INTERFERENCE ANALYSIS AND MITIGATION FOR HETEROGENEOUS CELLULAR NETWORKS

A Dissertation
Presented to
The Academic Faculty

By

David Manuel Gutierrez Estevez

In Partial Fulfillment
of the Requirements for the Degree
Doctor of Philosophy
in
Electrical and Computer Engineering

School of Electrical and Computer Engineering
Georgia Institute of Technology
December 2014

INTERFERENCE ANALYSIS AND MITIGATION FOR HETEROGENEOUS CELLULAR NETWORKS

Approved by:

Dr. Ian F. Akyildiz, Advisor
Ken Byers Chair Professor in Telecommunications, School of Electrical and Computer Engineering
Georgia Institute of Technology

Dr. Matthieu Bloch
Assistant Professor, School of Electrical and Computer Engineering
Georgia Institute of Technology

Dr. Geoffrey Ye Li
Professor, School of Electrical and Computer Engineering
Georgia Institute of Technology

Dr. John R. Barry
Asst. Professor, School of Electrical and Computer Engineering
Georgia Institute of Technology

Dr. Jun (Jim) Xu
Professor, College of Computing
Georgia Institute of Technology

Date Approved: December 2014

To my grandma

A mi wely

ACKNOWLEDGMENT

Writing the acknowledgement section of a PhD thesis after five years of intense *roller-coasting* work does not seem less challenging than writing its technical contents. However, although unavoidably imperfect and incomplete like any other human work, this is my humble effort to express my deepest gratitude to people and institutions that have been key in the development of this thesis, either because they directly helped me with the work itself, or because their support was essential in its attainment.

First of all, an infinite gratitude arises towards the place that hosted me throughout the development of this work. The BWN Lab Family, whose soul and spirit comes from my advisor and mentor Prof. Ian F. Akyildiz, is a work of art that need not envy the best Italian Renaissance painters. For having embraced me, for having let me be part of it, and for having allowed me to fulfill my professional and personal dreams, I am truly grateful to Prof. Akyildiz. His countless hours of support, his close relationship more similar to a father than an advisor, and his infinite energy and motivation have left a mark in me that will accompany me during the rest of my life. Equally remarkable is Prof. Akyildiz's ability to find truly exceptional people to expand our BWN Lab Family, a meaningful name that conveys how we all eventually become much more than simple colleagues. Hence my gratitude towards all my fantastic labmates, who have been the best travel companions anyone can wish for. I would like to particularly thank Max, Josep, and Zhi, for being my reference and support; to Elias for always being there and saving me in countless tough moments; and to the newer members Kiko, Xavi, Alba, Ahyoung, Bige and Hazar, for contributing to an inconceivably beautiful end of journey. Thanks to Anna, Sara, and Marcello, because their friendship is a treasure I will carry with me for the rest of my life. Last but not least, thanks to the fellowship programs of *Fundacion la Caixa* and *Fundacion Caja Madrid*, without whose support and trust this work would have never been carried out.

But the intense Atlanta experience has gone far beyond the walls of the lab, and to be

fair I would need an infinite list to name everyone I feel grateful to after these five years of PhD life. It is astonishing the amount of interesting people I have met from all over the world, and although sad at times because most of them come and go, I feel I have been shaped by each and one of them. Although the full list does not fit here, I would not forgive myself if I don't mention Mauro and Ciccio, who allowed me to discover the Italian part of my soul; Neus, the best roommate anyone could wish for; and Nico and Giovanni, who enjoyed the hours of conversation as much as I do. Thanks also to Marco, Spyros, Chlo, and Matt, my battle companions in the at times craziness of the PhD journey. And thanks to Almu, my most admired source of inspiration.

It has also been during the last few years of my life that I have discovered the real power of connection. I could not have survived this journey had I not felt the strength and proximity of relationships essential to who I am now, even with an ocean in-between. A heartfelt thank you to my *marbles* Agu, Richi, Maria, Rosa, and Zoraida, for their lifelong friendship; to Vicky and Gracia, for shaping my intense multi-dimensional universe of connection; and to Matteo, because the depth of our relationship redefined my idea of friendship beyond any existing conception. My insatiable search for connection culminated last year in San Diego, where the essentiality I had always longed for took a human shape. So thank you, Carme, because by your side my past, present, and future lives are given a fulfilling meaning.

The last words of this acknowledgement could not go to anybody else other than my family. My mother, my father, and my brother are the core of my roots, my most fundamental identity trait, the only place I really belong to. Without you, my family, no stage of this journey would have been traversed. Because of your infinite love, understanding, and support; because of your vision and sacrifice throughout the years; and because thinking of what we have lived together during the last years brings tears to my eyes - because of all of that, I owe you what I have done and who I have become. My dear family: Thank you. Words can't properly express that feeling, but I'm sure the shared joy will speak for itself.

TABLE OF CONTENTS

LIST OF FIGURES

SUMMARY

The architecture of cellular networks has been undergoing an extraordinarily fast evolution in the last years to keep up with the ever increasing user demands for wireless data and services. Motivated by a search for a breakthrough in network capacity, the paradigm of heterogeneous networks (HetNets) has become prominent in modern cellular systems, where carefully deployed macrocells coexist with layers of irregularly deployed cells of reduced coverage sizes. Users can thus be offloaded from the macrocell and the capacity of the network increases. However, universal frequency reuse is usually employed to maximize capacity gains, thereby introducing the fundamental problem of inter-cell interference (ICI) in the network caused by the sharing of the spectrum among the different tiers of the HetNet.

The objective of this PhD thesis is to provide analysis and mitigation techniques for the fundamental problem of interference in heterogeneous cellular networks. First, the interference of a two-tier network is modeled and analyzed by making use of spatial statistics tools that allow the reconstruction of complete coverage maps. A correlation analysis is then performed by deriving a spatial coverage cross-tier correlation function. Second, a novel architecture design is proposed to minimize interference in HetNets whose base stations may be equipped with very large antenna arrays, another key technology of future wireless systems. Then, we present interference mitigation techniques for different types of small cells, namely picocells and femtocells. In the third contribution of this thesis, we analyze the case of clustered deployments by proposing and comparing techniques suitable for this scenario. Fourth, we tackle the case of femtocell deployments by analyzing the degrading effect of interference and proposing new mitigation methods. Fifth, we introduce femtorelays, a novel small cell access technology that combats interference in femtocell networks and provides higher backhaul capacity.

CHAPTER 1

OVERVIEW OF NEXT GENERATION CELLULAR SYSTEMS

1.1 Introduction

Cellular networks have been undergoing an extraordinarily fast evolution in the past years. With commercial deployments of Release 8 (Rel-8) Long Term Evolution (LTE) already carried out worldwide, a significant effort is being put forth by the research and standardization communities on the development and specification of next generation cellular systems. Currently, the most prominent example is LTE-Advanced, which was conceived as an evolution of LTE systems [1] [2], [3], [4], [5], [6]. The work started in Rel-10 by the Third Generation Partnership Project (3GPP) had the initial objective of meeting the International Mobile Telecommunications-Advanced (IMT-Advanced) requirements set by the International Telecommunications Union (ITU) which truly defined fourth generation (4G) systems. However, current predictions for future systems point out tremendous challenges far beyond what the ITU initially established for 4G. Driven by both the explosion of users' demands for mobile data along with new services and applications, and the need for a ubiquitous and wirelessly accessible cloud platform, the evolution of future mobile traffic is expected to boom. Applications and services demand ever-increasing data rates. A traffic growth of up to 30 times was predicted to take place between the years 2010 and 2015 [7]. By 2016, more than 10 exabytes of traffic per month will be circulating across cellular networks and more than 4 billion 3GPP wireless subscriptions will be operating in the network [6]. With these forecasts in mind, it becomes critical to provide not only very high broadband capacity, but also efficient support for a variety of traffic types, flexible and cost-efficient deployments, energy efficient communications strategies, robust systems against emergencies, and a balance between backward compatibility and future enhancements.

To progressively tackle these challenging requirements, 3GPP has been organizing its work based on releases. Figure 1 shows a roadmap of all releases spanning LTE-Advanced

and the main technologies that were developed in each of them. Rel-10 started early in 2010 and was functionally frozen in March 2011 after its approval by the ITU for having met all the requirements for IMT-Advanced. Technologies introduced during that release include carrier aggregation for transmissions in several frequency bands, enhanced multiple input-multiple output (MIMO) techniques, relays, and self-organizing networks (SON). Then, Rel-11 was started and further enhancements were included to the basic LTE-Advanced technologies developed for Rel-10. The major contribution during Rel-11 was cooperative multipoint transmission and reception (CoMP), which allows different cells to cooperate for serving users. In addition, several important enhancements were introduced for heterogeneous networks (HetNets) such as enhanced inter-cell interference coordination (eICIC) and mobility management enhancements. After the completion of Rel-11, the standardization work started focusing on Rel-12 LTE-Advanced with a calendar that lasted through 2013 until its predicted freezing in late 2014. For Rel-12, further enhancements and new technologies are being proposed at the 3GPP meetings [8], [9]. Although no actual conclusions have been drawn yet, there is a clear view on which key technologies will be addressed in Rel-12, as shown in Fig. 1. Enhancements to CoMP (inter-site CoMP), carrier aggregation (multi-stream and multi-flow carrier aggregation), and MIMO (Full-dimension MIMO) are key items in the agenda of 3GPP. Moreover, radically new technologies are also being introduced: Machine-Type Communication (MTC) will enable machines to interact among themselves as part of a large network, and Device-to-device (D2D) communication will allow mobile users to interact with each other without the need to go through the network. Rel-13 is expected to further enhance LTE-Advanced technologies while Rel-14 and Rel-15 could potentially define a new access technology.

In parallel to the work of 3GPP, the challenge of ever-increasing demands for wireless data boosted by smartphones, tablets, and video streaming has led to the recent proposal by most of the relevant industrial players of a 1000x target for network capacity in next generation cellular systems [10], [11]. Hence, informal discussions regarding what will be

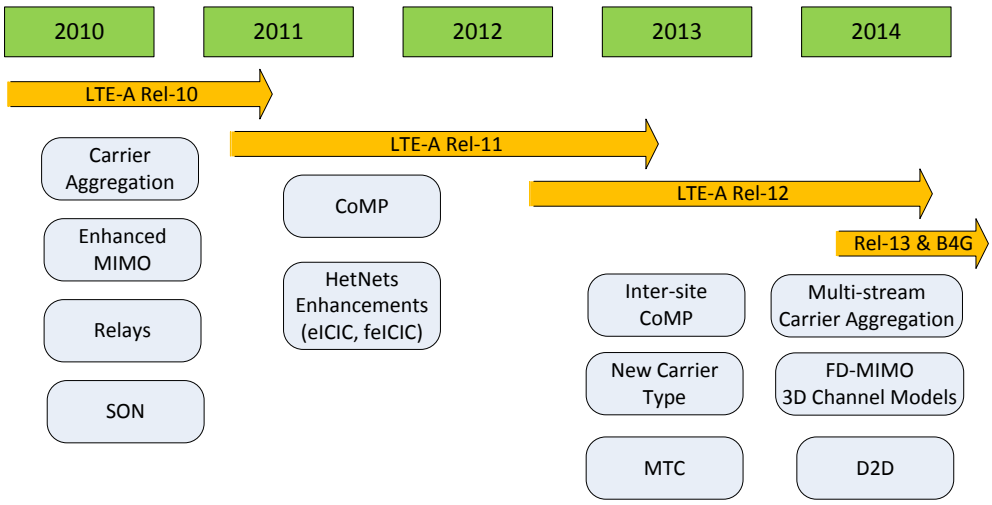

Figure 1. 3GPP releases roadmap

the fifth generation (5G) of cellular systems have started taking this figure as a major design goal [12], [13]. Furthermore, large collaborative projects between industry and academia such as METIS [14] and 5GNOW [15] have been recently established with the purpose of setting the fundamentals of 5G and target first deployments by 2020.

This introductory chapter of this thesis contains a brief overview of the main key technologies that play an important role in the different releases spanned by LTE-Advanced so far. It also includes new concepts currently under discussion and research challenges that will pave the way towards 5G. The remainder of this chapter is organized as follows. Section 1.2 presents carrier aggregation techniques. Enhanced MIMO techniques are summarized in Section 1.3 followed by cooperative communications in Section 1.4. Basic fundamentals of HetNets are explained in Section 1.5. Then, newer key technologies of Rel-12 are introduced: Section 1.6 presents MTC and Section 1.7 introduces D2D. Finally, Section 1.8 gives a very brief overview of other technologies expected to have a key role in future 5G systems.

1.2 Carrier Aggregation

One of the most effective methods to improve the network performance is to increase the amount of utilized bandwidth. Therefore, in order to meet the requirements of IMT-Advanced as well as those of 3GPP operators, LTE-Advanced considers the use of bandwidths of up to 100 MHz in several frequency bands. Carrier aggregation (CA) consists of grouping several "component carriers" (CC) to achieve wider transmission bandwidths. An LTE-Advanced device can aggregate up to five CCs, each of up to 20 MHz. With the largest configuration, this implies a total bandwidth of 100 MHz. To support backward compatibility with LTE devices, CCs shall be configured as a typical LTE carrier. Therefore, any of the CCs used for CA should also be accessible to LTE user equipments (UEs). Nevertheless, mechanisms, such as barring [16], already exist in order to prevent LTE UEs from camping on specific CCs. This way, operators have the flexibility of adjusting the characteristics of the CCs to support a mixture of LTE and LTE-Advanced devices. In addition to supporting wider bandwidths, carrier aggregation provides additional benefits, namely inter-cell interference mitigation, handover improvement, energy savings, and load balancing [1].

LTE-Advanced supports three schemes of carrier aggregation. The basic scheme of CA occurs when contiguous CCs are aggregated, as shown in Fig. 2(a). It depicts the aggregation of five CCs of different bandwidths, where the two rightmost are used exclusively by LTE-Advanced devices and the rest are shared among LTE and LTE-Advanced devices. While this scenario is the easiest to implement from a technical point of view, operators do not always have enough contiguous spectrum to perform this type of deployment. Therefore, non-contiguous CA is also supported. In this case, the CCs may belong to the same or to different spectrum bands, also called intra-band CA and inter-band CA, respectively. These two scenarios are depicted in Fig. 2(b) and Fig. 2(c). These two types of CA are extremely useful to operators that have fragmented spectrum along multiple frequency bands, since they can effectively reuse their spectrum fragments to provide improved service to

their users.

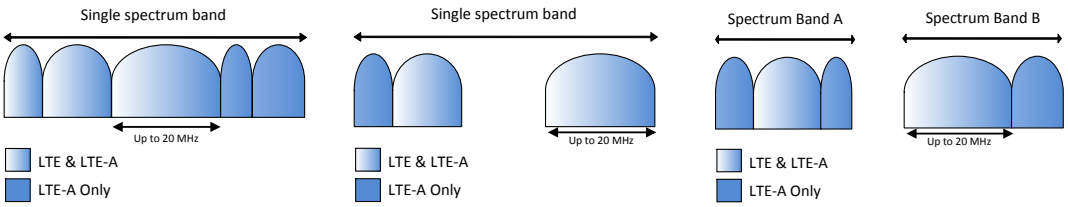

(a) Intra-band contiguous (b) Intra-band non-contiguous (c) Inter-band non-contiguous

Figure 2. Carrier aggregation schemes within 3GPP

The initial scope of carrier aggregation was to enable a single evolved NodeB (eNB) to serve its users utilizing two or more CCs. However, cellular networks have been evolving to become heterogeneous, where several small cells are deployed within the coverage region of the larger macrocell, as shown in Fig. 3. In this type of scenario, it is envisioned that an LTE-Advanced device will be capable of aggregating CCs belonging to the small cells and the macrocell. However, this scheme requires increased coordination between the small cells and the macrocell in order to avoid inter-cell interference. As a further evolution of the multi-stream concept (also called multi-flow), it is also being studied to support CA not only among LTE and LTE-Advanced eNBs working in TDD and FDD [17], but also across base stations belonging to other technologies. This will provide significant improvement in the network, specially when there is an unbalance in the utilization of the radio access technologies (RATs). The technique must be carefully utilized since it also increases the amount of energy consumed by the UE, the amount of signalling in the air inteface and the core network, and requires the introduction of new data aggregation entities common to the multiple RATs.

1.3 Enhanced Multiple Antenna Techniques

The use of multiple antennas both at the transmitter and the receiver is known as MIMO and has become an essential technology for every current or future wireless system attempting to achieve very high data rates. Although MIMO techniques were already introduced

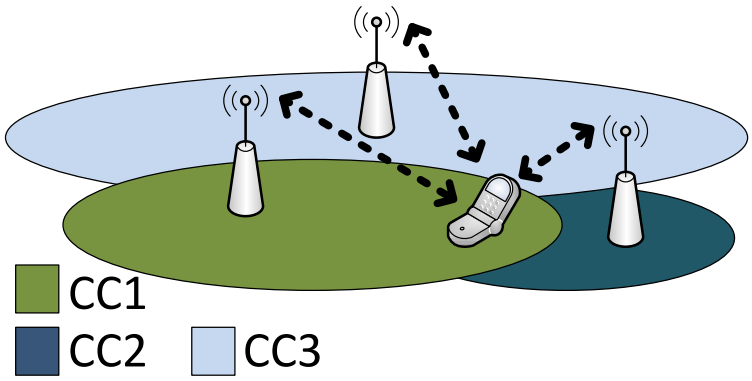

Figure 3. Multi-stream carrier aggregation

in LTE systems [18], significant work has been carried out in the past years to boost the potential gains of this set of techniques for LTE-Advanced in Rel-10, Rel-11 and Rel-12 [19], [20], [21]. Therefore, the name of *enhanced MIMO* was selected for the set of LTE-Advanced techniques. Most of the major enhancements over LTE MIMO were introduced in Rel-10, although during Rel-11 some further refinements were made. The maximum antenna configuration was increased to 8x8 for the downlink and 4x4 for the uplink. In addition, an important novel feature is the introduction of a dynamic framework for switching at the eNB between single-user MIMO (SU-MIMO) and multi-user MIMO (MU-MIMO), where the mode of operation for each user can be adapted transparently to higher layers in a fast timescale. This feature is important to optimize system performance since the MIMO channel and the UE's signal-to-interference-and-noise (SINR) conditions, as well as the traffic demands, may vary from one subframe to another. Furthermore, although improved techniques in terms of advanced beamforming and precoding for both SU-MIMO and MU-MIMO have been introduced, the latter mode has been given preference since it is considered to be a key capacity-enabling feature to meet spectral efficiency targets in LTE-Advanced systems. These new features have implications on different system aspects, such as reference signals, feedback design, or precoding codebooks.

More recently, the use of very large arrays at base stations has been proposed as a very

promising way of drastically improving the capacity of cellular networks [22], [23], [24]. Because of its great potential, it has been indeed identified as a key technology for future 5G systems [1], [12], [13]. By massive MIMO it is usually understood that the order of magnitude of the number of antennas is greater than the current one, e.g., 100 or more. A number of very appealing advantages can be potentially achieved out of this technology. First, dramatic capacity improvements can be obtained, especially when it is used to serve multiple users (MU-MIMO) [24]. In addition, random matrix theory shows that the effects of uncorrelated noise and multipath fading vanish when the number of antennas grows to infinity [25]. Moreover, the directivity of the beams can be greatly improved, hence reducing the side-lobe interference, and the radiated energy can be significantly reduced due to the large array gains [26]. However, massive MIMO is not exempt of challenges. In the first place, the so-called pilot contamination problem has been assessed as the ultimate performance-limiting factor in massive MIMO cellular systems [25]. Its mitigation is probably the center of current research efforts in this field, as it will be summarized later in this section. But other challenges related to hardware impairments, channel and propagation models, or complexity of the detector need also to be addressed [23], [24].

In addition to the plain massive MIMO idea, a promising concept currently under investigation within 3GPP is *Full-dimension MIMO* (FD-MIMO), where a large two-dimensional array of transmit antenna ports (16, 32, or 64) at the eNB makes use of the so-called active antenna system (AAS) technology to provide accurate 3D beamforming to targeted users [27], [28]. The main idea of AAS is to integrate the active transceiver component and the passive antenna array into just one radome, thus allowing improved beamforming capabilities in the azimuth and elevation planes for a full utilization of the spatial domain [29]. Allowing the AAS to have additional control over the elevation dimension enables the eNB to direct beams in different horizontal and vertical directions, thus improving the accuracy of the beams directivity while allowing beams for different operations, dedicated tilts, frequency bands, network standards and link directions.

Figure 4 shows a sample scenario for the FD-MIMO concept. Three different potential uses of FD-MIMO are shown: First, a smoother experience of users benefiting from eNB cooperation can be achieved with well-focused 3D beamforming. Second, users at the same horizontal position in the cell but different vertical positions are simultaneously served by means of vertical beam adaptation. Third, vertical coverage is extended in scenarios such as tall buildings in dense urban areas. As with the case of plain massive MIMO, multiple research challenges such as the feedback design or suitable 3D channel models still remain to make FD-MIMO fully implementable [1], thus establishing FD-MIMO as an interesting research topic for the future.

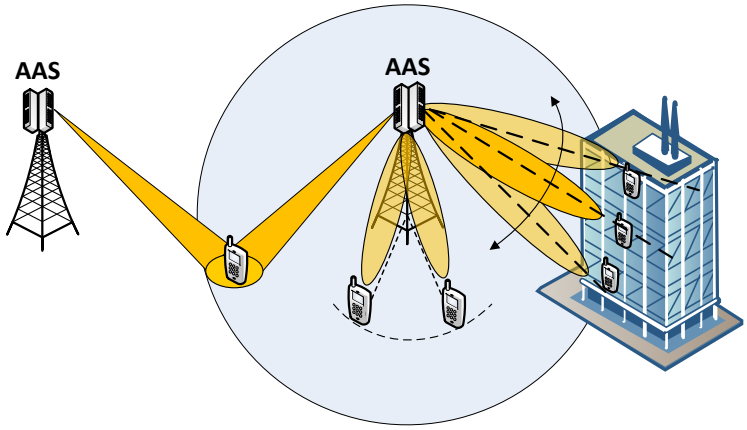

Figure 4. Full-dimension MIMO concept

Chapter 4 of this thesis proposes a solution for in this novel area by presenting an architectural design for HetNets where one or several of the base stations are equipped with massive MIMO antenna arrays.

1.4 Cooperative Multipoint Transmission and Reception

A key tool to improve system efficiency, cell-edge throughput, and coverage of future 3GPP cellular networks is coordinated multipoint transmission and reception (CoMP) [2], [30], [31]. Although the concept started to be discussed in Rel-10 LTE-Advanced, it was not included in the specifications until Rel-11 due to initial high complexity concerns. The

main principle of CoMP is based on the idea that UEs close to the cell-edge region can benefit from the downlink cooperation of multiple cell sites, thus transforming a problem of interference into an opportunity for improved service. Similarly, CoMP can be also applied in the uplink in such a way that multiple sites coordinate the reception of signals coming from the UEs.

Different CoMP architectures can be envisioned depending on whether the cooperation takes place intra-site (i.e., within the same eNB) or inter-site (i.e., among different eNBs). Intra-site CoMP was achievable in earlier releases since communication takes place just within one site and does not involve backhaul. Furthermore, the deployments can be carried out in homogeneous or heterogeneous environments, implying that the cell can have same or different coverage area sizes. According to these possible architectures, 3GPP has considered the utilization of CoMP in four different scenarios, as Fig. 5 depicts. Scenarios 1 and 2 represent homogeneous deployments, where the coordination takes place intra-eNB and inter-eNB, respectively; Scenario 3 represents inter-cell CoMP in heterogeneous deployments; and Scenario 4 depicts a distributed antenna system (DAS) with shared identification number (ID). Scenarios 1 and 4 have been included already in Rel-11 while scenarios 2 and 3 are currently being developed within Rel-12 [6].

Different CoMP approaches with different levels of coordination exist both for the downlink and uplink. In the downlink, three main CoMP modes exist. In increasing order of complexity, they are the following: (i) Coordinated scheduling/beamforming (CS/CB) where each UE is served by a single cell and scheduling decisions and precoding at each eNB are coordinated among different eNBs to reduce inter-cell interference; (ii) dynamic point selection (DPS), where the transmission to the intended UE only takes place from one point at a time. This point is drawn from the CoMP cooperating set and may vary as fast as on a subframe-by-subframe basis; and (iii) joint transmission (JT), where data intended for a particular UE is simultaneously transmitted from multiple sites to coherently or non-coherently improve the signal quality received in a time-frequency resource.

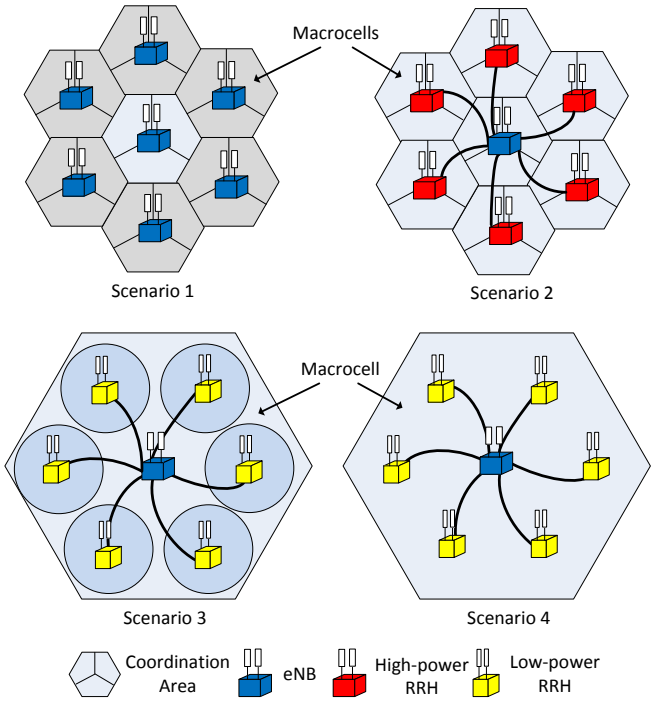

Figure 5. CoMP scenarios considered within 3GPP

1.5 Heterogeneous Networks

The ubiquituous coverage and ever-increasing capacity requirements for current cellular networks are the major drivers for the paradigm of HetNets, where cells of different sizes and different radio access technologies (RATs) must coexist within the same network. The reason for the prominence of this technology can be found in the fact that studies on past network capacity enhancements were performed and it was observed that reducing the distance from base stations to users have contributed to capacity gains of 1600-fold [32]. After a tremendous activity on small cells has been conducted in recent years by academia, industry, and standardization bodies, every operator across the world is currently carrying out the deployment of HetNets comprised of a macrocell network underlaid by one or several tiers of small cells [33]. Femtocells, metrocells, picocells, WiFi access points or remote radio heads (RRHs) are representative technologies of this family, as Fig. 20 shows.

HetNets introduce a number of technical challenges, among which inter-cell interference (ICI) probably stands out as the most critical issue to guarantee the attainment of

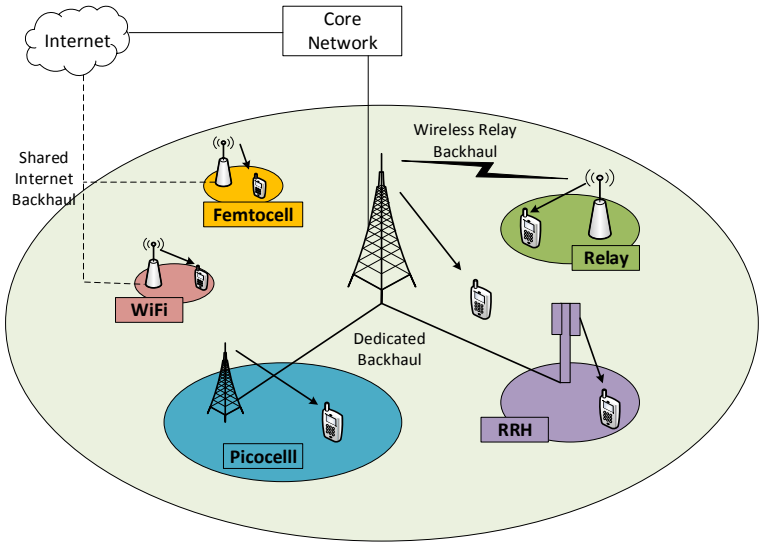

Figure 6. HetNet

the potential benefits that HetNets offer. This thesis is mostly dedicated to this particular challenge and Chapter 2 gives a detailed introduction and literature review of the topic. However, this is not the only technical challenge affecting HetNets. Other important issues of HetNets are cell association, mobility management, and energy consumption. We briefly introduce them in this section.

- *Cell association:* The problem of cell association in the case of homogeneous cell deployments comprised only of macrocells is typically decided based on a criterion that selects the largest downlink signal strength or SINR at the user's receiver [34], [35]. However, in a HetNet, the assignment of users to a particular base station is a non-trivial problem. The above mentioned association criterion leads to a high underutilization of the small cells as the reduced available power of small cells would cause very few users to be attached to them. To solve this problem and boost the capacity gains of small cells, the state-of-the-art solution for HetNets is to expand the range of the small cells by introducing a so-called bias factor [36] that allows the user to attach to the small cell before its received power is larger than the power received

from the macrocell. This factor is applied at the receiver of the users as a a multiplicative term modifying the actual received power from the small cell base station [37]. However, the current cell biasing approach has the fundamental drawback of increasing the amount of ICI in the network, thus coupling the ICI and cell association problems. Expensive time-domain techniques need to be used where the macrocell stops transmission during certain subframes, called almost blank subframes (ABS), causing macrocell users to experience a large performance loss [38].

- *Mobility management:* Seamless and robust mobility is a bigger challenge in HetNets compared to homogeneous macrocell deployments. A detailed study of mobility performance for HetNets show that the handover failure rates and ping-pong effects are far greater in HetNet environments compared to homogeneous deployments [39]. The poor handover performance of users in HetNets is owing to several factors. One of the major factors is the need to account for the unique characteristics of HetNets when performing user mobility state estimation in addition to accounting for parameters such as the number of cross-overs. Another factor is the need to perform efficient small cell discovery over different carriers at the base stations. This is essential to enable traffic offload from macro to small cells as well as to reduce the battery consumption for the users and the overall system. Furthermore, since the handover failures can be larger in the HetNet case, more robust recovery procedures are required to mitigate the impact of a failed handover. Some examples of improved mobility schemes for HetNets can be found in the 3GPP documents [40], [41], and [42], among others.

- *Energy consumption:* Industry and academia have engaged in addressing the energy efficiency in cellular networks, also called green cellular networks, through several large-scale projects and consortia [43], [44]. The common agreements across all these initiatives are that (i) for operators, the major energy inefficiencies and wastage

occur at the RAN, and (ii) for mobile devices, the energy requirements are increasing due to the new services that demand higher data rates and quality of service (QoS). At the RAN, it is imperative to improve the energy efficiency given the tremendous amount of energy that it not only consumes, but also wastes. On the other hand, at the UE, the concern about the energy consumption arises from the combination of two key factors. First, the UE has a very limited battery life. Second, the exponential traffic growth is driven by services with higher QoS requirements and data rates. Particularly, video service is expected to account for half of the global mobile data traffic by 2018 [45]. Even though the amount of energy consumed at the UE does not directly change the operators energy bill, it significantly influences the quality of experience (QoE) of the end-user. Such QoE is critical for user satisfaction, churn rate, and, therefore, the overall economic performance of operators.

1.6 Machine-type Communication

In addition to the proliferation of human users, there is a fast-growing tendency of automation (Internet of Things, Smartgrids) where machines are able to interact between themselves as part of a large network. This type of communication is referred to as machine-type communications (MTC) or machine-to-machine communication (M2M). The number of MTC devices is predicted to grow at a compound annual growth rate of over 25% [46], [47]. Several technologies have been proposed to realize MTC communications among which WiFi, Zigbee, Bluetooth are more prominent. However, MTC solutions utilizing mobile cellular networks can offer several benefits. They are easier to install and can provide reliable data delivery to remote MTC servers. Moreover, mobile networks are crucial for supporting a large range of MTC devices including the highly mobile ones. One of the first studies on MTC for 3GPP systems was presented in [48].

The M2M communication scenarios according to 3GPP can be classified as follows:

(1) Communication between MTC Devices and one or more MTC Servers, (2) Communication between different MTC Devices. This is illustrated in Fig. 7. The MTC devices can exist in groups and each of the devices have similar capabilities to LTE-Advanced users to communicate with the LTE-Advanced base stations. The core network of LTE-Advanced is connected to an MTC server that is controlled by MTC users (such as an organization or individual). In the first case, an MTC user can control several MTC devices (such as a set of sensors performing measurements) through an MTC server and hence the communication takes place between the MTC devices and the MTC servers. In the second case, different MTC devices either under the same/different operator can communicate between themselves without an intermediate MTC server.

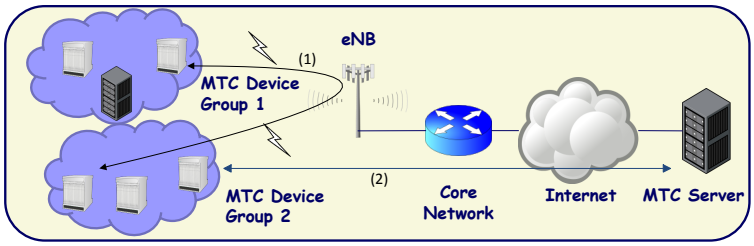

Figure 7. MTC architecture for LTE-Advanced with communication scenarios

The support of MTC for 3GPP systems raises quite a few challenges, both at the air interface level and the network level. Particularly for the case of LTE-A, there would be several millions of MTC devices, each one requiring only a fraction of the bandwidth for transmitting data. This could result in the wastage of a significant amount of resource due to the heavy signaling and data overheads involved for communication in LTE-A. In addition, this could also result in a reduction of the resources available for other devices that actually require high data rate communications. A 3GPP work item was organized to identify and propose novel solutions for supporting MTC devices at the LTE-Advanced air interface [40]. Similarly, the service requirements for MTC was laid out in [49].

1.7 Device-to-device Communication

The paradigm of device-to-device communication (D2D), also known as proximity services (ProSe), is another key enabling technology for LTE-Advanced that has been included in Rel-12 for consideration [50], [51]. It refers to the ability of cellular devices to communicate directly among each other without the need to access the network infrastructure. Although currently existing technologies such as Bluetooth or WiFi-direct already allow this functionality, they do not allow the operator to control the communication process and guarantee certain user experience. Furthermore, they are not designed to be integrated within the cellular network, while D2D should minimize the impact on the cellular network and enable users to transparently switch between D2D modes and regular cellular communication.

The applications driving this new communication technology are already numerous as of today, but it is likely that many others are yet to be found in the near future. We describe some of them in this paragraph: First, operators are becoming increasingly interested in context-aware applications where a plurality of services can be provided depending on the user's location. To make the context-aware functionality of the network as flexible as possible, optimized direct communication of the user with other devices should be enabled. Second, the support for public safety networks in cases where network infrastucture is not available is a major current concern that 3GPP is addressing with the introduction of D2D. Third, the rapid emergence of M2M applications and the Internet of Things makes a use case for D2D, since it would be desirable to control electronic consumer devices directly from the cell phone of the owner without the need to overload the network. Fourth, D2D can be seen as an additional method to offload traffic from the congested macrocell networks, so operators are currently exploring the option of exploiting D2D functionalities with that purpose.

There are some aspects of D2D that deserve special attention. First, some similarities are shared between D2D and mobile ad hoc networks, which have been extensively studied

in the literature. However, a significant difference is that D2D can rely on limited assitance from the network for control functions or, if necessary, to carry out the communication. How to select the best network mode for operation is still a research challenge, as it is pointed out later in this section. Second, a question of vital importance is what spectrum to use, and how to distribute it. The direct link between UEs can be established over a variety of air interfaces including both licensed and unlicensed spectrum. The classical advantages and disadvantages of both options apply here, with the particularity that this type of communication must take place in a integrated fashion with the rest of the network. Therefore, network operators may also benefit from less congestion and interference in their network when using D2D in the unlicensed band.

Device-to-device communication (D2D) is an emerging technology with high disruptive potential in the network. However, a large number of challenges still remain unsolved and constitute an exciting field of research for the next few years. Among them, the following can be highlighted: (i) mode selection to establish the level of involvement of the network in the D2D communications [50], [51], (ii) group communications strategies for direct communication among multiple terminals [52], [53], (iii) interference and resource management [54], [55], (iv) multi-hop communication [56], and (v) neighbor discovery procedures [57], [58].

1.8 Other Key Enabling Technologies for Future 5G Systems

Besides the above explained technologies currently under discussion within 3GPP, the conversation has also started to seek other revolutionary technologies for 5G. In this last section, we briefly introduce some of the newest topics in cellular communications that could become cornerstones of future 5G systems.

- *Milimiter Wave:* Even though all the above advanced communication techniques contribute to improving the spectral efficiency of the networked communication, there is currently no doubt among researchers, practitioners, and regulatory bodies that

new spectrum will be needed to significantly increase the capacity of current cellular networks. This naturally means going up in the spectrum to higher frequencies. Currently, there is large interest in the study of the so-called milimiter wave (mmWave) band spanning the frequency band of 3 GHz to 300 GHz for cellular transmission [59], [60], [61], [12], [13]. The most immediate challenges for making cellular communications feasible in this band are those related to propagation: Pathloss, shadowing, and absorption can scale up significantly when compared to transmission in traditional spectrum. However, beamforming techniques based on the use of massive MIMO in the mmW band can overcome the pathloss problem, while the high sensitivity to blockages induced by the shadowing can be assumed as a new system design parameter that can be mitigated through different techniques. For example, multi-stream carrier aggregation could provide fallback solutions to the inherent intermittent service characteristics of mmWave transmission. Other aspects of mmWave-enabled cellular systems that deserve in-depth study are the cell association policies, the separation of data and control, the hardware design for these high-frequency components, or the MIMO solutions suitable for this frequency band [59].

- *New Air Interface Concepts:* The characteristics of the air interface that will be utilized in 5G systems is currently a topic under discussion [13], [14]. In the first place, there is currently no general agreement on whether orthogonal frequency division multimlexing (OFDM) should be kept as the main waveform for 5G systems. It is clear that its strong advantages in terms of robustness against frequency selectivity and inter-symbol interference (ISI), computational efficiency, and suitability for MIMO communications still make it a good candidate. However, it also presents shortcomings in terms of synchronization and orthogonality requirements that have become a major issue for enabling other communication techniques such as CoMP [15]. Hence, other options currently discussed encompass filterbank multi-carrier

solutions (FBMC), nonorthogonal signals, faster than Nyquist (FTN) techniques, or generalized frequency division multiplexing (GFDM). Besides the waveform, additional key elements of the air interface need also be designed: The multiple access scheme, previously based on OFDMA, should also be revisited since non-orthogonal techniques and advanced coded multi-carrier schemes should be proposed and evaluated. Moreover, multiple-access solutions for D2D as well as MTC scenarios are required. Finally, the medium access control (MAC) and radio resource management (RRM) layers as well as novel hybrid automatic repeat request (HARQ) schemes may require further improvements or even re-design.

- *Ultra Dense Networks:* Densification of base stations is a classical means of providing increased capacity in wireless communication. When the range of the cells decreases and the number of base station increases, this leads to a very dense small cell scenario where the number of served users per base station would be very small. Transmit powers of base stations and terminals would become very similar. In the limit, one base station may only serve one user with same transmit power as the terminal, hence eliminating differences between traditional cellular concepts like access node and terminal as well as uplink and downlink. In this envisioned network scenario, all access network components would be identified just as devices communicating through symmetric wireless links [12], [14].

CHAPTER 2

THE CHALLENGE OF INTERFERENCE IN HETEROGENEOUS NETWORKS

2.1 Introduction

The general interest on small cells was triggered after it was noticed that the reduction of the coverage size in serving cells is a major source of capacity increase for cellular networks [62], [63]. Since the electromagnetic spectrum is a very scarce resource for operators, to maximize the gains the irregularly deployed layers of small cells must operate in the same frequency bands as the macrocell. That is clearly a more efficient option than partitioning the resources. However, this approach causes ICI, which can be further classified into cross-tier when it happens among elements in different layers of the network, or co-tier for the case of cells of the same layer.

The challenge of interference in HetNets has become central in the study and design of future cellular systems. The study of ICI has always been a major research issue also in homogeneous systems: Interference coming from adjacent cells in the traditional cellular grid has always caused performance degradation to the cell edge users, which suffered both from a weaker signal reception and increased interference. The reason for the resurgence of interference in HetNets lies in several factors. First, it is almost imperative to think of universal frequency reuse deployments, since the amount of cells in each tier does not allow efficient resource partitioning schemes. But maybe more importantly, in the past interference affected just the cell edge users of the macrocell whereas the topology of a HetNet deployment and the number of base stations make virtually every user in the network susceptible to suffer or cause interference. Therefore, the system-level implications of ICI are more significant in the HetNet case. Last but not least, the unplanned and even random nature of a HetNet deployment makes the problem of managing interference more challenging than the case of well-thought homogeneous deployments.

Proper handling of interference in a HetNet requires two major tasks: Understanding of the interference phenomenon (i.e., interference modeling and analysis), and methods to mitigate it as efficiently as possible. This thesis deals with the two aspects of the problem. In this chapter, we provide an overview of the state of the art as well as the organization of the reminder of this thesis.

2.2 Overview of the State of the Art

In this section, we present an overview of the state of the art of the field of interference analysis and mitigation for HetNets. Since this is a topic of very high interest for both academia and industry, efforts in the last few years have been carried out both at the academic institutions side and the standardization bodies composed of the major industry players in the field. In the following, we survey the most significant contributions at both sides.

2.2.1 Academic Efforts

An extensive body of research tackling the problem of interference in HetNets can be found in the academic literature. After HetNets were identified as a key technology for increasing network capacity, it became clearly imperative to understand and model the effect of interference, and to design mitigation techniques that tackle all types of ICI, namely the cross-tier and the co-tier cases. In the interference analysis field, a large portion of the work carried out by the research community has been oriented towards finding mathematical models that represent the HetNet architecture, thus allowing the derivation of closed-form expressions for performance metrics in the average sense. On the interference mitigation side, an overwhelming amount of solutions have been proposed in the literature in the form of algorithms and procedures that mitigate ICI in a HetNet, although this part of the work related to the interference problem has been extensively studied at the standardization bodies. Their solutions are currently the most prevalent ones and will be surveyed in detail in Section 2.2.2.

The first paper in the above direction by Andrews et al. is [64], where the framework

of stochastic geometry for the analysis of wireless networks was presented. In particular, expressions for the key metrics of SINR and rate as well as well as coverage gain were developed in closed-form expressions using stochastic geometry for the first time. The work in [65] extended this analysis for the case of HetNets consisting of up to K-tiers of randomly deployed base stations of different transmit power. Assuming the classical max-SINR association criterion, expressions for the probability of coverage and rate are derived for this new scenario. A similar analytical work was performed in [66], where a closed expression for the SINR distribution of HetNet users at random locations is derived. Another relevant piece of analytical work was presented in [67], where the interference management efficiency of universal frequency reuse in HetNets is compared against a fractional frequency reuse deployment. Other relevant papers include [68], where coverage expressions for HetNets equipped with multiple antennas are found taking into account both cross-tier and co-tier interference, and the more recent [69], where a novel hybrid stochastic model for interference is developed to simplify the study of its impact in cellular systems. Finally, some prominent academic papers on the interference mitigation side are [70] and [71], which propose innovative interference coordination techniques suitable for HetNets.

Nevertheless, there is still an important lack of analytical models to represent the state and fluctuations of interference in real time. The dynamics of the network should be characterized for a better operation of the network at each time. Furthermore, the inherent cross-tier correlation existing among tiers due to ICI has not been investigated so far. In this thesis, we approach the interference analysis problem in a novel way: An analytical framework is presented based on random field theory that tracks the two-tier coverage, and the cross-tier correlation will be exploited via a cross-correlation function that we derive. The work on interference analysis is presented in Chapter 3. On the mitigation side, there is a lack of interference studies on scenarios with non-uniform user distributions as well as HetNet topologies where the small cells are deployed targeting hotspot locations in

clustered fashion. Chapter 5 explores interference suppression techniques in this scenario.

Besides the plain ICI problem simply arising from the universal frequency reuse, other aspects of HetNets can also play an important role in the amount of interference that is created in the network. In particular, in this thesis we examine two of them, namely the cell association problem and massive MIMO techniques for HetNets. In the following, we survey some relevant literature in the former topics and their relationship to the interference problem.

Cell association: The cell association problem in HetNets was briefly introduced in Section 1.5. Several works in the literature have dealt with this issue and its coupling with the interference problem. In [72], analytical expressions for optimal range expansion biases in different scenarios are derived, where coverage regions are found to be elliptical. In addition, a cooperative scheduling scheme between macrocells and picocells is proposed to mitigate the created interference when biased association is applied. The authors of [70] propose ICIC and cell association solutions for the correct operation of HetNets focused on cell splitting, range expansion, resource negotiation, and dynamic interference management for QoS via over-the-air signaling. Other theoretical works include an analytical study of the downlink SINR distribution of a heterogeneous network [37], where the impact of cell biasing in outage probability and average ergodic rate is investigated. Additional mathematical frameworks to find optimal association bias have also been proposed: In [73], a semidefinite relaxation of the maximum sum rate is presented along with a randomized heuristic to find a feasible association. Finally, [74] presents an optimization formulation for the load balancing problem by jointly considering resource allocation and cell association while it also introduces a distributed algorithm of low complexity with near optimal performance. A common denominator of all these works is that cell association is interference-agnostic, and its management is only triggered *a posteriori*. In Section 3.4.1, we propose a novel approach to cope with the interference and association coupling.

Massive MIMO techniques: In addition to the densification of the number of cells

in the network introduced by the HetNet paradigm, multiple antennas have traditionally been one of the preferred approaches to increase the capacity of networks. Furthermore, beamforming has been a very effective means of reducing interference in the network by concentrating the energy of the signal in one direction, Currently, the number of antennas deployed per unit area is also becoming denser under the concept of massive MIMO as explained in Section 1.3. When the number of antennas is large, the utilization of time-division duplex mode (TDD) in the network is preferred to avoid unaffordable pilot overhead. This consideration will be further explained in detail in Chapter 4. In massive MIMO systems, the major performance degrading factor is a type of interference effect known as *pilot contamination*. Pilot contamination appears due to the channel estimation error that is caused by the reuse of non-orthogonal pilot sequences at different users. The particularity of the pilot contamination effect in a TDD system is that the channel estimate may exhibit a strong correlation with the interfering channel, hence making this effect quite dangerous when the number of antennas is large for the following reason: The interference may end up being directed through beamforming towards a user or a base station that does not intend to receive that signal. To handle this effect, a number of solutions have been proposed in the literature already. A common approach is to rely on precoding to mitigate it: A single-cell precoding method is proposed in [75], multi-cell cooperation methods can be found in [76] and [77], and a more realistic solution limiting the information exchange overhead among base stations is proposed in [78]. Another family of methods is known as blind methods or eigenvalue-decomposition-based channel estimation [79], [80]. These methods are based on subspace partitioning under the assumption that the channel vectors from different users are orthogonal. Finally, the piece of work most related to the approach presented in this thesis is the proposal of time-shifted pilots as a means to reduce pilot contamination [81]. It is shown that in the asymptotic regime, i.e., when the number of antennas grows to infinity, it is beneficial to divide the base stations in groups that transmit their pilots simultaneously, thus reducing the interfering channels contributing to the pilot contamination effect.

We envision massive MIMO systems as a powerful means to avoid interference among small cells in HetNets. Hence, the technologies of HetNets and MIMO can be effectively combined to achieve larger system gains if the pilot contamination effect is properly managed, as it will be shown in Chapter 4.

Femtocells

A particular type of small cell that has drawn a lot of attention in the research community are femtocells. A femtocell access point (FAP) is a short-range low-power device owned and installed by the subscriber that aims to achieve better service at places like a home, an office, a supermarket, etc. by transmitting in licensed spectrum. The traffic is sent over the IP (Internet Protocol) backhaul, thus offloading macrocell traffic and releasing resources for other macrocell users. Figure 8 shows the architecture of a femtocell. A first comprehensive overview of the concept and its main technical challenges was presented in [82], and the overall status of the technology was later reviewd in [83]. Numerous aspects for investigation were pointed out, such as the cross/co-tier interference, QoS provisioning via internet-based backhaul, timing/synchronization, and access method. Interference was already identified as the major technical concern.

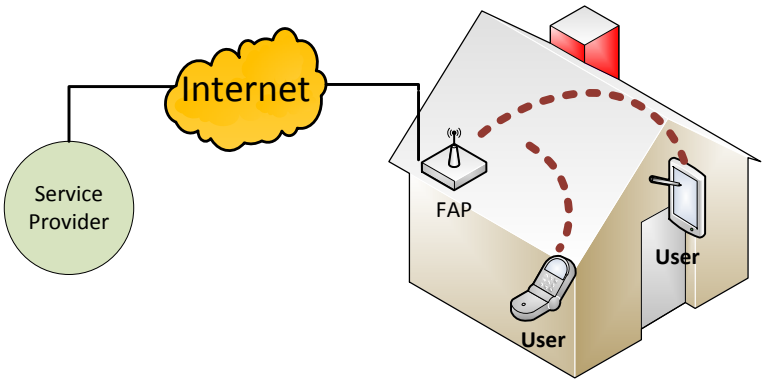

Figure 8. Femtocell architecture

In a typical femtocell scenario, the uplink transmission of the femtocell user (FU) will cause interference to the base station, while the downlink transmission of the base station

will cause interference to the FU. In a closed femtocell scenario, non-authorized macrocell users (MUs) can get as close as they desire to the FAP and still not be able to access the femtocell service. This causes the interference problems to increase even more. The non-authorized user may receive strong downlink interference from the FAP, while at the same time the FAP may receive strong uplink interference from the non-authorized user. In open and hybrid femtocells the non-authorized user could be switched as to be served by the FAP. However, in a closed femtocell the non-authorized user is not allowed to connect to the FAP. These scenarios have been studied in detail and several techniques to mitigate the interference issues have been proposed. In [84], the use of a different carrier for High Speed Packet Access (HSPA) FAPs is proposed to mitigate downlink interference, as well as the dynamic adjustment of their transmission power. However, reducing the transmission power has the side effect of reducing the coverage and capacity of the FAPs. To mitigate uplink interference, limiting the transmission power of the FU is proposed in [85]. For OFDMA FAPs, several techniques are proposed in [86] for orthogonal and co-channel FAP deployments. In general, the techniques can be classified as static or dynamic, centralized or distributed, and cooperative or noncooperative. Within this framework, the concept of self-organizing networks has gained significant importance as a tool to tackle the interference problem [87], [88], due to the dynamic nature of femtocell deployments.

2.2.2 Standardization Efforts

The topic of interference in HetNets has also sparked strong interest in the industry and standardization bodies. Most of the work on interference management has been carried out by 3GPP, the leading standards body for cellular communicacations. The work carried out so far has spanned several releases: Initial techniques were developed under the work item of inter-cell interference coordination (ICIC) of Rel-8 and Rel-9, and more advanced techniques were further developed in its enhanced version (eICIC) for Rel-10 and beyond. More recently, a new work item known as further enhanced ICIC (feICIC) was created

containing the latest techniques to mitigate interference in HetNets [89]. While ICIC algorithms use less sophisticated approaches such as carrier frequency separation, adaptive fractional frequency reuse, or basic MIMO, eICIC techniques introduce physical layer enhancements that address some of the shortcomings of the former techniques such as the interference at the control channel transmitted over the entire bandwidth. In this section, we review the most important techniques of those introduced in the last years.

Figure 9 illustrates the different scenarios of inter-cell interference considered within 3GPP. Interference mitigation techniques are needed both for the uplink and the downlink, as Fig. 9 points out. In addition, the interference may be caused by the macrocell to the small cell, by the small cell to the macrocell (both cross-tier), or among small cells (co-tier). The gravity of the interference case may vary depending on several factors like the transmit power of the interfering device, or the location of the small cell with respect to the macrocell and other small cells.

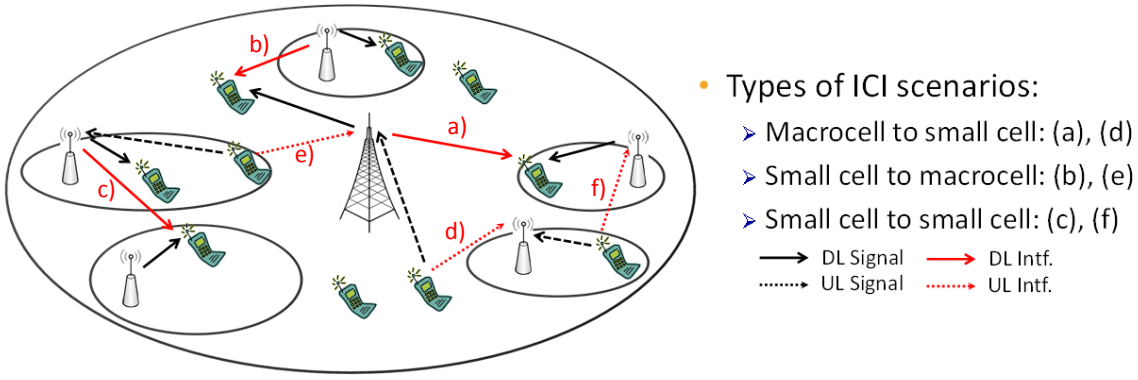

Figure 9. Inter-cell interference scenarios in a HetNet

In order to overcome the above interference, several ICIC methods were proposed as part of Rel-8/Rel-9. One of the common approaches is to use different carrier frequencies for different cell layers [90]. This is an effective means to mitigate the ICI but at the expense of utilizing more frequency resources. In the more common case when the cell layers utilize the same carrier frequency, power control schemes are recommended to reduce the transmission power of at least one of the cell layers to reduce the interference on

other layers. Other schemes proposed for ICIC based on Rel-8 and Rel-9 capabilities include adaptive fractional frequency reuse, spatial antenna techniques including MIMO and SDMA, and adaptive beamforming [91].

A majority of the solutions proposed in the Rel-8 and Rel-9 do not address the interference at the control signaling channel (PDCCH) since it is transmitted over the entire bandwidth in order to achieve diversity gain in the frequency domain. With the enhancements in the physical layer enabled for Rel-10 and Rel-11 such as carrier aggregation, more sophisticated methods appeared as part of the eICIC family. These solutions are basically categorized as (i) time domain-based, (ii) frequency domain-based, (iii) power control based, and (iv) advanced receiver at the terminal.

2.2.2.1 Time Domain-based Techniques

The time domain-based techniques basically rely on reducing the transmission activity on the ABS subframes by each of the cell layers to minimize interference to the victim layers. The knowledge of the subframe timing is assumed to be available at the different base stations. The ABS are implemented by either utilizing the MBSFN (Multicast/Broadcast over single-frequency network) subframes or by deliberately not scheduling (or using power control) over other subframes. Figure 10 illustrates the frame configuration of a victim cell and an aggressor cell when the above time domain-based eICIC scheme is applied. The aggressor uses the ABS subframe during the transmission of control signaling (broadcast and synchronization signals) by the victim cell. In the ABS subframe, the aggressor applies power control and transmits only common reference signals (CRS), critical control channels or broadcast and paging information for legacy support. Thus the victim's control signals are protected during the ABS subframe duration.

The transmission by the aggressor cell in the ABS subframe, particularly the CRS, cannot be avoided whereas the rest of the control signaling or broadcast signals can be suppressed for some of the ABS subframes. This transmission of CRS will result in interference experienced at the victim cell. Many of the existing time domain-based ICIC

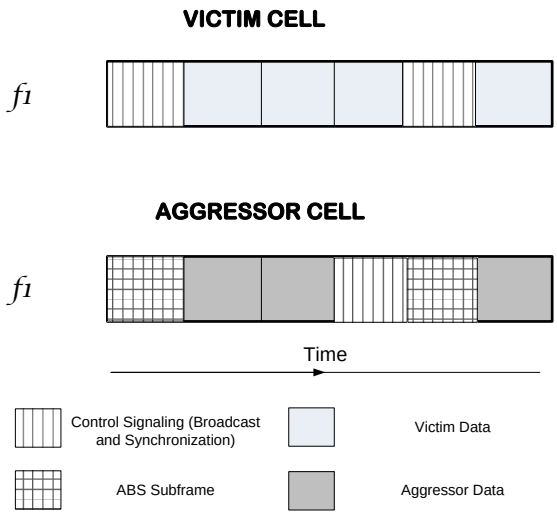

Figure 10. Frame configuration for time domain-based ICIC scheme

schemes assume that perfect cancellation of CRS interference from the received signal at the victim cells. The performance of time domain eICIC schemes when imperfect CRS interference cancellation is analyzed in [92]. A non-ideal reference signal received power (RSRP) measurement-based CRS cancellation scheme is proposed accompanied by the time domain-based eICIC. The results show that imperfect CRS cancellation can still result in user throughput that is comparable to the ideal cancellation case.

The time domain schemes require that the different cell layers exchange the ABS subframe information. This can be enabled using the X2 interface existing between the base stations. In addition, it is also highly desired that time synchronization is achieved, at least at the subframe boundaries between the cell layers.

2.2.2.2 Frequency Domain-based Techniques

Among the frequency domain-based techniques, carrier aggregation with cross-carrier scheduling is widely regarded as a prominent method for performing interference mitigation. The control channel interference on the downlink can be mitigated by partitioning the component carriers in the cell layers into two different sets, one for data and control while the other mainly for data and perhaps also control signaling with power control applied. Figure 11

illustrates such a carrier aggregation-based eICIC scheme. Carrier aggregation is used by both macrocell and small cell layers where both layers enable data communication over $f1$ and $f2$. The macrocell includes the control information only on $f1$ for data transmitted on both $f1$ and $f2$. In a similar manner, the small cell includes the control information only on $f2$. Using this simple mechanism, the control signaling for the different layers are separated. In such a case, the macrocell adopts the carrier $f1$ as the primary carrier while applying power control schemes on carrier $f2$ to minimize interference to the small cell tier. Similarly, the small cell utilizes $f2$ as the primary carrier and applies power control schemes on $f1$. The above scheme, however, has the constraint that the different layers need to be time synchronized.

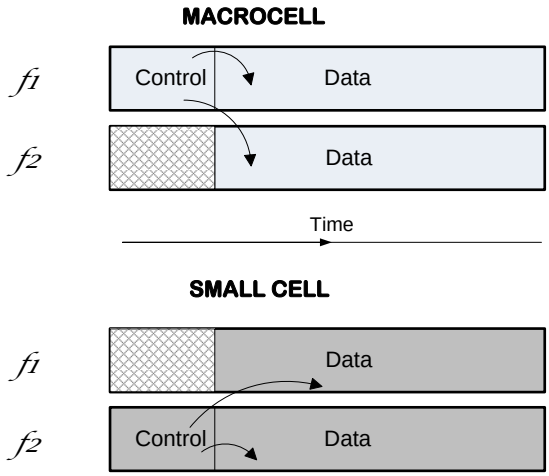

Figure 11. Frame configuration for carrier aggregation-based eICIC scheme

In Rel-11, further support for performing frequency domain-based eICIC was provisioned in the form of enhanced PDCCH (EPDCCH) [93]. One of the key design aspects of the EPDCCH is that it enables each UE to be configured with up to two EPDCCH sets. Each of these sets consist of 2, 4 or 8 physical resource block (PRB) pairs. The locations of these PRBs in the LTE-A frame indicating the EPDCCH are provided with signaling messages with minimum overhead [94]. Such a flexible allocation of EPDCCH control

signaling within the frame enables coordination between different tiers to avoid overlapping EPDCCH and hence the control signal interference.

2.2.2.3 Power Control Techniques

Power control techniques are still part of the eICIC family of schemes. Although they were already proposed for Rel-8/Rel-9 ICIC, several new approaches were introduced explicitely considering the heterogeneous nature of the network. In particular, power control techniques are recommended for the case of femtocell networks [89]. All of the approaches are based in setting the optimal transmit power value but the criteria to select the value may differ since decreasing power to reduce interference also decreases the QoS received at the femtocell users. Examples of criteria for the transmit power at the small cell are the following: (i) proportional to the strongest macrocell interference, (ii) large enough to overcome the pathloss between base station and user, (iii) large enough to satisfy the femtocell users' QoS requirements, or (iv) small enough to let the macrocell users achieve their target QoS.

2.2.2.4 Advanced UE Receivers

Finally, interference can also be handled at the mobile user side via advanced receivers that perform interference cancellation and/or suppression to increase system capacity and user experience [38]. A typical example is an interference canceller at the terminal: It first decodes the strongest interfering signal, performs channel estimation towards that interfering cell, and cancels the interference before actually decoding the signal. This process can be repeated for as many interferers as needed before the signal from the serving cell is decoded.

These types of advanced receivers have been defined in 3GPP in the course of a few releases starting from Rel-10, and were continued through Rel-12 within the HetNet feICIC work item. Furthermore, in Rel-12, there is another on-going study item that focuses on interference cancellation and/or suppression of data and control channels extended with possible network coordination. There are three different categories under this type of feICIC that differ in the knowledge of interferer parameters. They may be applied to deal

with inter-cell, intra-cell, and/or inter-stream interference. Proposed implementations for the receivers include linear filters, maximum likelihood receivers, and interference cancellation receivers [6].

In Chapter 5 of this thesis, we investigate techniques of this category for clustered deployments of picocells.

2.3 Organization of this Thesis

This thesis tackles the problem of interference analysis and mitigation for heterogeneous cellular networks. The two first chapters have dealt with introductory material relevant to the problem at hand: In Chapter 1, the key enabling technologies of future cellular systems are briefly discussed, among which the paradigm of HetNets stands out as a major capacity-increasing technique. Then, Chapter 2 has focused on surveying the state of the art of the problem of interference in HetNets.

The reminder of this thesis presents analysis and solutions to different aspects of the problem under investigation. The subsequent chapters can be divided into two parts. Part I deals with interference in generic HetNets where the type of the small cells deployed in the network may be of different kind. Part II, comprising Chapter 5 through Chapter 7 focuses on providing interference management solutions for specific types of small cells, namely picocells and femtocells. A summary of the contribution of each chapter is provided in the following.

- Chapter 3 introduces new models and their application for the investigation of ICI in HetNets: First, a coverage estimation model is introduced based on the feedback of the users to their serving base stations. Second, a cross-tier correlation study is performed to assess the level of correlation that exists between the tiers of a HetNet due to the ICI. Third, the former model is applied to the problem of cell association in HetNets, providing a new method to set the bias value of small cells affected by ICI.

- Chapter 4 proposes a new architecture design method for generic HetNets where one or several of the base stations in the networks are equipped with a massive MIMO array of antennas. The network operates in TDD mode and the selection of the transmission path in each time slot is performed based on interference-related criterion that tries to minimize the degrading effect of pilot contamination in the network.

- Chapter 5 presents interference suppression techniques for clustered deployments of picocells. In particular, two techniques are proposed and compared: One of them belongs to the category of interference cancellation at the receiver although some level of network assistance is required while the second technique just coordinates the transmission of the picocells in the cluster. The performance of these techniques is analyzed for the whole rate distribution of the network.

- Chapter 6 deals with femtocell deployments. Three aspects are covered: First, an assessment of the performance degradation caused by interference is performed using a high-fidely network simulation platform. Then, two methods for interference management are proposed. The first one proposes spatio-temporal interference estimation for improved resource allocation decisions at the femtocell; the second explores the use of hybrid access in femtocells to reduce interference while guaranteeing the QoS requirements of the users.

- Chapter 7 introduces a novel small cell access point intended to overcome the shortcomings of FAPs, namely the interference and the backhaul problems. Our proposal, known as femtorelay, is a smart combination of femtocells and relays providing open access to users of the network while introducing a relay-based additional backaul connection that eliminates privacy concerns of open access femtocells while increasing the capacity of the access point. This chapter presents a detailed description of the femtorelay architecture as well as the solution to provide seamless integration of femtorelays in standardized networks.

- Chapter 8 presents the conclusions of this PhD thesis.

CHAPTER 3

INTER-CELL INTERFERENCE MODELS, ANALYSIS, AND APPLICATIONS FOR HETEROGENEOUS NETWORKS

3.1 Introduction

In the interference analysis field, most of the work carried out by the research community has been oriented towards finding mathematical models that represent the HetNet architecture, thus allowing the derivation of closed-form expressions for performance metrics in the average sense. However, there is an important lack of analytical models to represent the state and fluctuations of interference in real time. The dynamics of the network should be characterized for a better operation of the network at each time. Furthermore, the inherent cross-tier correlation existing among tiers due to ICI has not been investigated so far.

In this chapter of the thesis, we approach the interference analysis problem in a different way: An analytical framework is presented based on random field theory that estimates and therefore tracks the two-tier coverage, and the cross-tier correlation between the tiers will be investigated. Moreover, we apply this modeling to develop a solution of the cell association problem based on cell-specific bias, as it will be explained later in this chapter. The observation that coverage in both tiers may have some level of correlation in both the spatial and temporal domains due to the existing interference is informally assumed in most previous studies. However, to the best of our knowledge there exists no previous paper explicitly addressing the spatial coverage cross-tier correlation, and accordingly there exists no analytical characterization of this correlation. Since we focus on the spatial dimension in this paper, we make use of spatial statistics techniques to derive analytical expressions for the two-tier coverage maps suitable for a subsequent cross-correlation analysis. In particular, we use random field estimation techniques to generate coverage fields, formalized in terms of downlink SINR fields, using the position and SINR values of the users in the network. A cross-validation is performed across different estimation models seeking for

the best choice. To the best of our knowledge, only our interference management scheme of Section 6.3 has applied this framework to the present two-tier cellular scenario. In addition, we derive an explicit formulation of the spatial coverage cross-tier correlation function depending on the previous model's parameters. Moreover, we present a novel approach for small cell association where the range of the small cells is expanded following the cell biasing approach as proposed in 3GPP [38]. However, our bias value is specific to each small and is set taking into account coverage correlation considerations that can be extracted from our mathematical framework.

The remainder of this chapter is organized as follows. In Section 3.2 we present the two-tier network model based on stochastic geometry utilized for this work. Section 3.3 introduces both the estimation and correlation models: In Section 3.3.1 we develop the estimation of the two-tier SINR fields using random field theory while Section 3.3.2 shows the derivation of the analytical cross-correlation function. Performance evaluation for these two models is carried out in Section 3.3.3. Then, Section 3.4 presents the novel correlation-aware cell-specific bias solution based on the previous estimation model, with simulation results regarding this application shown in 3.4.2. Finally, the conclusions are presented in Section 3.5.

3.2 System Model

We consider a two-tier cellular network consisting of a single macrocell base station (MBS) and multiple small-cell base stations (SBS) deployed within the coverage area of the macrocell, as shown in Fig. 35. The small cells share the properties of co-channel deployment, open subscriber group operation, and lack of coordination. This means that small cells share the same channels both with the macrocell and among themselves, any user assigned by the network can camp on any small cell, and no careful frequency planning has been carried out by the operator in order to minimize interference. Their coverage area will be determined by their transmit power ratio with respect to the MBS, which is assumed to be

the same for all SBSs present in the network.

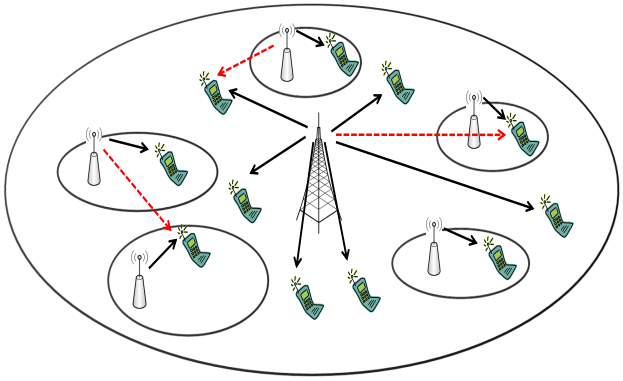

Figure 12. The two-tier considered topology

Fig. 35 also shows the different types of downlink interference present in this co-channel deployment, represented as dotted red lines. Cross-tier interference shows in two ways: MUs receive interference from SBSs, and small cell users (SCUs) receive interference coming from the MBS. In addition, co-tier interference is also modeled as the interference caused by a SBS to an SCU of an adjacent small cell.

Since there is no planning on the locations of the SBSs, these are drawn from a stochastic point process [95]. The model assumes a Poisson Point Process (PPP) Φ_s for the spatial distribution of the base stations with density λ. Similarly, mobile users are also modeled by an independent PPP, Φ_u, with different density, namely β. The location of the users plays an important role in the performance of the estimation framework presented in section 3.3.1, which utilizes the users positions as inputs for the generation of the coverage maps. Further, the employed channel model between the base station and the user accounts for fading and pathloss. The fading effect follows a Rayleigh distribution and hence the channel coefficients are assumed to be drawn from i.i.d. exponential distributions. The pathloss effect is modeled using the standard pathloss function given by $PL = \|d\|^{-\alpha}$, where $\alpha > 2$ corresponds to the pathloss exponent.

The approach that is followed for the attachment of a user to a base station is the maximum SINR criterion: for each user, a set of SINRs is calculated with respect to the base

stations from which signal is being received, and the maximum is selected for attachment. We call $\mathcal{B}$ the set of base stations present in the network serving both macro- and small cell areas. Using the former criterion and the model described above, the resulting SINR S of user u attached to max-SINR base station b can be expressed as follows:

$$S(u,b) = \frac{P^b h_u^b \, \|d(u,b)\|^{-\alpha}}{\sum_{a \in \mathcal{B} \setminus b} P^a h_u^a \, \|d(u,a)\|^{-\alpha} + \sigma^2} \tag{1}$$

where P^b is the transmitted power from base station b, $h_u^b \sim \exp(1)$ is the channel coefficient from base station b to user u, and σ^2 is the constant additive noise power. Figure 13 shows one deployment example generated with this model and the attachment results. In addition to the differences in macro/small cell transmit power, channel effects and interference also contribute to the users not always attaching to the closest base station. In Fig. 13, users being served by a small cell are depicted as such whereas macrocell users are represented as points without any attachment.

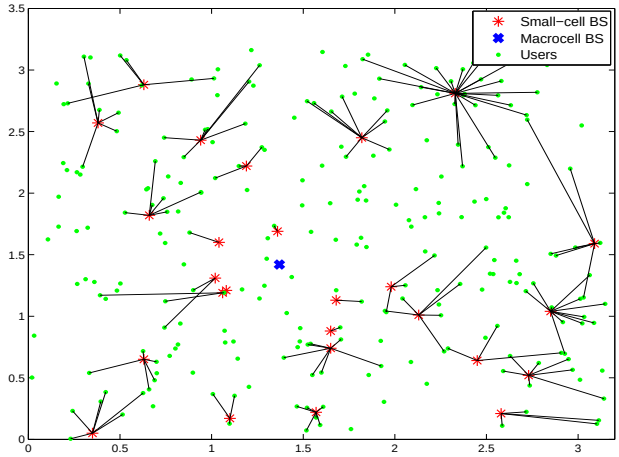

Figure 13. Sample deployment scenario. SBSs and users are distributed as PPPs with densities $\lambda = 2$ and $\beta = 12\lambda$ respectively. Transmit power ratio of macrocell to SBSs is given by $P_{mc} = 100P_{sc}$

3.3 Coverage-based Estimation and Correlation Models

In this section, we present a spatial coverage estimation method for HetNets followed by a cross-tier correlation analysis of the estimated two-tier coverage maps.

3.3.1 Coverage Map Estimation Using Random Fields

Spatial statistics constitute a powerful tool utilized in the solution of a broad spectrum of problems in different fields ranging from sociology or medicine to engineering and technology. A comprehensive literature review of the field can be found in [96] and [97]. The particular field of wireless communications has also made use of different techniques drawn from this field [98], as section 3.2 just showed for the case of point processes. In this section, we focus on the particular subfield of random fields, a set of techniques previously utilized in the wireless network literature for problems such as the characterization of spectrum in dynamic spectrum access systems [99] or the PSD estimation of signal and interference in traditional cellular systems [100]. In most cases, the focus of these works is centered on modeling and learning about the state of a wireless network at runtime. Our objective is to make use of these techniques to derive suitable analytical SINR coverage expressions for cross-correlation analysis of the two tiers.

Originally developed in the field of geostatistics to describe the properties of soil [101], a random field $Z(\mathbf{x})$ is a stochastic process defined over some metric space or region of interest W. It is characterized by its mean and covariance function as Eq. (2) shows.

$$\begin{aligned} \mu(\mathbf{x}) &= E[Z(\mathbf{x})] \\ C(\mathbf{x},\mathbf{y}) &= E[Z(\mathbf{x})Z(\mathbf{y})] - \mu(\mathbf{x})\mu(\mathbf{y}) \end{aligned} \tag{2}$$

The application of this framework had the initial objective of reliably estimating soil properties at locations that cannot be sampled using correlation properties of the field. To characterize the spatial correlation of the collected signals in a given random field, the concept of *semivariogram* was introduced, which is calculated as shown in Eq. (55).

$$\gamma(\mathbf{x},\mathbf{y}) = 0.5 \times E\left[(Z(\mathbf{x}) - Z(\mathbf{y}))^2\right] \tag{3}$$

The semivariogram will only depend on $\mathbf{h} = \mathbf{x} - \mathbf{y}$ if the random process Z is intrinsically stationary. Further, if Z is also isotropic, the semivariogram γ will only depend on the distance between the two points $\|\mathbf{h}\| = \sqrt{(x_1 - y_1)^2 + (x_2 - y_2)^2}$. Hence, our analysis is

confined to planar deployments due to the irregular distribution of users in the vertical domain. Since the definition of semivariogram requires an infinite number of samples, we use the popular *empirical semivariogram* model to perform the estimation, which estimates a semivariogram value for each pair of samples. Equation (4) shows the expression, where $N(\mathbf{h})$ represents the pooled number of pairs separared by lag $\mathbf{h}$, grouped into lag bins.

$$\widehat{\gamma}(\mathbf{h}) = \frac{1}{2N(\mathbf{h})} \sum_{\alpha=1}^{N(\mathbf{h})} [Z(\mathbf{x}_\alpha + \mathbf{h}) - Z(\mathbf{x}_\alpha)]^2 \tag{4}$$

The empirical semivariogram provides only a limited number of points. Hence, for the sake of providing reliable subsequent field estimation, we need semivariogram fitting models. Different parametric models exist, all of which are characterized in terms of three key empirical parameters: (i) *sill*, defined as the maximum spatial correlation level for any two points; (ii) *range*, defined as the lag between two points at which the semivariogram reaches the sill value; and (iii) *nugget*, defined as the semivariogram value for a lag value of zero. The three models considered in this work are the exponential model γ_{exp}, the Gaussian model γ_{gauss}, and the linear model γ_{lin}, given by Eqs (5), (6), and (7), where a represents the range, b the nugget, and c the sill.

$$\gamma_{exp}(\mathbf{h}) = b + c \times (1 - \exp(-3||\mathbf{h}||/a)) \tag{5}$$

$$\gamma_{gauss}(\mathbf{h}) = b + c \times \left(1 - \exp(-3||\mathbf{h}||^2/a)\right) \tag{6}$$

$$\gamma_{lin}(\mathbf{h}) = b + c + a \times ||\mathbf{h}|| \tag{7}$$

In wireless systems, different continuous spatial phenomena can be modeled as random fields. Examples are signal strength, interference power, shadow fading or the coverage metric SINR. In this work, we shall treat the two-tier downlink SINRs, $S^M(\mathbf{x})$ for the macrocell and $S^F(\mathbf{x})$ for the small cell tier, as random fields and assume that a collection of sample measurements will be available provided by the scattered mobile users. In order to obtain the full coverage maps over the region of interest, we need to estimate the values of S^M and S^F at every position $\mathbf{x}_0$ for which a measurement is not directly available.

We select an ordinary Kriging estimator, a linear estimator of great simplicity extensively used in geostatics. Kriging interpolates the values of observations of a random field at unobserved locations. For this purpose, a best linear unbiased estimator (BLUE) is used based on a stochastic model of the spatial dependence quantified by the semivariogram. For a complete discussion and derivation the reader is referred to [96]. In order to obtain the field value in a generic location given by the vector $\mathbf{x}$, the macrocell estimated field $\widehat{S}^M(\mathbf{x})$ can be calculated as follows:

$$\widehat{S}^M(\mathbf{x}) = \sum_{i=1}^{m} \lambda_i^M(\mathbf{x}) S^M(\mathbf{x}_i), \tag{8}$$

where m represents the total number of available measurements, $S^M(\mathbf{x}_i)$ represents the sample field measurements provided by the macrocell users, and the weights $\lambda_i^M(\mathbf{x})$ correspond to the Kriging coefficients of the estimator representing how much amount of the measured field in a particular point will be contained in the estimation. The search for a solution to the BLUE optimization problem yields the following system of equations:

$$\begin{pmatrix} \boldsymbol{\Gamma}^M & \mathbf{1} \\ \mathbf{1}^T & 0 \end{pmatrix} \begin{pmatrix} \boldsymbol{\lambda}^M \\ \mu^M \end{pmatrix} = \begin{pmatrix} \boldsymbol{\gamma}^M(\mathbf{x}) \\ 1 \end{pmatrix}, \tag{9}$$

where $\boldsymbol{\lambda}^M$ is the desired vector of Kriging weights, $\boldsymbol{\gamma}^M(\mathbf{x})$ is a vector of semivariogram values relating the position at which one wishes to estimate ($\mathbf{x}$) to the macrocell users measurements locations ($\mathbf{x}_i^M$). Therefore, $\gamma_i^M(\mathbf{x}) = \gamma(\mathbf{x} - \mathbf{x}_i)$. The parameter μ is a Lagrange multiplier used in the minimization of the estimator variance whose value can be obtained from the above equations. Finally, Γ^M is the matrix of macrocell measurement semivariograms, given by the following expression:

$$\boldsymbol{\Gamma}^M = \begin{pmatrix} \gamma(\mathbf{0}) & \gamma(\mathbf{x}_1^M - \mathbf{x}_2^M) & \dots & \gamma(\mathbf{x}_1^M - \mathbf{x}_m^M) \\ \gamma(\mathbf{x}_2^M - \mathbf{x}_1^M) & \gamma(\mathbf{0}) & \dots & \gamma(\mathbf{x}_2^M - \mathbf{x}_m^M) \\ \vdots & \vdots & \ddots & \vdots \\ \gamma(\mathbf{x}_m^M - \mathbf{x}_1^M) & \gamma(\mathbf{x}_m^M - \mathbf{x}_2^M) & \dots & \gamma(\mathbf{0}) \end{pmatrix} \tag{10}$$

In the above matrix, the vectors $\mathbf{x}_i$ correspond to the positions of the m users providing measurements of the macrocell coverage field. A remark worth noting is the fact that, in general, the nugget value will be zero ($b = 0$) since this parameter is used to account for the variability at distances smaller than the typical sample spacing, including the measurement error. Thus, for the selected semivariogram fitting models in this work, the diagonal of Γ^M will consist of zeros.

Back to Eq. (9), a simplified expression containing the weight vector is given by

$$\boldsymbol{\Gamma}^M \cdot \boldsymbol{\lambda}^M + \mu^M = \boldsymbol{\gamma}^M. \tag{11}$$

Simple manipulation of the above equation yields:

$$\boldsymbol{\lambda}^M = \left(\boldsymbol{\Gamma}^M\right)^{-1} \cdot \boldsymbol{\gamma}_\mu^M, \tag{12}$$

where

$$\boldsymbol{\gamma}_\mu^M(\mathbf{x}) = \begin{pmatrix} \gamma(\mathbf{x} - \mathbf{x}_1^M) \\ \gamma(\mathbf{x} - \mathbf{x}_2^M) \\ \vdots \\ \gamma(\mathbf{x} - \mathbf{x}_m^M) \end{pmatrix} - \mu^M. \tag{13}$$

Equation (12) shows in a compact matrix form an expression for the Kriging weight vectors, which will be obtained according to the selected semivariogram model. Equation (13) contains the semivariogram values of the macrocell users minus the Lagrange multiplier of the Kriging equations.

Similarly, the derivation of the estimated small cell tier field $\widehat{S}^F$ with measurements provided by f mobile users will be performed in an analogous manner. The small cell coverage field $\widehat{S}^F$ is defined as the maximum SINR value that a mobile user could achieve at each point of the region of interest if a small cell were serving it.

We are now in place to give analytical expressions for the coverage fields of the two-tier

network, which are given by Eqs. (14) and (15) in compact matrix form:

$$\begin{aligned}\widehat{S}^M(\mathbf{x}) &= \boldsymbol{\lambda}^M(\mathbf{x}) \cdot \mathbf{s}^M \\ &= \left[\left(\boldsymbol{\Gamma}^M\right)^{-1} \cdot \boldsymbol{\gamma}_\mu^M(\mathbf{x})\right]^T \cdot \mathbf{s}^M \\ &= \boldsymbol{\gamma}_\mu^M(\mathbf{x})^T \cdot \left(\boldsymbol{\Gamma}^M\right)^{-1} \cdot \mathbf{s}^M,\end{aligned} \tag{14}$$

$$\begin{aligned}\widehat{S}^F(\mathbf{x}) &= \boldsymbol{\lambda}^F(\mathbf{x}) \cdot \mathbf{s}^F \\ &= \left[\left(\boldsymbol{\Gamma}^F\right)^{-1} \cdot \boldsymbol{\gamma}_\mu^F(\mathbf{x})\right]^T \cdot \mathbf{s}^F \\ &= \boldsymbol{\gamma}_\mu^F(\mathbf{x})^T \cdot \left(\boldsymbol{\Gamma}^F\right)^{-1} \cdot \mathbf{s}^F.\end{aligned} \tag{15}$$

Here, T represents the transpose operator and $\mathbf{s}^F$ and $\mathbf{s}^M$ represent the macrocell and small cell tiers measurement vectors, respectively. The macrocell case is shown as example in Eq. (16).

$$\mathbf{s}^M = \begin{pmatrix} S(\mathbf{x}_1^M) \\ S(\mathbf{x}_2^M) \\ \vdots \\ S(\mathbf{x}_m^M) \end{pmatrix} \tag{16}$$

As a final remark in this section, it is important to acknowledge the dependence of the model on the density of users per cell since the coverage maps are generated based on users' measurements. This work considers a scenario with a realistic proportion of users to base stations according to the literature and 3GPP, but coverage estimation with this same model for underutilized cells would deserve further study.

3.3.2 Spatial Cross-tier Correlation Function

Equations (14) and (15) provide *continuous* field estimations since they allow the calculation of the field values for any location $\mathbf{x}$ belonging to the region of interest W. Therefore, we can define the cross-tier correlation function as follows:

$$R_{\widehat{S}_M,\widehat{S}_F}(\mathbf{x}) = \int_{W_{ux}} \int_{W_{uy}} \widehat{S}_M(\mathbf{u})\, \widehat{S}_F(\mathbf{u}+\mathbf{x})\, d\mathbf{u}, \tag{17}$$

where W_{u_x} and W_{u_y} represent the region of interest in the two spatial dimensions over which the network is deployed. Utilizing Eqs. (14) and (15) and making some change of notation yields the following expression:

$$\begin{aligned}
&\int_{W_{u_x}} \int_{W_{u_y}} \widehat{S}_M(\mathbf{u})\, \widehat{S}_F(\mathbf{u}+\mathbf{x})\, d\mathbf{u} \\
&= \int_{W_{u_x}} \int_{W_{u_y}} \boldsymbol{\gamma}_\mu^M(\mathbf{u}) \cdot \underbrace{\left(\boldsymbol{\Gamma}^M\right)^{-1} \cdot \mathbf{s}^M}_{\mathbf{b}^M} \\
&\qquad\qquad \cdot \boldsymbol{\gamma}_\mu^F(\mathbf{u}+\mathbf{x}) \cdot \underbrace{\left(\boldsymbol{\Gamma}^F\right)^{-1} \cdot \mathbf{s}^F}_{\mathbf{b}^F} d\mathbf{u} \\
&= \int_{W_{u_x}} \int_{W_{u_y}} \boldsymbol{\gamma}_\mu^M(\mathbf{u}) \cdot \mathbf{b}^M \cdot \boldsymbol{\gamma}_\mu^F(\mathbf{u}+\mathbf{x}) \cdot \mathbf{b}^F d\mathbf{u},
\end{aligned} \tag{18}$$

where the vectors $\mathbf{b^M}$ and $\mathbf{b^F}$ capturing the information of the semivariogram matrix and measurements are introduced for the ease of notation. Further mathematical manipulation yields:

$$\begin{aligned}
&\int_{W_{u_x}} \int_{W_{u_y}} \boldsymbol{\gamma}_\mu^M(\mathbf{u}) \cdot \mathbf{b}^M \cdot \boldsymbol{\gamma}_\mu^F(\mathbf{u}+\mathbf{x}) \cdot \mathbf{b}^F d\mathbf{u} \\
&= \int_{W_{u_x}} \int_{W_{u_y}} \left(\gamma_\mu\left(\mathbf{u}-\mathbf{x}_1^M\right) b_1^M + \ldots + \gamma_\mu\left(\mathbf{u}-\mathbf{x}_m^M\right) b_m^M\right) \\
&\qquad\qquad \cdot \left(\gamma_\mu\left(\mathbf{u}-\mathbf{x}_1^F\right) b_1^F + \ldots + \gamma_\mu\left(\mathbf{u}-\mathbf{x}_f^F\right) b_f^F\right) d\mathbf{u} \\
&= \int_{W_{u_x}} \int_{W_{u_y}} \sum_{i=1}^{mf} \gamma_\mu\left(\mathbf{u}-\mathbf{x}_{f(i)}^M\right) b_{f(i)}^M \gamma_\mu\left(\mathbf{u}-\mathbf{x}_{g(i)}^F\right) b_{g(i)}^F d\mathbf{u},
\end{aligned} \tag{19}$$

where the subindices $f(i)$ and $g(i)$ have been introduced for determining either a specific measurement location or an element of a vector. The functions f and g are defined as follows:

$$\begin{aligned}
f(i) &= \left\lfloor \frac{i}{f} \right\rfloor \\
g(i) &= i \bmod f
\end{aligned} \tag{20}$$

Switching the order of the sum and the integrals allows us to obtain the final cross-tier correlation expression given by Eq. (21) as follows:

$$R_{\widehat{S}^M,\widehat{S}^F}(\mathbf{x}) = \sum_{i=1}^{mf} b_{f(i)}^M b_{g(i)}^F K_i(\mathbf{x}), \tag{21}$$

where the correlation terms $K_i(\mathbf{x})$ are calculated according to the following expression:

$$K_i(\mathbf{x}) = \int_{W_{u_x}} \int_{W_{u_y}} \gamma_\mu^M \left(\mathbf{u} - \mathbf{x}_{f(i)}^M\right) \gamma_\mu^F \left(\mathbf{u} + \mathbf{x} - \mathbf{x}_{g(i)}^F\right) d\mathbf{u}. \tag{22}$$

3.3.3 Performance Evaluation

In this section, we show numerical results and performance evaluation with the target of illustrating the correlation analysis of the previous sections. The objective is to validate the analytical equations for a two-tier network consisting of a macrocell underlaid by a tier of open access small cells that use the same transmit power. The employed methodology can be summarized as follows: Following the system model described in Section 3.2, we simulate two networks with the parameters given by Table 7. Network 1 is a simplified case with a reduced number of small cell base stations where the channel effects are limited to the pathloss due to distance. Network 2 is a more realistic case containing numerous base stations and the channel model presented in Section 3.2. The simulated scenario is used to obtain the SINR values of the mobile users in the network and their base station attachment. With those values at hand, we show and analyze in section 3.3.3.1 the complete two-tier SINR field estimations obtained according to Eqs. (14) and (15). In section 3.3.3.2 we perform a cross-validation of the three semivariogram models presented in Section 3.3.1 to determine which of them performs the best estimation. Finally, Section 3.3.3.3 shows the novel cross-tier correlation functions of Network 1 and Network 2 obtained by evaluating the derived expressions (21) and (22).

3.3.3.1 Coverage Fields Generation

The estimations of the macrocell and small cell coverage fields are depicted in Fig. 14 and Fig. 15 for Networks 1 and 2, respectively. Both of them have used the exponential semivariogram model for their generation. In the case of Network 1, the structure of the SINR fields is very *clean* since the only present channel effect is the pathloss, and hence no randomness affects the estimation. As expected, the macrocell SINR field exhibits a

Table 1. Network Simulation Parameters

Parameter	Network 1	Network 2
Macrocell area (km)	5	10
Number of MBSs	1	1
SBSs density (λ)	1	2
Mobile user density (β)	10	24
Power ratio (S/F)	100	100
Pathloss exponent	3	3
Channel exponential mean	-	1
Attachment criterion	max-SINR	max-SINR

maximum at the location of the MBS. The quality of the field goes down with the distance to the base station due to the pathloss effect and the interference coming from the three small cells present in the network. Minima of the SINR field are precisely met at the location of these SBSs. Reciprocally, the small cell tier exhibits also an expected structure, with maxima located at the SBS locations and a minimum at the location of the MBS. Thus, a clear cross-correlation exists between the two fields.

The case of Network 2 is illustrated in Fig. 15. Here, we observe fields of a less smooth structure. The randomness of the Rayleigh fading channel and the more complex nature of the network are responsible for it. However, since our final objective is to determine and characterize a possible cross-correlation between the fields, we do observe reciprocal behavior in the two-tier field despite the channel. Maxima and minima are still located at the positions of the base stations, while the type of base station depends on whether it corresponds to the macrocell or small cell tier. Thus, a characterization of the cross-correlation is still meaningful, as it will be shown in section 3.3.3.3.

3.3.3.2 Semivariogram Model Cross-Validation

We now explore the different semivariogram fitting models introduced in section 3.3.1. The three cases that will be analyzed correspond to the exponential, Gaussian, and linear models employed for the best possible fitting of user measurements to an analytical semivariogram function. The method that we follow is a cross-validation of the estimation

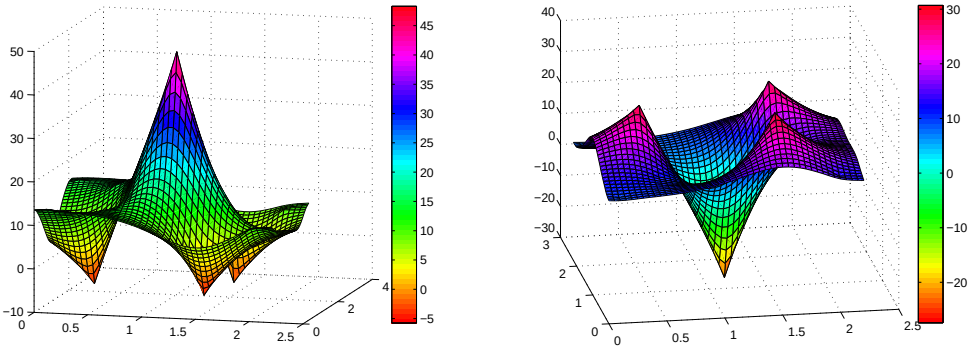

(a) Macrocell SINR field (b) small cell SINR field

Figure 14. Two-tier coverage field estimation with exponential semivariogram model for Network 1

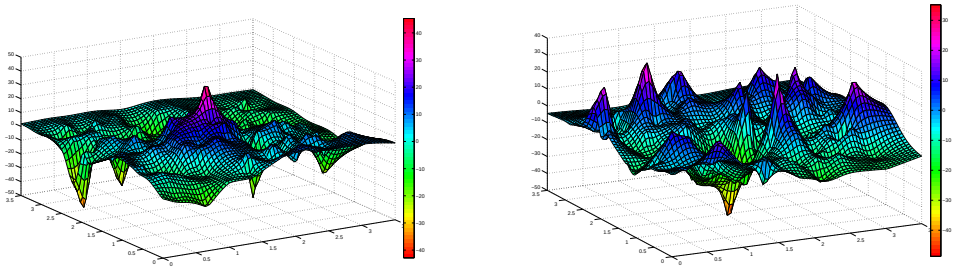

(a) Macrocell SINR field (b) small cell SINR field

Figure 15. Two-tier coverage field estimation with exponential semivariogram model for Network 2

results for the case of Network 2, where a larger pool of measurements is available. An estimation is performed at each location for which a measurement is available, and the error of the estimation is obtained by subtracting the estimated value from the real value. This method is repeated for the three models. Furthermore, two error metrics are shown: The complete cross-validation error distribution where all the estimation errors for both fields are captured, and the mean squared error (MSE) given by

$$E = \frac{\sum_i^N \left(\widehat{Z}(i) - Z(i)\right)^2}{N}, \tag{23}$$

where N is the total number of measurements.

The results of the cross-validation experiment are shown in Fig. 16. In all cases, the distribution of the cross-validation error has a shape resembling a Gaussian distribution

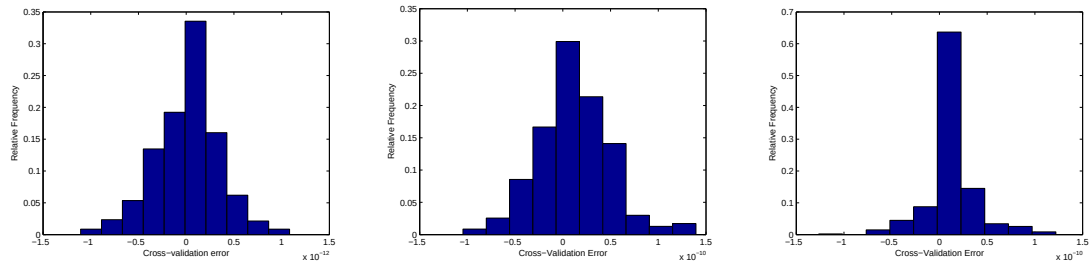

(a) Exponential: $E = 1.23 \cdot 10^{-25}$ (b) Gaussian: $E = 1.48 \cdot 10^{-21}$ (c) Linear: $E = 6.49 \cdot 10^{-22}$

Figure 16. Cross-validation error distribution of the two-tier field estimation.

centered around an error of zero. Furthermore, all three models exhibit an acceptable estimation MSE, with the exponential model being the one that more accurately estimates the coverage values. Therefore, the exponential semivariogram model is the most suitable for reconstructing the coverage fields in a two-tier cellular network.

3.3.3.3 Cross-correlation Function

This section shows the numerical results obtained by implementing the analytical expression for the cross-correlation function obtained in section 3.3.2. Again, the cases of both Network 1 and 2 are illustrated. A two-dimensional grid is generated for the calculation of the cross-correlation function. Additionally, the raw results obtained with Eq. (21) for every grid position are informative only when compared to each other in a relative fashion. Therefore, it makes sense to further normalize them to obtain a metric similar to a cross-correlation coefficient with values between -1 and +1. However, as opposed to a cross-correlation coefficient, a value of +1 would not mean that the fields are identical but their correlation would be just maximum. The normalizing operation is given by

$$\mathbf{R}_{norm} = 2 \times \frac{\mathbf{R} - R_{min}}{R_{max} - R_{min}} - 1, \tag{24}$$

where R_{min} and R_{R_max} correspond to the minimum and maximum values of the analytical cross-correlation function.

Figure 17 shows the cross-correlation results. The cross-tier correlation function of both networks exhibits a similar structure. A minimum is obtained exactly at the position $(0, 0)$,

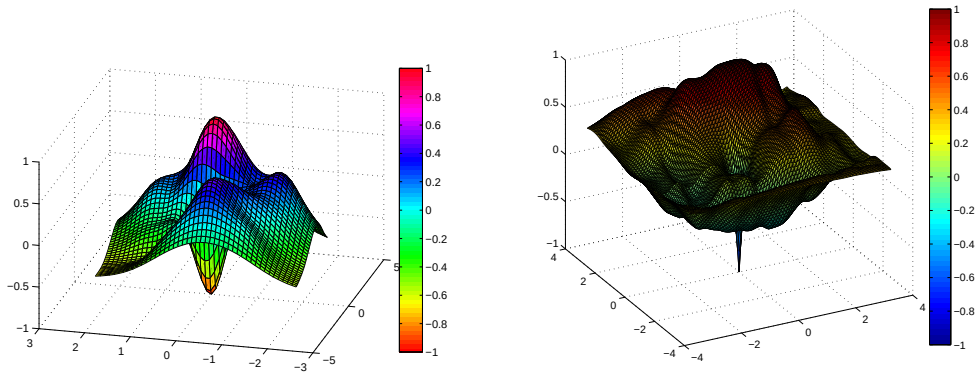

(a) Network 1 (b) Network 2

Figure 17. Analytical cross-tier correlation results

a meaningful remark since it is precisely when the two unshifted fields overlap, causing minima and maxima to coincide in space and largely contribute to the cross-correlation value. Thus, it is in this location that the integral in (17) should yield a result of highest absolute value. However, the two-tier fields can be considered as *phase shifted* 180° since maxima in one field are mapped to minima in the reciprocal field. Hence the value -1.

The cross-correlation function provides also some information regarding the location of the small cells within the network. No phase shift exists in this case between the two fields since the maximum corresponding to the MBS in the macrocell field is matched with the maxima corresponding to the SBS in the small cell tier. In the case of Network 1, the function is smoother due to the simplified architecture of the network and three maxima can be detected, corresponding to the three small cells existing in the network. The complexity of Network 2 does not allow to differentiate the locations of the small cells but it does convey an idea of the density of SBSs contained in a certain area.

Beyond the intuitive meaningfulness of the results, we further validate the cross-correlation model by obtaining a normalized spatial cross-correlation coefficient of the two fields with the built-in function of MATLAB *normxcorr2*. We compare these results with the analytical ones shown above. The graphs are omitted from the manuscript due to lack of space

but MSEs in the order of 10^{-8} and 10^{-6} for Network 1 and Network 2 respectively suggest an analytical model accurate enough for the representation of the cross-tier correlation function.

These results validate the intuitive idea of coverage correlation between tiers due to interference. Hence, understanding the level of this correlation in the spatial dimension is very useful knowledge that can be applied in the design of practical solution for tiered networks, as it will be shown in future chapters of this thesis.

3.4 Application to the Cell Association Problem

In addition to interference, cell association is another important challenge for HetNets. Deciding which users should be attached to which base station is a trivial problem in the case of homogeneous networks: The SINR is maximized and the base station providing the highest SINR is always selected. However, this approach in the case of HetNets leads to a high underutilization of the small cells since very few users would be attached to them. To solve this problem and increase the capacity gains of small cells, the current agreed solution is to expand the range of the small cells by introducing a so-called bias factor [36]. However, this increases the interference on the user, thus coupling the ICI and cell association problems [102]. In this section, we present one application of how two-tier coverage correlation can be used to solve the problem of cell association for HetNets.

3.4.1 Correlation-aware Cell-specific Bias for Range Expansion

As explained above, a bias factor is utilized to expand the range of small cells. This factor, applied at the receiver of the users, acts as a positive offset in dB added to the actual received power from the SBS that makes the user believe the received power is higher and so that it performs the handover at an earlier point. As a consequence, it allows more users to be associated with the small cell. In linear scale, the factor is a multiplicative term modifying the actual received power from the small cell base station, as Eq. (25) shows [37].

$$P_{r,j} = P_j L_0 \left(R_j / r_0\right)^{-\alpha_j} B_j \tag{25}$$

Here, $P_{r,j}$ is the received power from the a base station in tier j, P_j is the common transmit power of base stations in tier j, L_0 is the path loss at a reference distance r_0 where $-\alpha_j$ is a per-tier path loss exponent, R_j is the distance to the nearest base station in tier j, and B_j is an identical bias factor for each tier j. Without modifying the transmit power, that adjustment makes the user believe the received power is higher than what it actually is. Hence, it performs the handover at an earlier point, allowing more users to be associated with the small cell. Figure 18 shows the concept of cell biasing for a picocell network.

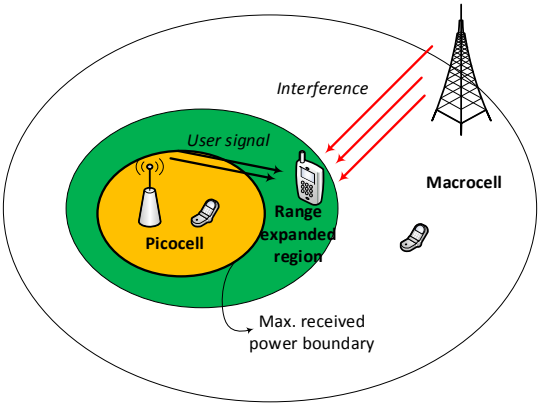

Figure 18. Biased picocell coverage.

Several problems arise in this scenario: First, interference is incurred in the users as they will hand over to the small cell when they are still receiving strong signal from the macrocell. Second, setting a universal bias factor for all the small cells in the network is a very rigid approach that may undermine performance since not all the coverage regions of the different small cells have the same features, even when their transmit powers are the same. For this reason, we introduce a correlation-aware cell-specific bias solution where the cross-tier correlation of the fields is exploited to provide a suitable cell bias value for each small cell.

The approach can be summarized as follows: *The cell-specific bias will approximately keep its universal value when the respective increase and decrease of coverage in each of the two network tiers moving away from the small cell are correlated, i.e., when one is*

cause of the other. Otherwise its value will be modified in such a way that steep falls in the coverage of a small cell when moving away from its base station without a correlated increasing field of the surrounding macrocell will decrease the value of the bias factor. Similarly, steep falls in the macrocell coverage when approaching a SBS that does not present a correlated small cell field will increase the bias value. By doing this, the bias will adapt to the dual behavior of both fields: It will increase its value when there is gain in further extending small cell coverage, and it will decrease when the universal bias value is already causing losses. This adaptation can be also very useful to optimize the cell association when the two strongest powers come from two small cells, but that problem is now left as future work.

To implement the above scheme, the coverage maps need to be generated in order to obtain relevant information regarding the fields. Then, the cell-specific bias value should be calculated. A simple implementation of the above principle for the derivation of the cell-specific bias is

$$B_i = B_{un} \cdot \frac{\delta}{\frac{|\widehat{m}_{F_i}|}{|\widehat{m}_M|}} = B_{un} \cdot \frac{\delta|\widehat{m}_M|}{|\widehat{m}_{F_i}|} \tag{26}$$

where B_i is the cell bias of small cell i, B_{un} is the universal bias value, and both m_{F_i} and $\widehat{m}_M$ are estimations of the steepness of the fields around small cell i. These values can be estimated in different ways. In Section 3.4.2 we show one particularly simple method using the coverage maps derived in Section 3.3.1. Finally, δ is a system parameter that adjusts the ratio to make it close to one for the highest correlated case where the universal bias value is a wise design choice.

It is worthwhile to include a remark on the low implementation costs of this approach. Small cell base stations just need to collect SINR values of their users -which they do already- while some signalling exchange between the two tiers would be carried out regarding the macrocell coverage map around the small cell area. This communication could take place over a wired or over-the-air (OTA) backhaul connection. However, other implementations of correlation-aware cell-specific bias can also be easily designed.

3.4.2 Performance Evaluation

To evaluate the performance of the cell-specific bias approach we simulate user rates and per-cell throughput values for a network without bias, with several universal bias values, and with cell-specific bias. For the latter case, the steepness of the fields $\widehat{m}_M$ and $\widehat{m}_{F_i}$ is estimated by averaging the spatial slope of the coverage maps in the four main spatial directions (north, east, south, west) when going away from the small cell base station. For this experiment, the average is performed over the coverage radius of a bias-free small cell. Furthermore, the experiment dismisses users with too low rates that are considered in outage. The boundary is given by the 80% of the lowest rate in a bias-free scenario.

Figure 19 shows the cumulative density functions (CDF) of user rates and per-cell throughput for the case of Network 2. The considered universal bias values are 10%, 15%, and 20% of the average received power across the network, and the reference B_{un} value for the cell specific case is 15%. When the rates of all users are shown, the bias-free case shows the best results because the few users in the small cells will experience a high SINR. The larger the bias, the worse the geometry of the small cell. Cell-specific bias performs better than its reference value and all other larger bias values. However, when the cell throughput is considered, i.e., all the user rates per small cell are aggregated, the cell-specific bias solution performs the best. These results show that depending on the characteristics of the coverage map, a universal bias value may be too large for some small cells and too small for some others. In the former case, the geometry of the cell is hurt, i.e., users attached to it suffer from low SINR and subsequent low data rates. In the latter case, there is a loss of capacity since more users could be supported. Thus, both cases show a degradation of their throughputs when the bias values are not correctly chosen. On the other hand, a cell-specific bias is capable of providing each cell with an appropriate tradeoff value that allows it to increase the number of supported users and the overall throughput.

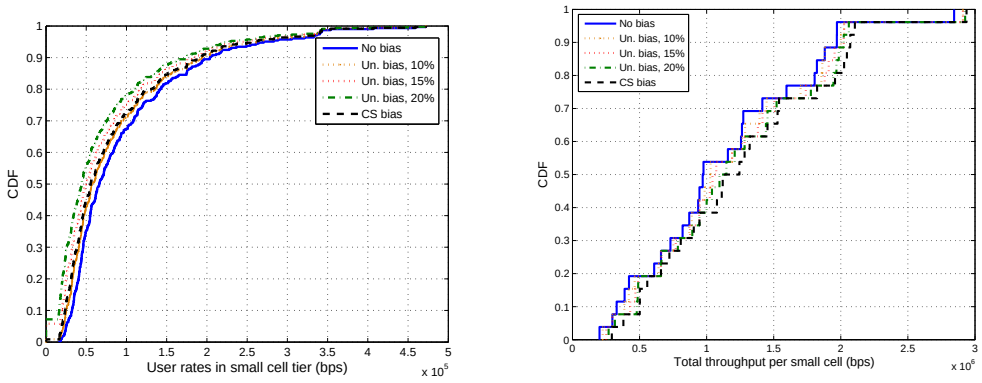

(a) Rates (b) Throughput

Figure 19. Cell-specific bias results

3.5 Conclusions

Inter-cell interference stands out as major performance degrading effects in HetNets. In this chapter, we have addressed the fundamental issue of the spatial coverage cross-tier correlation between the macrocell and the small cell tiers in the presence of interference by introducing a new mathematical framework. First, we derived analytical expressions for the estimated two-tier coverage fields using techniques from the random field theory. We utilized different estimation models and cross-validated them for an assessment of their suitability for the task at hand. Stemming from these expressions, we derived a novel closed-form expression for the cross-tier correlation function exclusively dependent on the estimator's parameters. Results have shown the suitability of the model for the estimation of the fields and their correlation as well as the potential of using cross-correlation to efficiently solve practical problems of HetNets.

CHAPTER 4

INTERFERENCE AVOIDANCE FOR MASSIVE MIMO-ENABLED TIME-DIVISION DUPLEX HETEROGENEOUS NETWORKS

4.1 Introduction

In this chapter, we present a novel architecture design for time-division duplex (TDD) HetNets suitable for massive MIMO systems that minimizes the the pilot contamination effect of the system. The pilot contamination effect and the most relevant literature on the topic were presented in Section 2.2.1. None of the papers referenced in that section dealing with pilot contamination considers the case of a HetNet scenario. However, the particularities of a HetNet architecture can have a great impact in the design of the best strategy to cope with pilot contamination.

The concept of massive MIMO was introduced in Section 1.3 since it has been indeed identified as a key technology for future 5G systems. One particularly important feature of massive MIMO cellular systems is the need for an underlying TDD architecture. It is well known that the exploitation of MIMO communication requires full channel knowledge at knowledge at the transmitter [103]. Although some research has been carried out investigating the applicability of frequency-division duplex (FDD) in massive MIMO systems [104], [105], [106], it is generally accepted that this approach would require an unaffordable overhead in terms of pilots to estimate the large amount of channels [24]. Unlike FDD systems where the uplink and downlink transmissions take place over different frequencies, TDD benefits from channel reciprocity because the same frequencies are used for both transmission paths. This means that in TDD systems both the uplink and downlink channels can be estimated directly at the base station by using just uplink pilots, thus avoiding both the forward link and feedback overhead required by FDD systems.

It is important for this work to review the currently proposed TDD architectures since

the smart design of such an architecture will be the method employed in this paper to eliminate the pilot contamination effect. 3GPP defines the TDD version of LTE systems, known as TD-LTE, with an architecture consisting of a radio frame divided in subframes where each subframe can be configured in uplink (U) or downlink (D) mode [107]. The reference signals or pilots (P) are transmitted both for the uplink and downlink directions in particularly designated subframes shared for the two transmission paths. The configuration is static and equal for all cells of the network. Table 2 shows the possible standard configurations of TD-LTE systems.

Table 2. TD-LTE Configurations

Configuration	Periodicity	Subframe Number									
		0	**1**	**2**	**3**	**4**	**5**	**6**	**7**	**8**	**9**
0	5 ms	D	P	U	U	U	D	P	U	U	U
1	5 ms	D	P	U	U	D	D	P	U	U	D
2	5 ms	D	P	U	D	D	D	P	U	D	D
3	10 ms	D	P	U	U	U	D	P	D	D	D
4	10 ms	D	P	U	U	D	D	P	D	D	D
5	10 ms	D	P	U	D	D	D	P	D	D	D
6	5 ms	D	P	U	U	U	D	P	U	U	D

However, current work within LTE-A Rel-12 suggests the adaptive configuration of the transmission path for each subframe to match load requirements more precisely. This feature is known as enhanced International Mobile Telecommunications Advanced (eIMTA) [6]. Furthermore, some recent work in the literature explores a TDD architecture for massive MIMO HetNets where the regular TDD mode can be replaced by the reverse TDD mode, hence letting downlink and uplink communication in different cells coexist in time [108], [109]. However, pilot contamination effect is completely ignored in the analysis.

The motivation for this work lies in the need to provide an architectural framework optimized for the coexistence of HetNets and massive MIMO. The significance of this problem is very high since both of the former technologies will constitute key elements of future 5G systems. The contributions of this paper can be summarized as follows:

- *Novel TDD HetNet Architecture:* A novel architecture for massive MIMO-enabled

HetNets is proposed where the characteristics of TDD systems are exploited to mitigate the pilot contamination effect. In particular, the configuration of each time slot of each cell belonging to each network tier will be selected in such a way that the interference caused in the system is minimized. Four configurations for each time slot will be possible: Downlink (D), uplink (U), downlink pilot (P_D), and uplink pilot (P_U). However, certain constraints will need to be satisfied within the radio frame of each cell.

- *Interference Analysis of Novel Architecture:* The interference pattern of the proposed architecture is analyzed in depth. In particular, two fundamental interference regimes are defined where pilot contamination will or will not be present. Whether a certain cell is operating in one or another regime depends on the design of the TDD architecture, since only certain configurations will cause pilot contamination to appear. Furthermore, the optimal basic TDD configuration for one serving cell and one interfering cell is investigated based on interference criteria, and further considerations based on the reciprocity of interference, the transmit power, and the interferer's mode of operation are also included in our analysis.

- *Problem Formulation and Solution Strategies for the TDD HetNet Grid:* The TDD HetNet grid represents the set of multi-tier cells whose TDD configuration must be chosen on a per-time-slot basis. Thus, the problem of selecting the optimal TDD configuration is mathematically formulated using the above interference-based criteria and the framework of a grid. Since its integer combinatorial nature makes it very hard to solve it analytically, we propose two different strategies that can be used as guidelines to develop efficient algorithmic solutions to the TDD HetNet Grid problem.

The remainder of this chapter is organized as follows. In Section 4.2 we present the system model for this paper covering the signal model and the basics of a generic TDD

architecture. Section 4.3 introduces our novel TDD HetNet architecture and the problem of its design. The interference analysis of such an architecture is shown in Section 4.4, while the formal TDD HetNet grid problem and the proposed strategies for its solution are covered in Section 4.5. Performance evaluation is carried out within those same sections. Finally, conclusions as well as directions for future work are pointed out in Section 4.7.

4.2 System Model

This section introduces the system model for this paper. In particular, we describe how the signal and frame transmission is represented, and the model for a TDD HetNet architecture.

4.2.1 Signal and Frame Model

It is assumed that all cells of all tiers utilize OFDM. The channel model for each subcarrier is flat-fading where the small-scale fading vector $\mathbf{h}_i^j$ from network element i to network element j is independent across users and base stations and follows the complex gaussian distribution given by $\mathbb{C}\mathcal{N}(\mathbf{0}, \mathbf{I})$. The estimated channel vector is denoted as $\widehat{\mathbf{h}}_i^j$. If the channel is MIMO, we represent it with a matrix $\mathbf{H}$. The pathloss effect is modeled using the standard pathloss function given by $\alpha_i^j = \|d(i, j)\|^{-\alpha_e}$, where $d(i, j)$ is the distance between network elements i and j, and $\alpha_e > 2$ corresponds to the pathloss exponent. We further assume a block fading model both in time and frequency: First, the channel vectors $\mathbf{h}_{ij}$ remain constant during cherence blocks of N time slots, and the channel vectors in different time slots are assumed to be independent. The pathloss, however, is assumed to remain constant since it changes much more slowlier. Second, the channel vectors remain also constant across a certain number of subcarriers. In this work, it is enough to assume that the number of pilots in each cell will be suited to the channel coherence badnwidth. Channel reciprocity is assumed for both multipath fading and pathloss.

The pilot-based channel estimation is key in this work. Using channel reciprocity and the N-coherence-block assumption, we safely further assume that pilots will be sent in each cell once every N time slots and just over one transmission path, being this either downlink

or uplink. If the base station managing the cell is equipped with massive MIMO, the pilots can only be sent in the uplink; otherwise the cell has freedom to choose it. As we will show, this design decision has an impact on interference performance. The number of time slots dedicated to uplink (n_U) and downlink (n_D) communication will be assumed to be equal in all cells.

Regarding the pilots, we assume that a set of K time-frequency orthogonal pilots exists for each cell regardless of its tier. This means that the maximum number of supported users for each cell without pilot contamination within the same cell is also K. A different pilot signal Ψ_i is used in the communication with each user i of one cell, and the received signal is multiplied by a reciprocal signal Ψ'_i such that Eq. (27) holds.

$$\begin{aligned} \Psi'_i \cdot \Psi_i &= 1 \quad \forall i \\ \Psi'_i \cdot \Psi_j &= 0 \quad \forall i \neq j \end{aligned} \tag{27}$$

It is assumed that regardless of the transmission path that is chosen to transmit the pilots, a single pilot signal will be allocated for the channel estimation phase of the communication of a base station with each of its served users. Furthermore, the value of K is assumed large enough to serve all MUs under the MBS; hence, base stations in lower tiers are assumed to have enough pilots to serve their users. No coordinating mechanism among base stations is assumed, thus pilots from different base stations at each tier may be subject to contaminate each other.

In this work, base stations will use the multiple number of antennas to perform beamforming in the downlink. The precoding vector is obtained by calculating the normalized version of the estimated channel, as Eq. (28) shows:

$$\mathbf{w} = \frac{\widehat{\mathbf{h}}}{\|\widehat{\mathbf{h}}\|} \tag{28}$$

Similarly, the multiple antennas are exploited at the receiver of the base station by decoding the signal using Maximal Ratio Combining (MRC) as Eq. (29) shows, where $\mathbf{y}_b$ is the

received signal at base station b.

$$\widehat{q} = \widehat{\mathbf{h}} \cdot \mathbf{y}_b \tag{29}$$

The total number of base stations in the network is known as B. Furthermore, we denote by K_b the number of users associated to base station b. For data transmission, we denote by q_k the symbol sent by user k in the uplink, and by s_k^b the symbol sent by base station b to user k in the downlink.

4.2.2 HetNet Topology

The HetNet topology considered in this work is depicted in Fig. 20. A three-tier network is considered consisting of a macrocell tier (MT), a picocell tier (PT), and a femtocell tier (FT), all of them deployed using a universal frequency resue approach. The MT has only one MBS while picocell base stations (PBSs) and femtocell base stations (FBSs) are distributed following the usual PPP distribution widely used in the literature to model HetNet topologies [95]. We denote the PBS and FBS densities as λ_P and λ_F, respectively. Similarly, the users are also distributed following one single PPP distribution across the network, thus spanning the three tiers. We denote its density by λ_U.

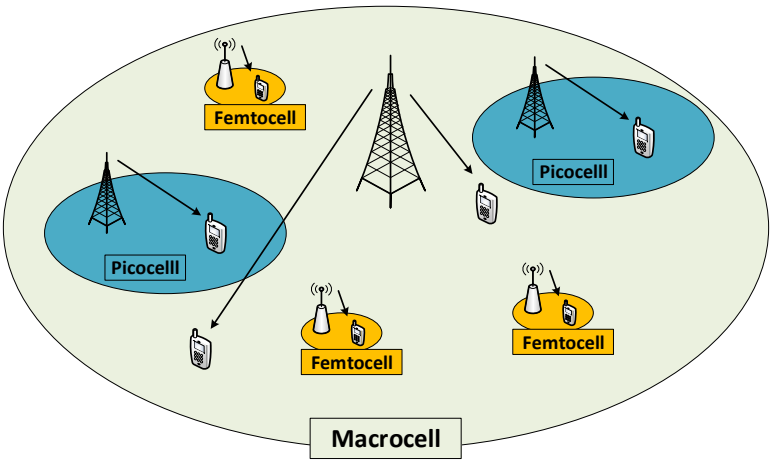

Figure 20. Considered HetNet topology

In this work, each tier is characterized by two power values, namely the transmit power of the base stations belonging to one tier (assumed constant and equal among base stations

of the same tier), and the *average* transmit power of a user in each tier. The former parameter is denoted as S_M, S_P, and S_F for the MT, PT, and FT, respectively. The latter parameter is also assumed different for each tier and directly proportional to the average distance to the serving base station in each tier. The assumption is reasonable since users closer to their serving base station should employ less amount of power in the downlink. The average power values for the MT, PT, and FT are denoted as S_{U_M}, S_{U_P}, and S_{U_F}, respectively.

4.3 Novel TDD HetNet Architecture

In this section, we present a novel TDD architecture for massive MIMO-enabled HetNets. The goal of our proposed architecture design is to mitigate the overall interference of the network. As mentioned in Section 2.2.1, the most critical factor in massive MIMO systems is the pilot contamination effect; hence, our design is targeted at minimizing pilot contamination effect and overall interference.

The proposed architecture makes use of a frame structure coarsely related to that of a radio frame in TD-LTE systems. Each frame consists of N time slots, each of which is configured in one of the following modes of operation:

- Downlink Pilot (P_D), for reference signals transmitted in the downlink.
- Uplink Pilot (P_U), for reference signals transmitted in the uplink.
- Downlink (D), for downlink data transmission.
- Uplink (U), for uplink data transmission.

Each TDD frame is assumed to last less than the channel coherence time, hence only one time slot out of N needs to transport pilot signals for each cell. Furthermore, cells where the base station is massive MIMO-enabled can only transport pilots using P_U mode. Each base station in the network may have a different configuration for its TDD frame although the number of downlink and uplink time slots must be the same across cells. In

this paper we further consider such configuration to be static during the network operation time, i.e., it does not change for each TDD frame.

The objective of this work is to provide insight on the optimal design for such a TDD HetNet architecture. The most important elements of the design that need to be figured out are the following: (i) the position of the pilots within the TDD frame, (ii) the transmission path over which the pilots will be sent, and (iii) the selection of *D* or *U* modes of operation for the data transmission time slots. The extent to which these three design elements are related among themselves and represent a crucial factor for the gravity of the pilot contamination effect will become apparent during the interfere analysis of Section 4.4. In addition, the freedom to select the *D* and *U* time slots independently in each cell introduces a *generalized* TDD version of the regular and reverse TDD modes [108]. This creates interference patterns that can be classified as base-station-to-user (B2U), base-station-to-base-station (B2B), user-to-base-station (U2B), and user-to-user (U2U). Although these modes are independent of the pilot contamination effect, they will greatly impact the overall interference performance of the system and must be therefore taken into account when providing a TDD design solution.

Figure 21 shows the architecture design problem depicted as a grid where the rows represent the cells and the columns represent the time slots. In the particular example of Fig. 21, three base stations are depicted, each of them belonging to one network tier. Each of them is characterized by two power values as explained in Section 4.2. The problem is thus to fill out the TDD grid minimizing the interference of the system.

4.4 Interference Analysis

In this section, we perform an interference analysis of a TDD HetNet whose architecture has to be designed according to the principles specified in Section 4.3. In particular, we investigate how to fill out the TDD grid in Fig. 21 when one or several of the base stations in the system are equipped with a very large number of antennas. This requires us to

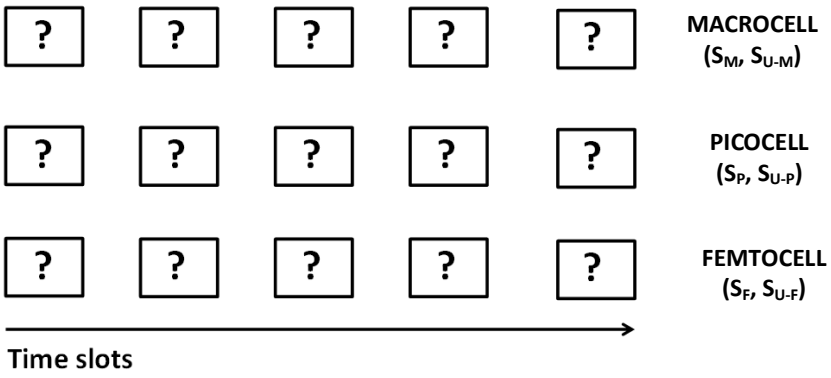

Figure 21. The HetNet TDD grid

pay special attention to the pilot contamination effect introduced in Section 4.1 and to the interference source, which can be both users and base stations, thus impacting the received interference power.

Here, we provide expressions for the received signal at each of the four possible modes of operation described in Section 4.3. In the uplink, we assume that the transmission from different users is performed on the same resources. In the downlink, however, we assume an OFDMA scheduler allocates resources in orthogonal subcarriers to the different users. We distinguish between training phase (i.e., time slots during which the channel estimation is performed) and data transmission phase, which encompass both U and D modes of operation.

We call $\mathbf{r}$ the received signal coming within the serving cell, free of ICI. During the training phase, the received signal at base station b_i if P_U mode is used is given by Eq. (30) while the received signal at user k_i if P_D mode is used is given by Eq. (31) as follows:

$$\mathbf{r}_{b_i}^{P_U} = \sum_{k=1}^{K_{b_i}} \alpha_k^{b_i} S_{U_{T(b_i)}} \mathbf{h}_k^{b_i} \Psi_k, \tag{30}$$

$$\mathbf{r}_{k_i}^{P_D} = \alpha_{k_i}^{b_i} S_{T(b_i)} \bar{\mathbf{h}}_{k_i}^{b_i} \cdot \mathbf{\Psi}_{k_i}, \tag{31}$$

where it has been assumed that b_i is the serving cell of user k_i during P_D mode, and $T(b_i)$ represents the network tier of base station b_i, i.e., MT, PT, or FT. During the data transmission phases, the received signals in the uplink and downlink are given by Eqs. (32) and

(33), respectively:

$$\mathbf{r}_{b_i}^{U} = \sum_{k=1}^{K_{b_i}} \alpha_k^{b_i} S_{U_{T(b_i)}} \mathbf{h}_k^{b_i} q_k, \tag{32}$$

$$\mathbf{r}_{k_i}^{D} = \alpha_{k_i}^{b_i} S_{T(b_i)} \bar{\mathbf{h}}_{k_i}^{b_i} \cdot \mathbf{w}_{k_i}^{b_i} s_{k_i}^{b_i}, \tag{33}$$

where the precoding weights of the downlink transmission are obtained using Eq. (28).

We now introduce ICI to the above expressions. Since each cell may have a different TDD configuration, it is possible for each time slot to receive interference in any of the four modes of operation: P_U, P_D, U, or D. For convenience, we define the binary matrix $\mathbf{\Gamma}$ of size $b \times 4$ per time slot, where an entry of 1 per row indicates which of the four modes of operation is used in each base station. We denote by γ_{ij} the element in row i and column j of matrix $\mathbf{\Gamma}$. With that in mind, we define the interference metric I_x, where the x may stand for b_i or k_i depending on whether the interference is received at a base station or a user. In Eq. (34), the channel $\mathbf{h}$ may be a vector if $x = b_i$ or a scalar in case $x = k_i$. Similarly, $\mathbf{H}$ will be a matrix if $x = b_i$ or a vector if $x = k_i$.

$$\begin{aligned} I_x =& I_x^{P_U} + I_x^{P_D} + I_x^{U} + I_x^{D} \\ =& \underbrace{\sum_{\substack{b=1 \\ b \neq b_i}}^{B} \gamma_{b1} \sum_{k=1}^{K_b} \alpha_k^x S_{U_{T(b)}} \mathbf{h}_k^b \Psi_k}_{I_x^{P_U}} + \underbrace{\sum_{\substack{b=1 \\ b \neq b_i}}^{B} \gamma_{b2} \sum_{k=1}^{K_b} \alpha_x^b S_{T(b)} \bar{\mathbf{H}}_x^b \cdot \mathbf{\Psi}_{u_k}}_{I_x^{P_D}} \\ &+ \underbrace{\sum_{\substack{b=1 \\ b \neq b_i}}^{B} \gamma_{b3} \sum_{k=1}^{K_b} \alpha_k^x S_{U_{T(b)}} \mathbf{h}_k^b q_k}_{I_x^{U}} + \underbrace{\sum_{\substack{b=1 \\ b \neq b_i}}^{B} \gamma_{b4} \sum_{k=1}^{K_b} \alpha_x^b S_{T(b)} \bar{\mathbf{H}}_x^b \cdot \mathbf{w}_k^b s_k^b}_{I_x^{D}}, \end{aligned} \tag{34}$$

4.4.1 Fundamental Interference Regimes

In this section, we introduce the concept of fundamental interference regimes. A cell will operate in a particular interference regime *with respect to another interfering cell* depending on (i) the existence of pilot contamination effect, i.e., the interferer's TDD configuration during the training phase, and (ii) the selection of the mode of operation at both the

serving and interfering cells during the data transmission phase. We define two fundamental regimes, namely the Pilot Contamination Regime (PCR) and the Regular Interference Regime (RIR). As the names suggest, the former occurs when the channel estimate is contaminated by another existing channel in the system, thus introducing the risk of beamformed interference. The latter represents the more usual case where interference can be thought of as noise in the system. We explain these two concepts more in detail in the following.

4.4.1.1 Pilot Contamination Regime (PCR)

The case of PCR implies that the channel estimate is contaminated in such a way that beamforming the transmit signal at the base station using, e.g., the expression in (28), will imply directing interference to another existing element in the network. For that effect to happen, the interference received during the training phase of the cell must come from another cell (uplink or downlink) that is using the same pilot signal as the particular user being served. In our proposed TDD HetNet architecture, the network elements subject to contaminating the pilot estimation may be both users and base stations, since transmission paths for each time slot at each base station can be configured independently.

Let us first investigate the case where the pilots in the serving cell are sent over the uplink, i.e., the mode P_U is used during the training phase. To set this cell in PCR with respect to an interfering cell, the interfering cell must be also executing its training phase during the same time slot. If that happens, pilot contamination will occur when the same pilot sequence is reused in two different users of the two cells. The reason follows from Eq. (27). Since we are assuming P_U mode for the training phase, the estimation is performed at the base station, and the contaminated estimates correspond to the (reciprocal) channels between the receiving base station and the interfering element. Two possibilities exist for the interfering element: Either a user (uplink) or a base station (downlink). We call the first regime *PCR-U* and the second *PCR-D*. The former implies that the interfering cell is operating in P_U mode while the latter imples a P_D mode. Figure 22 summarizes these

concepts for a two-base station scenario.

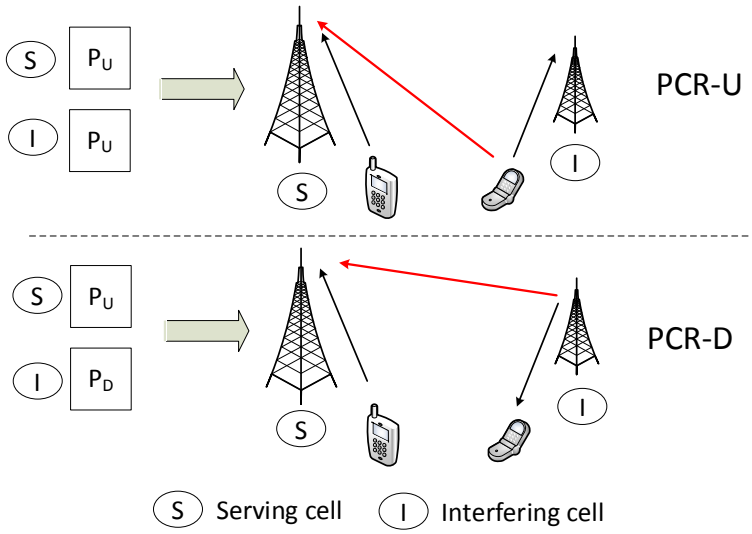

Figure 22. TDD configurations during training phase and their corresponding interference scenarios for PCR-U and PCR-D regimes.

Assuming that during PCR-U all interfering cells are operating in P_U mode, the received signal at base station b_i can be expressed as follows:

$$\mathbf{y}_{b_i}^{PCR-U} = \mathbf{r}_{b_i}^{P_U} + I_{b_i}^{P_U} + \mathbf{z}, \tag{35}$$

where $\mathbf{z}$ is the additive white gaussian noise (AWGN) and $I_{b_i}^{P_U}$ represents one of the four components of I_x in (34) when x stands for a base station. Then, the pilot-based channel estimation is performed by multiplying the received signal with the pilot as follows:

$$\begin{aligned} \widehat{\mathbf{h}}_{k'}^{b_i} &= \Psi'_{k'} \mathbf{y}_{b_i}^{PCR-U} \\ &= \alpha_{k'}^{b_i} S_{U_{T(b_i)}} \mathbf{h}_{k'}^{b_i} + \sum_{b=1}^{B^{k'}} \alpha_{k''_b}^{b_i} S_{U_{T(b)}} \mathbf{h}_{k''_b}^{b_i} + \mathbf{z}, \end{aligned} \tag{36}$$

where $B^{k'}$ is the number of base stations using the pilot sequence k' for channel estimation. The most interesting element of Eq. (36) is the channel vector $\mathbf{h}_{k''_b}^{b_i}$, which represents the channels from all interfering users using the same pilot sequence to the serving base station b_i. These particular channels that have contaminated the estimates become a very degrading interfering when beamforming is performed, since the precoding vector is just the normalized version of the channel estimate.

Let us now look at the PCR-D case assuming all interfering cells are operating in P_D mode. The received signal at base station b_i is given by

$$\mathbf{y}_{b_i}^{PCR-D} = \mathbf{r}_{b_i}^{P_U} + I_{b_i}^{P_D} + \mathbf{z}, \tag{37}$$

and the channel estimate is given by

$$\begin{aligned}
\widehat{\mathbf{h}}_{k'}^{b_i} &= \Psi'_{k'} \mathbf{y}_{b_i}^{PCR-D} \\
&= \alpha_{k'}^{b_i} S_{U_{T(b_i)}} \mathbf{h}_{k'}^{b_i} + \sum_{b=1}^{B} \alpha_{k'}^{b} S_{T(b)} \left(\Psi'_{k'} \bar{\mathbf{H}}_b^{b_i} \cdot \mathbf{\Psi}_{k'} \right) + \mathbf{z} \\
&= \alpha_{k'}^{b_i} S_{U_{T(b_i)}} \mathbf{h}_{k'}^{b_i} + \sum_{b=1}^{B^{k'}} \alpha_{k'}^{b} S_{T(b)} \left(\bar{\mathbf{H}}_l \right)_b^{b_i} + \mathbf{z},
\end{aligned} \tag{38}$$

where $\left(\bar{\mathbf{H}}_l \right)_b^{b_i}$ represents the l-th SIMO channel from the interfering base station b to the serving base station b_i using the same pilot signal as user k'. Hence, we observe a major difference between PCR-U and PCR-D modes: *The contaminating contributions represent a B2U channel in the case of PCR-U and a B2B channel in the case of PCR-D.*

The above observation has important implications in the TDD design. It is well known that the main directivity gains of beamforming come from pre-multiplying the transmit signal by the same channel vector that will be undergone by the signal before being received, hence increasing its energy in that particular direction. Precoding the signal with a channel estimate that contains the interfering channel during the training phase will boost therefore the transmission in that particular direction, increasing interference.

Assuming a single interferer case, let us focus our attention in the scalar product $\mathbf{h} \cdot \mathbf{w}$ that takes place after transmitting a beamformed signal. The mentioned scalar product when the channel estimate is contaminated can be expressed as follows:

$$\begin{aligned}
\bar{\mathbf{h}}_x \cdot \mathbf{w}_{k'}^{b_i} &= \bar{\mathbf{h}}_x \cdot \frac{\widehat{\mathbf{h}}_{k'}^{b_i}}{||\widehat{\mathbf{h}}_{k'}^{b_i}||} \\
&= \bar{\mathbf{h}}_x \cdot \frac{\mathbf{h}_{k'}^{b_i} + \mathbf{h}_j}{||\mathbf{h}_{k'}^{b_i} + \mathbf{h}_j||} \\
&= \frac{\bar{\mathbf{h}}_x \cdot \mathbf{h}_{k'}^{b_i}}{||\mathbf{h}_{k'}^{b_i} + \mathbf{h}_j||} + \frac{\bar{\mathbf{h}}_x \cdot \mathbf{h}_j}{||\mathbf{h}_{k'}^{b_i} + \mathbf{h}_j||}
\end{aligned} \tag{39}$$

where $\mathbf{h}_x$ is the channel experienced by the transmitted signal. It should be clear from Eq. (39) that the received power will be maximized when $\mathbf{h}_x$ is either equal to $\mathbf{h}_{k'}^{b_i}$ or to $\mathbf{h}_j$. One maximum will be attained at the user k' for which the signal is intended; however, it is up to design of the TDD architecture not to let the network element j to be listening to the wireless medium at that time slot. The element j can be either a user or a base station as it was previously explained.

An analog argument applies for data reception on the uplink using MRC combining since the channel estimate is also used for signal combining and decoding as shown in (29).

Both in the uplink and downlink, the problem of having a contaminated channel estimate can be severe, especially when the number of antennas is very large. However, the proposed TDD architecture provides the flexibility to avoid the reception of signal when a strong interering beam is directed towards the receiver. Or said in more plain words, to avoid listening when directed interference exists. Our proposed method to implement this interference avoidance scheme relies on selecting the appropriate transmission paths configuration given the training phase configuration of the cells. Let us call Reduced Contamination Regime (RCR) the TDD configuration that avoids listening when directed interference exists, and Increased Contamination Regime (ICR) the case when beamformed interference is received.

We seek the RCR and ICR configurations for both PCR-U and PCR-D regimes. In the case of PCR-U, we need to avoid the user who contaminated the pilot to be listening to the channel when the serving base station transmits. Hence, the D mode should be avoided in the interfering cell when D is selected in the serving cell. Similarly, when the serving cell is receiving data in D mode using MRC combining, the U mode should not be utilized in the interfering cell. Hence, these two configurations represent ICR in PCR-U. An analog reflection follows for PCR-D regime: The interfering base station should not be listening (i.e., set in U mode) when the serving base station is transmitting (D mode),

while a simultaneous downlink transmission of the interfering cell (D) while the serving base station is receiving data (U) would greatly degrade performance.

Table 3 shows the most fundamental findings of this contribution, where S stands for serving cell and I for interfering cell. In summary, we can state that two cells should have different TDD configuration for the data transmission slots if in PCR-U regime, whereas the configuration of the time slots should be the same for PCR-D mode. This rule provides powerful insights on how a TDD HetNet architecture should be designed to mitigate the critical pilot contamination effect of massive MIMO systems.

Table 3. Pilot Contamination Regime Classification

		RCR		ICR	
PCR-D	S	D	U	D	U
	I	D	U	U	D
PCR-U	S	D	U	D	U
	I	U	D	D	U

The reader may be wondering about the case of the serving cell using P_D mode for the training phase. In this case, the channel could be also contaminated by another exisisting channel in the system, but it would never be as harmful as in former case because it's the user who performs the estimation and feeds them back to the base station. Thus, the channels contaminating the estimate would always be between interfering network elements and the user. These channels will never be present when performing beamforming or combining at the serving base station. Therefore, the configuration of the TDD architecture would not have such a big impact on the interference performance.

4.4.1.2 Regular Interference Regime (RIR)

The interference in the system not caused by a contamination of the channel estimate falls under the category of RIR. We say that a serving cell operates under RIR with respect to an interfering cell when the latter has no way of causing beamformed interference to users or base stations in any of the two cells. Figure 23 shows the pairs of TDD configurations that cause RIR. When the channel estimation is performed while data transmission occurs in

the interfering cell, the estimation may lack precision because of noise-like effects but no other existing channel becomes part of the channel estimate since the pilot signal applied at the receiver was not used at the transmitter. In addition, we also classify as RIR the channel contamination suffered under P_D mode when the interfering cell is also on a training phase for the reasons stated above.

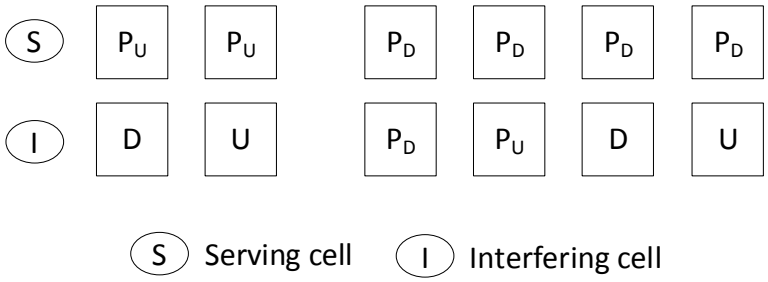

Figure 23. TDD configurations during training phase for RIR mode.

Later in this chapter we explore the differences between PCR and RIR. Although it is not intuitively clear whether it is more beneficial or not to induce more RIRs than PCRs in a grid, there is no doubt that some PCR configurations are unavoidable. In that case, RCR must be set at all cost to avoid the directed interference of ICR.

4.4.2 Other Important Considerations

Besides the fundamental interference regimes caused by the training phase configuration, there are other important factors that need to be taken into account when filling out the TDD grid. Those are summarized in the following.

4.4.2.1 Interfering Power Level

The level of received interference power at any receiver is critical to provide acceptable performance. While this is an obvious consideration for the data transmission phases, we show in the subsequent section that the impact of the interference power level during the training phase is also very high. In any case, the average level of interference primarily depends on the interferers' transmit power, location and, particularly for the downlink of massive MIMO system, on the pilot contamination effect. Furthermore, the transmit power of the

interfering device depends on both the network tier and the transmission path scheduled for the interfering cell in that time slot. With these elements in mind, it becomes crucial to provide a solution for the TDD grid that avoids highly degrading interference configurations (e.g., beamformed interference due to pilot contamination coming from a MBS) while allowing less degrading cases (e.g., non-beamformed interference coming from a FBS).

4.4.2.2 Interference Reciprocity

Two neighboring cells both cause and receive interference to/from one another. This means that the TDD configuration of two cells must be analyzed from two perspectives: When cell one acts as the serving cell and cell two as interfering cell, and when cell two acts as serving cell and cell one acts as interferer. This interference reciprocity feature makes an optimal solution to the grid more complex since both directions must be taken into account when evaluating a particular *filling* of the grid.

4.4.2.3 Number of Antennas at the Interferer

As a consequence of the interference reciprocity feature, the number of antennas at the interfering device also impacts the solution to the grid. While single-antenna transmitters do not perform beamforming, thus rendering the pilot contamination problem insignificant, multiple-antenna transmitters do. This means that the interference regime undergone by an interfering cell is not relevant when that interfering cell is operating in uplink (terminals are considered single-antenna in this work) or the base stations are single-antenna. Otherwise, the undergone fundamental interference regime does matter.

Section 4.5 formalizes these considerations in the formulation and solution of the TDD grid problem.

4.5 The TDD HetNet Grid Problem

In this section, we formally present the TDD HetNet Grid problem. As it was shown in Fig. 21, the TDD HetNet grid is composed of the frames belonging to each cell of the grid, with each subdivided in a number of time slots that is the same for the whole system.

The problem we are trying to solve is how to optimally decide the configuration of each time slot, i.e., which of the four possible modes (D, U, P_U, or P_D) is the most suitable one for each time slot of each cell. The criterion followed for the selection is based on the interference analysis described in the previous section. In particular, the highly degrading effect of pilot contamination should be avoided at all cost.

In the folloing, we present a mathematical formulation of the TDD HetNet Grid problem as an optimization problem. Unfortunately, this problem cannot be easily solved with conventional techniques and hence, we propose two different solution strategies that can be used as guidelines for any particular algorithmic solution of the problem at hand.

4.5.1 Problem Formulation

The TDD HetNet grid can be seen as a matrix $\mathbf{A}$ whose rows correspond to the cells present in the network and the columns represent the time slots. As the main target should be to minimize the interference in the system, the objective function must perform some sort of operation that allows the determination of the interference regime that is achieved between each possible pair of cells in the system. To determine the regime, it is necessary to observe the location of the pilot slots, and whethere these are transmitted in the uplink or in the downlink of the TDD system. As mentioned earlier, channels estimated at the users by non-massive MIMO cells do not present the problems of pilot contamination since the contaminating contribution does not affect the beamforming or combining. In addition to the matrix $\mathbf{A}$, it is convenient to have a vector $\mathbf{p}$ of length the number of cells in the system which indicates the position of the pilot time slot within the frame of each cell. As for the rest of variables that play a role in the formulation of our problem, Table 4 summarizes all of them as well as their description. Note that the different modes of operation are represented by $+1, 0, -1$ where we make the distinction of 0^- and 0^+ to differentiate pilots transmitted in the uplink and downlink, respectively.

The formulation of the problem can be found in Eqs. (40a) through (40h). Given as input the necessary system parameters, the challenge is to minimize a cost function that

Table 4. Elements of the TDD HetNet Grid Problem

Element	Description
N	Number of time slots in a frame
L	Number of base stations
n_D	Number of downlink time slots in a frame
n_U	Number of uplink time slots in a frame
$\mathbf{L}_{MM}$	Massive MIMO indicator vector
N_{MM}	Number of massive MIMO-enabled base stations
$\mathbf{A}$	TDD grid matrix
$\mathbf{p}$	Pilot location vector
$C(\cdot,\cdot,\cdot,\cdot)$	Cost function
$\{-1, 0^-, 0^+, +1\}$	$\{U, P_U, P_D, D\}$

accounts for the interference generated between each pair of cells in the system, and then aggregates it. For each pair, one cell is considered the serving cell and the second one is considered the interferer. The cost function $C(\cdot,\cdot,\cdot,\cdot)$ receives as arguments (i) the type of pilot used by the serving cell, (ii) the mode of operation used by the interfering cell at the interfering slot of (i), (iii) the mode of operation of the serving cell at the data transmission stage, and (iv) the mode of operation of the interfering cell at the data transmission stage. The cost function itself can be defined in different ways. The main idea is to define a mapping function that assigns weights (costs) to each combination of time slots interfering with each other based on the regime attained during the training phase. Higher costs will be thus allocated to ICR configurations, but the transmit power of the interfering network element also plays an important role when assigning the costs: The higher the interfering power, the higher the cost associated with that configuration. So one simple example of mapping would be to assign costs to ICR configurations based on the ratio average received power over average interfering power, and a weight of zero to RCR configurations. For RIR, the same reasoning applies except that costs are based just on power ratios since no

PCR exists.

$$\text{Given:} \quad N, L, n_D, n_U, \mathbf{L}_{MM}, N_{MM} \tag{40a}$$

$$\text{Find:} \quad \mathbf{A}, \mathbf{p} \tag{40b}$$

$$\text{Minimize:} \quad \sum_{i=1}^{L} \sum_{j=1}^{L} \sum_{\substack{n=1 \\ n \neq p(i)}}^{N} C\left(\mathbf{A}_{ip(i)}, \mathbf{A}_{jp(i)}, \mathbf{A}_{in}, \mathbf{A}_{jn}\right) \tag{40c}$$

$$\text{Subject to:} \quad \mathbf{A}_{ij} \in \{-1, +1\} \quad \forall i, \ \forall j \neq p(i) \tag{40d}$$

$$\mathbf{A}_{ip(i)} \in \{0^-, 0^+\} \quad \forall i \tag{40e}$$

$$p(i) \in \{1, \cdots, N\} \quad \forall i \leq L \tag{40f}$$

$$\sum_{j=1}^{L} \mathbf{A}_{ij} = n_D - n_U \quad \forall i \tag{40g}$$

$$\mathbf{A}_{i\mathbf{L}_{MM}(j)} = 0^- \quad \forall i, \ \forall j \leq N_{MM} \tag{40h}$$

In the above problem, constraints (40d) and (40e) make sure that each cell frame consists of one slot for pilots and the rest for downlink or uplink data transmission; constraint (40f) accounts for the possible location of the pilot within each frame; constraint (40g) makes sure that the number of uplink and downlink transmission slots is the right one; and finally constraint (40h) forces all massive MIMO-enabled cells to send their pilot signals in the uplink.

Unfortunately, the above problem does not have an analytical solution and must be solved by means of suboptimal algorithms. Due to space limitations and the former fact, we skip here the presentation of the different weighting approaches for the cost function that could be valid in the above optimization problem. In the following, we will present two different solution strategies that allow the design of suitable algorithms to fill out the TDD grid corresponding to a HetNet.

4.5.2 Solution Strategies

The impossibility to obtain an analytical solution to the above problems makes us resort to algorithmic solutions for the TDD HetNet grid problem inspired by the lessons of Section

4.4. The main message to take away so far is that it will be probably unavoidable to encounter the PCR regime in massive MIMO HetNets due to the reuse of the pilot signals. In that case, it is crucial to design the TDD layer so as to avoid configurations causing ICR. With this objective in mind, two alternatives seem possible: To avoid the PCR regime altogether when configuring the TDD network, hence rendering all interference regimes as RIR, or to provoke PCR but configure the system in such a way that RCR is the operating mode of each pairs of cells where at least one is enabled with massive MIMO. It is less obvious to differentiate between RIR and RCR since other factors out of the scope of this paper such as the resilience of the particular pilot sequence at use to *noise-like* interference, the channel estimation method, or the employed detection mechanism, may play a role in the post-detection SINR.

The two grid filling strategies are described in the following:

- **Avoid PCR:** This strategy starts by checking whether PCR can be avoided altogether in the grid given the topology configuration, that is, the number of slots, the number of base station, the MIMO capabilities of the base stations, etc. If this is not possible, then the unavoidable PCR cases must be identified first and solved in RCR mode. Then, the rest of RIR cases must be figured out. If the grid can be configured without incurring in PCR, then all pairs of cells operate in RIR mode and the selection of time slots must be such that minimizes the overall interence received power in the system.

- **Exploit PCR:** This second strategy, on the contrary, induces PCR in the system and configures the cells so that no ICR is induced and all the pilot contamination cases can be solved in RCR mode. Given the classification of Table 3 and the fact that massive MIMO cells require the pilots to be transported in the uplink, this implies that (i) no more than two slots in P_U should interfere to guarantee RCR, and (ii) the number of massive MIMO-enabled base stations in the system is limited by $2N$, where N is the number of time slots in each frame. Again, the application of this

strategy will result in different algorithms depending on the characteristics of the HetNet deployment.

These two strategies are not proper algorithms to solve the grid but guidelines to inspire the design of those. The reason why no exact algorithmic solution is provided lies in the fact the solution may greatly vary depending on the topology and configuration of the network. As discussed in Section 4.4.2, aspects such as the number of antennas in the interferer or the property of interference reciprocity should also shape the design of a particular solution. Hence, an algorithm to fill the grid when all base stations are equipped with very large antenna arrays would significantly differ from the same algorithm with single-antenna base stations which do not suffer from pilot contamination effect, or even just regular MIMO base stations that could transmit their pilots in the downlink. The design of optimal and efficient algorithms for each particular scenario is left as future work.

4.6 Performance Evaluation

In this section, we present simulation results that show the performance of the proposed TDD architecture on a HetNet where the MBS is equipped with a very large array of antennas. Two experiments are conducted: In the first case, we closely study the simple case of two cells operating in the Pilot Contamination Regime where one cell acts as the serving cell and the second one as interferer. The second set of experiments are targeted at evaluating the system-level performance of a HetNet whose TDD architecture is designed according to the principles proposed in this paper.

To perform the first experiment, we assume a two-base station scenario with one user each sharing the same pilot sequence. The serving base station is equipped with a very large array of antennas. We restrict the simulation to two time slots: A training phase followed by a data transmission phase. Trying to assess the performance difference between RCR and ICR when pilot contamination exists, we first assume that the serving base station gets

its channel estimate contaminated by interfering pilots carried first in the downlink (PCR-D) and then in the uplink (PCR-U). Then, we measure the signal-to-interference (SIR) ratio during the data transmission slot at the receiving ends: The interfered user in the case of downlink transmission, and the serving base station in the case of uplink transmission. The results are displayed in Fig. 26. The SIRs (y-axis) are measured for different contamination ratios (x-axis), where the contamination ratio is defined as the quotient between the received serving power and the received interfering power *at the training phase*. The main conclusions that can be extracted from the graphs are as follows. Clearly, the pilot contamination effect degrades SIRs both in the downlink and uplink, and the PCR-D and PCR-U modes of operation behave similarly. More interestingly, selecting the RCR configuration over ICR greatly increases the SIR of the downlink and uplink transmissions. Furthermore, the contamination ratio plays an important role: When the power level of the contamination is high, the beamformed interference experienced at the users increase, hence enlarging the SIR gap between RCR and ICR. This observation is crucial when designing a TDD configuration for a HetNet since beamformed interference coming from high-power elements (such as MBSs) is much more dangerous than the interference coming from low-power elements (such as FBSs). In summary, we have observed that the design of the TDD architecture is a critical parameter to control interference in massive MIMO systems.

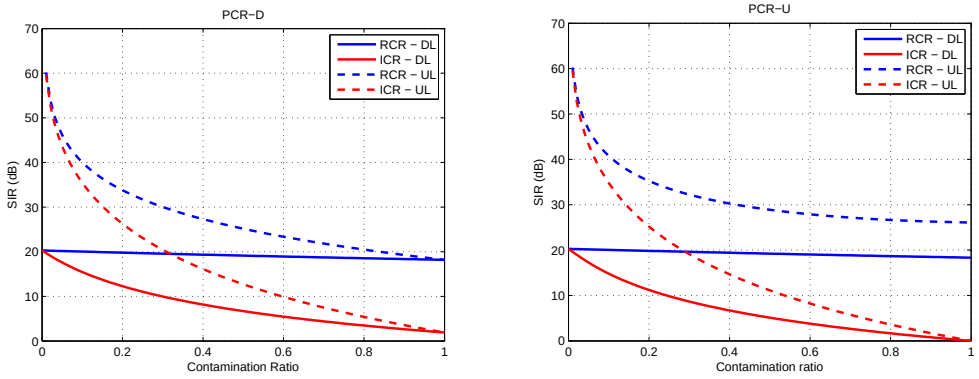

(a) PCR-D (b) PCR-U

Figure 24. Pilot Contamination Regime analysis for downlink and uplink transmission

For the second set of experiments, system-level simulations are conducted on a three-tier HetNet deployed across the area of one single macrocell. Hence, we just consider one MBS that is equipped with a very large antenna array. The rest of the base stations and users in the network are single-antenna. Table 7 shows the most relevant parameters to simulate the network described in Section 4.2. The first system-level evaluation will be performed with an array at the MBS of $M = 128$ antenna elements, while the second one will investigate the impact of the number of antennas on the network performance. The objective of this performance evaluation is to obtain the rate distribution of the users potentially affected by the pilot contamination effect using three different design approaches for the TDD configuration: Avoid PCR, Exploit PCR, and TD-LTE. We select a symmetric load scenario where $n_D = n_U$; hence, Configuration 1 of TD-LTE is chosen in Table 2 for a fair comparison. Each of the different TDD configurations compared in this section has a unique matrix

Table 5. Simulation Parameters

Parameter	Value
Macrocell area	100
Density of PBSs, FBs (λ_P, λ_F)	(0.2, 1)
Mobile user density (λ_U)	50
Transmit power of MBS, PBs, FBs (dBm)	(30, 10 , 0)
Transmit power of MUEs, PUEs, FUEs (dBm)	(0, -3, -6)
Pathloss exponent	3
Channel exponential mean	1
(N, n_D, n_U)	$(5, 2, 2)$

A representation that describes the configuration of each cell in the HetNet: The matrix $\mathbf{A}_{TD-LTE}$ is straightforward to obtain from Table 2 using Configuration 1 and a frame duration of $N = 5$ time slots; the matrices $\mathbf{A}_{aPCR}$ and $\mathbf{A}_{ePCR}$ correspond to the *Avoid PCR* and *Exploit PCR* strategies described in Section 4.5.2 and are obtained following the above principles for the particular HetNet topology investigated in this work where only the MBS had a very large array of antennas and the rest of base stations are single-antenna. In particular, $\mathbf{A}_{aPCR}$ has a first row corresponding to the macrocell configured as $[0^-, +1, -1, -1, +1]$

and the rest of rows follow the pattern $[+1, 0^{+}, -1, -1, +1]$, thus avoiding the pilot contamination effect, while $\mathbf{A}_{ePCR}$ has as first row the vector $[+1, 0^{-}, -1, -1, +1]$ and the rest of rows follow the pattern $[+1, 0^{-}, -1, -1, +1]$. Furthermore, this simulation assumes a pair of colliding pilots for each macrocell-small cell pair in the network. The design of the pilot sequences to minimize collisions as well as its distribution is beyond the scope of this research work.

The resulting uplink and downlink rate distributions are shown in Fig. 25, where the rates are expressed as spectral efficiency quantities measured in bps/Hz. Recall the downlink rates represent the rates of the interfered users (i.e., all small cell users) while uplink rates are measured at the MBS since no pilot contamination effect appears in single-antenna base stations. Several interesting observations can be made. First, managing the interference caused by the pilot contamination effect in a HetNet by means of the TDD architecture makes a very positive impact on the attainable user rates: By selecting the appropriate receiver when beamformed interference is present, the user rates can fully benefit from the advantages of massive MIMO systems. This advantage can be easily missed if the TDD architecture is not designed with this objective in mind, as in the case of TD-LTE. The effect, although troublesome for both downlink and uplink communications, is particularly bad for small cell users who see their rates very limited by the beamformed interference coming from the MBS. With the proposed simplified modeling for RIR based on AWGN interference, no significant difference can be observed between *Avoid PCR* and *Exploit PCR* strategies.

Finally, we investigate the performance dependence with the number of antennas for two of the three different TDD designs, namely *Avoid PCR* and TD-LTE. The results are shown in Fig. 26. The most important conclusion that can be extracted from these results is the difference in the evolution of the rate distribution curve when the number of antennas at the MBS M is increased. If the pilot contamination effect is well managed, i.e., the *Avoid PCR* strategy (*Exploit PCR*'s behavior is similar although not shown here for lack of space)

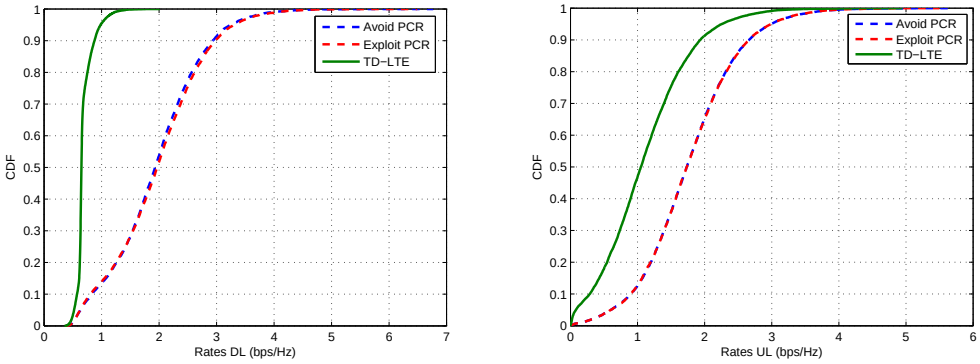

(a) Downlink (b) Uplink

Figure 25. Rate distribution for different TDD grid solutions

are selected to determine the **A** matrix, the rates of the users benefit from the increase of the number of antennas. However, if the underlying TDD architecture does not account for this effect such as the standard TD-LTE, the increase of antennas can be counter-productive and damage the attainable rates both in the downlink and the uplink.

4.7 Conclusions

In this chapter, we present a novel method to mitigate the strong interference caused by the pilot contamination effect present in a HetNet where the MBS is equipped with a very large number of antennas. The main idea in our proposed design is to prevent the reception of signal at time slots where certain network elements are receiving strong interference from a transmitter that uses a contaminated channel estimate. Besides the main architectural features, we conduct an interference analysis of our design and distinguish different fundamental interference regimes under which the network can operate. We then formalize the problem of a TDD HetNet grid and present two strategies to fill it out. Results show the potential of increasing the user rates via massive MIMO if the pilot contamination effect is properly managed with an appropiate TDD design.

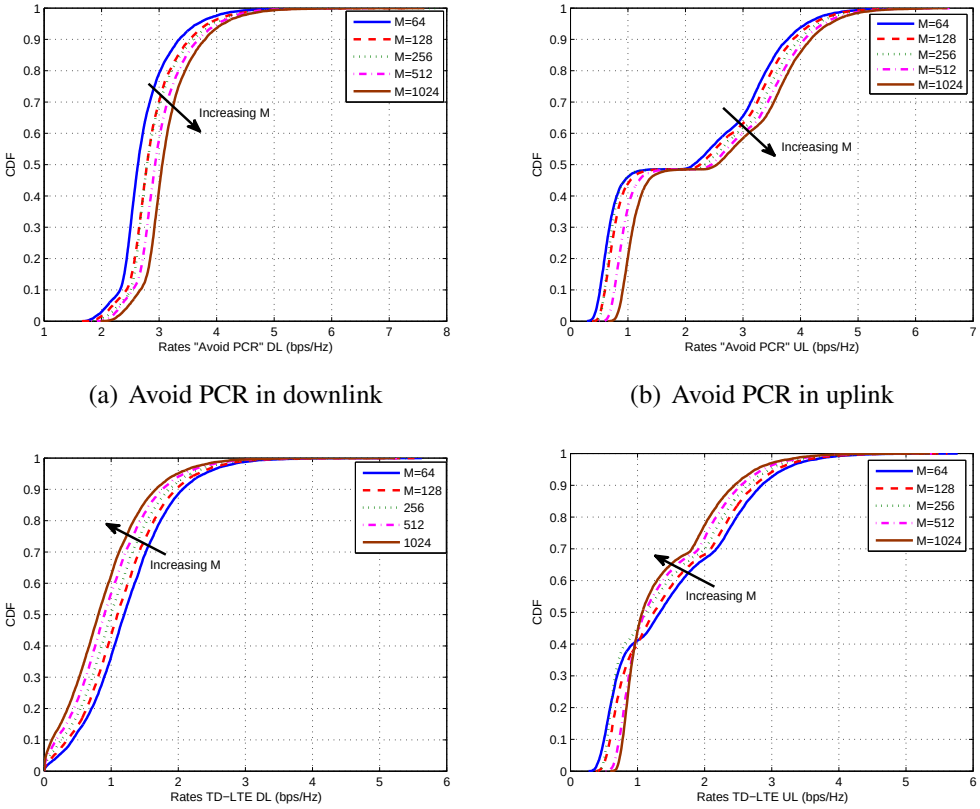

(a) Avoid PCR in downlink

(b) Avoid PCR in uplink

(c) TD-LTE in downlink

(d) TD-LTE in uplink

Figure 26. Rate distributions for different number of antennas at the MBS

CHAPTER 5

INTERFERENCE SUPPRESSION TECHNIQUES FOR PICOCELL DEPLOYMENTS

5.1 Introduction

As explained in Chapter 2, there are different ways of mitigating interference in small cell networks. First, 3GPP introduced in LTE Rel-10 a set of network-centric techniques grouped under the umbrella term of eICIC [110]. Although effective, these techniques usually require precise coordination and incur in relatively high network overhead. Alternatively, interference cancellation (IC) techniques at the mobile user can also be employed. Handheld receivers of future cellular systems such as LTE-Advanced will offer different IC techniques for control and data channels. They usually require less network overhead but transfer the complexity to the user receiver. The performance of both eICIC and IC techniques is highly influenced by the interference pattern of each particular network deployment. Therefore, different scenarios may require different techniques.

In this chapter of the thesis, we investigate interference suppression techniques for data channel in the scenario of clustered deployments of picocells. In particular, we focus on codeword-level interference cancellation (CWIC) and ABS. As with the well-known technique of successive interference cancellation (SIC), the elimination of the interference in CWIC takes place at the mobile user, which must decode the interference signal before subtracting it from the total received signal at the codeword level [111]. This decoding restriction imposes a fundamental tradeoff in the studied system since the interfering base station must constrain its transmission rate to a value supported by the interfering link. Both to keep the complexity of the scheme low and minimize the constraints in the system, we propose the case of decoding only the strongest interferer (SI). Hence, we call this technique CWIC-SI. The second investigated approach is ABS. The use of special subframes referred to as ABS where the macrocell mutes has been standardized as part of

eICIC to mitigate the strong interference of picocell users in the range expansion region [38], [89]. In these subframes, macrocells transmit only reference signals, which can be easily cancelled. Here, we investigate for the first time the use of ABS at the picocells as an interference suppression technique in the clustered scenario. Finally, it is worth noting that both CWIC-SI and ABS require some level of network coordination. To avoid additional network overhead, we assume some sort of backhaul coordination only among the picocells of the same cluster.

To the best of our knowledge, there is no existing literature on CWIC or ABS for clustered small cell deployments. Hence, the main contribution of this work is to provide insight into these interference suppression techniques for clustered small cell deployments. For that, we present a subframe-level coordinated scheduling scheme that allows the practical implementation of these techniques into real systems such as LTE. Both CWIC and ABS techniques are considered and adapted to this scheme, which further utilizes proportional fair (PF) resource allocation. Performance evaluation is carried out showing the impact of these techniques for users at the tail, median, and head of the picocells' rates distribution.

The remainder of this chapter is organized as follows. In Section 5.2, we introduce the scenario and system model utilized for this work. Section 5.3 presents the considered interference suppression schemes, namely CWIC and ABS, and analyze them in the context of clustered small cell deployments. Then, Section 5.4 introduces the proposed subframe-based coordinated scheduling scheme and tailors it to the techniques of CWIC and ABS. Performance evaluation results are shown in Section 5.5. Finally, conclusions are drawn in Section 5.6.

5.2 Deployment Scenario and System Model

This section describes the scenario of study as well as some system metrics relevant for this work. The picocell deployment follows the guidelines of 3GPP Small Cell Enhancement

(SCE) scenario 1 [112]: Co-channel deployment of macrocell and picocell clusters with seven wrap-around macrocells that have three sectors each. There is one picocell cluster per macrocell sector, and each cluster consists of four picocells. The users are dropped according to 3GPP configuration 4b [113], where 67% of the users are dropped around the picocell cluster and the remaining users are randomly dropped in the layout. Five different seeds are utilized for the simulations. Figure 27 shows the resulting deployment for one of the seeds.

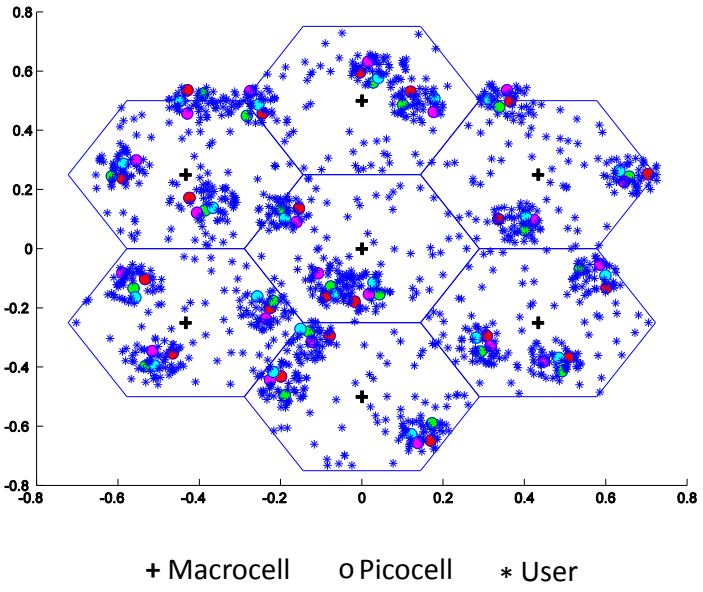

Figure 27. Considered 7-cell wrap around scenario with picocell clusters.

Two important assumptions of our system model are the cell association policy and the above mentioned cluster-restricted coordination. For this work, only RSRP association is considered, i.e., the serving cell is always the strongest received power. In addition, constraining the coordination to the cluster implies that in general only picocell users will be able to benefit from interference suppression techniques. Furthermore, particularly for the case of CWIC-SI, mostly only picocell users whose strongest interfer is a picocell will have the potential to cancel interference (this set of users is referred to as *pico-pico users* in the rest of this chapter). The reason for this is the inabilitity for the macrocell to constrain its rate when it does not belong to any cluster. Across all seeds, picocell users represent a

73.4% of all users while picocell users whose strongest interferer is a picocell account for 54.2% of all users.

There are five relevant link metrics in our system model. The first one is the conventional SINR of a user i defined as follows:

$$SINR(i) = \frac{P_r(i)}{I(i) + \sigma^2}, \tag{41}$$

where $P_r(i)$ is the received power from the serving cell of user i, $I(i)$ is total interference received at user i, and σ^2 is the constant additive noise power. For convenience, we express $I(i)$ in two different ways: (i) as $I(i) = I_{SI}(i) + \Delta I(i)$, where $I_{SI}(i)$ is the received power from the strongest interferer of i and $\Delta I(i)$ is the sum of the rest of interferers, or (ii) as $I(i) = \sum_{p \in \{\mathcal{P} - x_i\}} I_p(i)$ where x_i is the serving cell of user i, $\mathcal{P}$ is the set of all the picocells in network, and $I_p(i)$ is the interference received from picocell p at user i. In addition, we denote as C_i the cluster which the picocell x_i belongs to.

In addition, we consider the following four link metrics: (1) $SINR_{-1}(i)$, defined as the SINR of user i once the strongest interferer power has been completely removed (i.e., $I_{SI}(i) = 0$); (2) $SINR^{SI}(i)$, defined as the strongest interferer's SINR of user i, i.e., the ratio of the strongest interferer's power over the serving cell signal plus rest of interferers and noise; (3) $SINR^{SI}_{-0}(i)$, defined as the strongest interferer's SINR of user i after removing the serving cell power, i.e., the power ratio of the strongest interferer of user i over the rest of interferers; and (4) $SINR_{ABS(\mathcal{Y})}(i)$, defined as the SINR of user i when the set of picocells $\mathcal{Y}$ apply ABS, which is given by

$$SINR_{ABS(\mathcal{Y})}(i) = \frac{P_r(i)}{\sum_{p \in \{\mathcal{P} - x_i - \mathcal{Y}\}} I_p(i) + \sigma^2}. \tag{42}$$

Lastly, we provide two important definitions. A user i has a *dominant* interferer if the the link metric $SINR^{SI}_{-0}(i)$ is above some threshold T_D (dB). Furthermore, a user i has a *significant* interferer if its cancellation provides a gain equal or above some threshold T_S (dB), i.e., if Eq. (43) holds:

$$SINR_{-1}(i) - SINR(i) \geq T_S. \tag{43}$$

Figure 28 shows the cumulative density function (CDF) of the significance and dominance of the interferers across pico-pico users. Approximately 73% of those (40% of the total users) have gains of at least 3 dB by removing the strongest interferer while 49% of pico-pico users (27% of total users) have a dominant interferer with $T_D = 3dB$. These numbers tell us that a significant number of users can benefit from cancellation of just the strongest interferer.

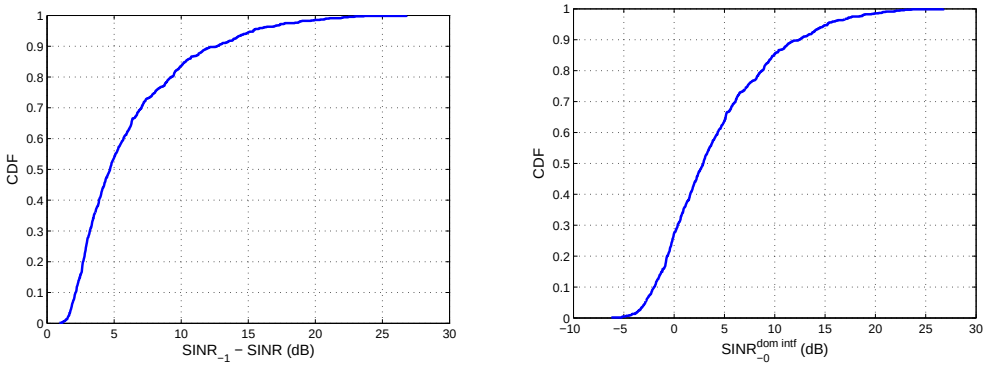

(a) Significant interferers (b) Dominant interferers

Figure 28. Distribution of interferers in the considered scenario .

5.3 Interference Suppression Techniques

In this section, we describe the two interference suppression techniques considered in this chapter. The system tradeoffs are explained, pointing the sources of gains as well as losses. For this and subsequent sections, the words spectral efficiencies and rates are used indistinctly.

5.3.1 Codeword-Level Interference Cancellation for Strongest Interferer

As explained in the introduction, CWIC is an interference cancellation technique implemented at the user's receiver. It is based on the decoding of the interference signal before this one is subtracted from the total received signal at the codeword level, thus completely removing it. The decodable or non decodable capability of a signal is given by Shannon's

famous capacity expression which, for a given SINR, establishes the maximum transmission rate for which an encoding scheme can be found with an arbitrarily low probability of error. In this work, we focus on CWIC applied only to the strongest interferer. By applying this restriction, the complexity of the receiver decreases and, more importantly, the constraints imposed in the system are fewer as it will be explained in the following. We refer to this technique as CWIC-SI throughout the rest of the paper.

The gains of CWIC-SI are obtained by boosting the rates of the IC-enabled users. The rate of a user i not applying CWIC-SI (or unsuccessfully trying to apply CWIC-SI) is bounded by Eq. (44) whereas the maximum achievable rate of i when this is IC-enabled is given by Eq. (45). In addition, to properly decode the interference signal at user i, the rate at which the the interfering base station transmits to its own user i must be supported by the interfering link. This link is characterized by the metric $SINR^{SI}$ as explained in Section 5.2. Hence, *for each interfered user* j, a rate constraint equation as the one shown in Eq. (46) must be applied. The immediate consequence of this constraint is that users being served by the interfering picocell experiment a significant performance loss in their rates. This is explained by the employed RSRP association rule, which generally causes $SINR$ values to be larger than $SINR^{SI}$ values of interfered users.

$$\rho_i \leq \log_2 \left(1 + SINR\left(i\right)\right). \tag{44}$$

$$\rho_i \leq \log_2 \left(1 + SINR_{-1}\left(i\right)\right). \tag{45}$$

$$\rho_i \leq \log_2 \left(1 + SINR^{SI}\left(j\right)\right). \tag{46}$$

Thus, the question that needs investigation is whether the gains of removing the strongest interferer are large enough to overcome the losses incurred at the users being served by the interfering cell. Furthermore, it is also not obvious how many users should be applying CWIC-SI to maximize gains. Finally, a coordination scheme among the picocells of the cluster is necessary both to select the subframes where the rate should be constrained and set the constrained rate value. All these research questions are answered in Section 5.4.

5.3.2 Almost Blank Subframes

In 3GPP, ABS has been proposed as the standard solution to avoid strong interference when users attach to the picocell base station in the range expansion region. During these subframes, the macrocell base station stops transmitting data, thus allowing the users in the range expansion region to receive signal from the picocell without macrocell interference. In this work, we use ABS in a different way. Only picocells within the same cluster can coordinate, therefore ABS is only used at the picocells. Furthermore, the scheduling of ABS does not depend on the existence of users at the coverage expansion region of the picocells since plain RSRP association is assumed. Unlike CWIC-SI, utilizing ABS at a certain picocell benefits all the users that are interfered by that picocell, regardless of whether the picocell is the strongest interferer or not. The SINR of all users will thus experience a boost. Moreover, users do not need to implement any kind of additional processing at the receiver. Nevertheless, the losses of this technique are potentially larger since no rate will be provided to the served users during an ABS subframe. As in the case of CWIC-SI, a coordination scheme among the picocells of a cluster is needed for the selection of ABS subframes. Section 5.4 deals with this issue.

5.4 Subframe-level Coordinated Scheduling

This section introduces a coordination scheme that allows the picocells belonging to the same cluster to apply the interference suppression techniques described in Section 5.3. The scheme is applied at a subframe level, hence making its application to any practical cellular system such as LTE an easy task.

5.4.1 Staggering

For both the cases of CWIC-SI and ABS, the first question is which subframes each picocell should select to constrain its rate so that users from other picocells can benefit from interference suppression techniques. If the employed technique is CWIC-SI, only users whose strongest interferer is constraining its rate may benefit from this technique. The value of the

constrained rate in picocell x, ρ_x^c, is specific to each picocell and must be calculated using a meaningful approach. This issue will be tackled later in the section. In the case of ABS, no signal is transmitted by a specific picocell and all users not attached to that particular picocell benefit from the technique, regardless of whether it is a strongest interferer or not. However, in both CWIC-SI and ABS cases, the users attached to the constraining picocell experiment losses due to a drastic reduction of their rates.

Given the above described premises, we propose the use of subframe-level staggering as a method to schedule when each picocell should constrain its rate. Staggering is a simple scheduling approach where each picocell constrains its rate in only one subframe in a non-overlapping fashion with the rest of picocells in the cluster. Figure 29 depicts the subframe-level staggering scheme for a cluster of four picocells. While the value of the constrained rate is always zero in all picocells for ABS, the selection of ρ_x^c needs some more careful consideration.

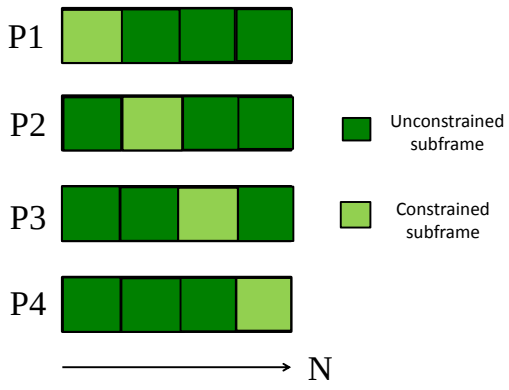

Figure 29. Staggered subframes for a cluster of four picocells.

To better illustrate the concept, Fig. 30 shows a snapshot of a cluster implementing CWIC-IC at the first subframe (n=1). The users under the serving picocell receive a signal of constrained rate, while a set of users whose strongest interferer is P1 receive a higher rate enabled by the suppression of their strongest interferer. How many of these users can successfully apply CWIC-SI depends on the value of ρ_{P1}^c. The rest of users do not see their rate altered.

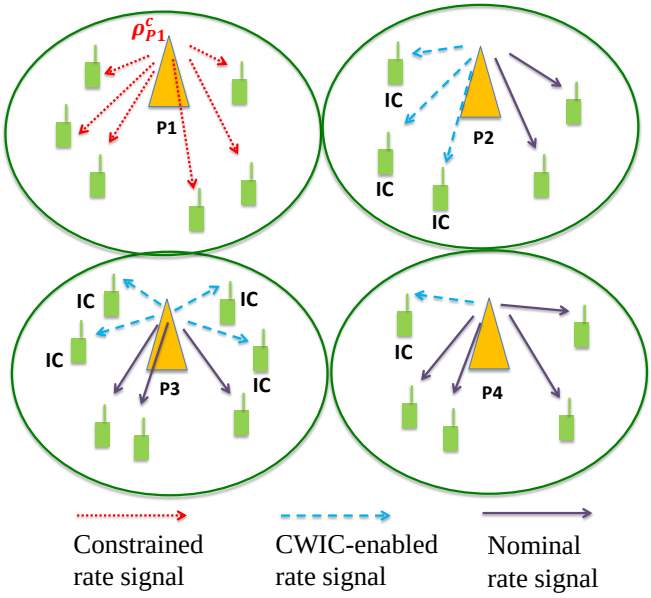

Figure 30. Staggering scenario snapshot for CWIC-SI at n=1.

5.4.2 Proportional Fair Rate Allocation

We now propose an optimization problem capturing the effects of the interference suppression techniques. Another important design parameter is the scheduler implemented at each picocell, which must distribute its available resources among its users. For that, we utilize the well-known proportional fair (PF) resource allocation approach that tries to maximize the log-utility metric [114], [70]. This metric for us is the total rate allocated to a single user given by the product of the amount of resources scheduled times the spectral efficiency achieved by that user.

Although the interference suppression techniques are applied per-cluster, we want to maximize the log-utility over the whole network, i.e., over all users of all cells existing in the network. The resulting optimization problem with PF resource allocation is given by

$$\max_{f_x(i,n)} \sum_{x\in\mathcal{P}} \sum_{i\in\mathcal{U}(x)} \log\left(\sum_{n=1}^{N} f_x(i,n)\cdot\rho_x(i,n)\right), \tag{47}$$

subject to

$$\sum_{i\in\mathcal{U}(x)} f_x(i,n) = \frac{1}{N} \quad \forall x, \forall n,$$

where $f_x(i,n)$ is the fraction of resources allocated by picocell x to user i in subframe n, and

$\rho_x(i,n)$ is the spectral efficiency of user i served by x on subframe n. In addition, $\mathcal{P}$ is the set of all picocells existing in the network, $\mathcal{U}(x)$ is the set of users being served by picocell x, and N is the number of subframes after which the staggering pattern repeats itself. The set of constraints in Eq. (47) accounts for fairness by forcing each picocell in a cluster to consume not more than $\frac{1}{N}$ of the cluster resources for its users.

The staggering pattern combined with any of the two proposed interference suppression techniques creates different possible interference patterns in every user for each subframe. Both CWIC-SI and ABS share the assumption that a macrocell will never constrain its rate. However, differences exist between the two techniques regarding the values of the spectral efficiencies $\rho_x(i,n)$, as Eq. (48) and Eq. (49) show. In those expressions, $\alpha_z(n)$ indicates whether picocell z constrains its rate (1) or not (0). For the case of CWIC-SI, we denote as $x'(x,i)$ the strongest interfering picocell of user i at picocell x, and the obtained rate during a constrained subframe depends on the value of ρ_x^c and the nominal user rate. For ABS, there will always be a picocell in the cluster muting in the cluster and hence users benefiting from it. Furthermore, the set $\mathcal{Y}$ represents the set of picocells in the network simultaneously applying ABS, showing that a user in one cluster can benefit from ABS applied in a picocell of an adjacent cluster.

$$\rho_x^{CWIC-SI}(i,n) = \begin{cases} \log_2(1+SINR(i)) & \text{if} \quad \alpha_x(n)=0 \;\&\; \alpha_{x'(x,i)}(n)=0 \\ \log_2(1+SINR_{-1}(i)) & \text{if} \quad \alpha_x(n)=0 \;\&\; \alpha_{x'(x,i)}(n)=1 \\ \min\left(\rho_x^c, \log_2(1+SINR(i))\right) & \text{if} \quad \alpha_x(n)=1 \;\&\; \alpha_{x'(x,i)}(n)=0 \end{cases} \tag{48}$$

$$\rho_x^{ABS}(i,n) = \begin{cases} \log_2(1+SINR_{ABS(\mathcal{Y})}(i)) & \text{if} \quad \alpha_x(n)=0 \;\&\; \alpha_y(n)=1 \;\forall y \in \mathcal{Y} \\ 0 & \text{if} \quad \alpha_x(n)=1 \end{cases} \tag{49}$$

Finally, it should be noted that since the coordination pattern is fixed, the optimization problem in (47) happens to be convex and thus solvable with regular convex solvers.

Selection of ρ_x^c: An important design choice for CWIC-SI is the calculation of the constrained rate ρ_x^c at each picocell x. This value determines how many users whose strongest

interferer is x will be able to apply CWIC-SI: The smaller ρ_x^c, the larger the number of users that will be able to apply CWIC-SI but the larger the losses of the users served by x. On the other hand, the larger ρ_x^c the fewer the users applying CWIC-SI and the smaller the losses in the users served by x. An optimum value should be sought that does not compromise the fairness of the system. Whichever the selection algorithm, it uses as input the $SINR^{SI}$ values of all users and, hence, the maximum rate supported by those links. We propose several approaches for the calculation of ρ_x^c:

- *Minimum*: The minimum $SINR^{SI}$ value of all users whose SI is x is selected for ρ_x^c. All users whose SI is x can thus apply CWIC-SI.

- *Maximum*: The maximum $SINR^{SI}$ value of all users whose SI is x is selected for ρ_x^c. Only one user can thus apply CWIC-SI.

- *Mean/Median*: The mean/median of the $SINR^{SI}$ CDF of all users whose SI is x is selected for ρ_x^c.

- *x% tail*: The value corresponding to the x% tail of the $SINR^{SI}$ CDF of all users whose SI is selected for ρ_x^c.

- *Threshold*: The minimum $SINR^{SI}$ of a subset of users is selected. The subset is comprised of users with an CWIC-SI gain $SINR_{-1} - SINR$ greater than a threshold T_S.

5.5 Performance Evaluation

In this section, we characterize the performance of both CWIC-SI and ABS, and compare them with the baseline case of not applying interference suppression. With this purpose, we generate realizations of channel gains based on the models defined in the 3GPP evaluation methodology [113] for the scenario described in Section 5.2. Relevant simulation parameters can all be found in the documentation.

We are interested in the rate distribution of the picocell users across the network. The plotted rates are obtained as solutions of the optimization problem in (47), where the total rate that each user receives is computed over the four subframes, i.e., $r_i = \sum_{n=1}^{N} f_x(i,n) \cdot \rho_x(i,n)$. We compute the allocated rates for the three main cases: No interference suppression, CWIC-SI, and ABS for all the clusters in the network. Furthermore, we obtain rate distributions for the different constrained rate selection approaches described in Section 5.4.2. Figures 31 and 32 show the results for CWIC-SI and ABS, respectively.

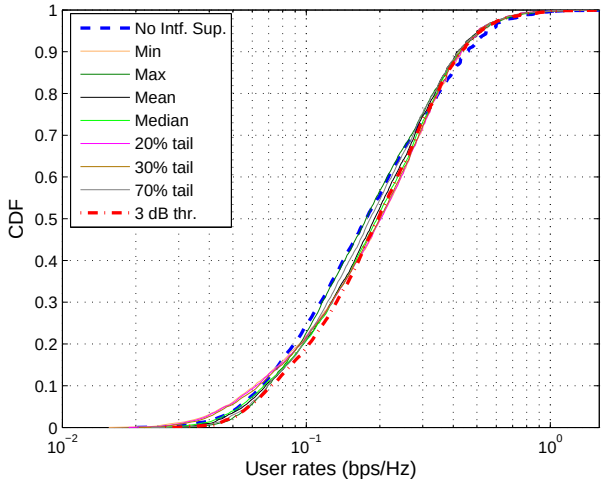

Figure 31. User rates CDF for staggered CWIC-SI.

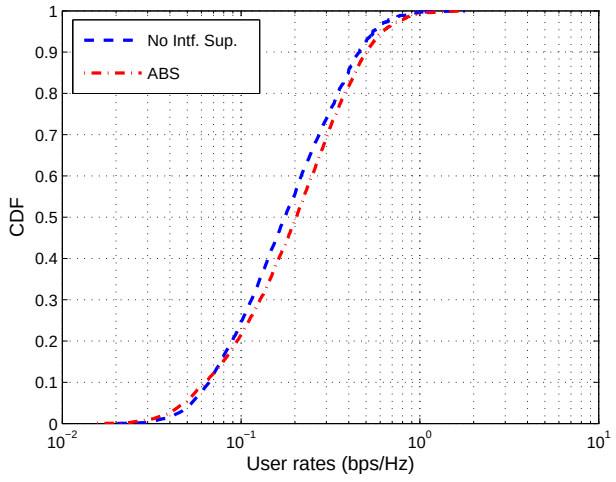

Figure 32. User rates CDF for staggered ABS.

It can be observed that, in general, interference suppression techniques bring gains to the rate distribution curve. The case of CWIC-SI seems to perform better when the constrained rate is selected using a threshold approach, i.e., when only users contributing with a minimum IC gain are considered. A separate search is conducted to select the best threshold value and 3 dB provides the largest gains although overall performance does not vary greatly with this parameter. Then, we break down the results into different regions of the rate distribution. Table 6 shows the gains or losses with respect to the baseline case of no interference suppression for the users at 5%, 50%, 95%, and mean, of the rate cumulative distribution. It should be noted that whereas some loss in the head of the distribution (95%) would be acceptable, the tail (5%) cannot be sacrificed. Losses in users at the center of the cell are tolerable, and sometimes they allow an improvement in the fairness of the system if the rates of the tail users simultaneously increase. However, the tail itself represents users such as those at the cell edge, which cannot afford losing more rate than what their location imposes.

Table 6 compares the baseline with the most relevant CWIC-SI cases and ABS. Some interesting insight can be extracted from these results. First, the maximum gains that can be achieved by these techniques are moderate, around 15%. Second, focusing on CWIC-SI a clear trend can be identified with respect to the tradeoff involved in the optimal number of users applying CWIC-SI. Letting all users apply this technique by selecting the *minimum* approach provides high median gains but the tail of the distribution is hurt (there is a loss of 13%). On the contrary, if only the user with best $SINR^{SI}$ in each cell applies CWIC-SI (*maximum*), no median gains appear but the tail does not suffer and even experiences a small gain of 9%. The tail behavior can be explained using the following intuition regarding the PF scheduler output: Given the logarithmic objective function in (47), some sort of fairness is imposed in the system. Hence, it seems reasonable to predict that most of the constrained subframes will be allocated to users with low rate to minimize system losses while maintaining fairness. If the constrained rate is very low as in the *minimum*, tail users

will futher lose rate. To prevent this system behavior, a compromise between gains and fairness should be selected. It turns out that the best tradeoff is achieved when only gainful users contribute to the selection of the constrained rate (*threshold*), providing acceptable median gains (12%), and some small tail gains (9%). Third, we look into ABS. The results show the largest mean gains of all schemes due to a mitigation of interference not restricted to the strongest interferer. Median and head users experiment gains of 16% and 13%, respectively. However, tail users do lose rate when the picocell completely stops transmitting during certain subframes. This is an issue that must be carefully addressed when designing a complete solution for a real system.

Table 6. User Rates Gains

Approach	**5%**	**50%**	**95%**	**Mean**
No Intf. Sup.	0.053	0.176	0.546	0.227
Minimum	0.87x	1.15x	0.92x	1.02x
Maximum	1.09x	1x	0.96x	0.98x
Median	1x	1.11x	0.95x	1.01x
30% tail	0.91x	1.14x	0.93x	1.02x
3 dB thr.	1.09x	1.12x	0.95x	1.03x
ABS	0.92x	1.16x	1.13x	1.11x

5.6 Conclusions

In this chapter, CWIC-SI and ABS have been introduced as interference suppression techniques for clustered small cell deployments along with a subframe-level coordination scheme for each picocell cluster. It has been shown that moderate gains can be obtained by applying either of these techniques but special care should be put on the system fairness. These results could be further improved by applying a biased cell association policy or a combination of interference suppression with other key LTE-Advanced technologies.

CHAPTER 6

INTERFERENCE AND RESOURCE MANAGEMENT FOR FEMTOCELL DEPLOYMENTS

6.1 Introduction

This chapter investigates the problem of interference for femtocell networks. As mentioned in previous chapters, an inexpensive solution that emerged to increase both network capacity and indoor coverage is the concept of femtocell [82]. Strictly speaking, a femtocell is the coverage area created by a FAP although the term femtocell is typically used for the hardware device as well. A FAP is a short-range low-power device owned and installed by the subscriber that aims to achieve better service at places like a home, an office, a supermarket, etc. by transmitting in licensed spectrum. The traffic is sent over the Internet Protocol (IP) backhaul, which also allows operators to offload macrocell traffic and release resources for other macrocell users. The major technical challenge and strongest performance limiting factor concerning femtocells is interference, which will be dealt with throughout this capter. Three different aspects of the interference problem are investigated in this chapter, namely (i) the degradation induced in the users' performance caused by un-managed interference, (ii) the improvement that can be obtained in performance with spatio-temporal interference estimation in femtocell netorks, and (iii) the hybrid mode of operation for a femtocell as a technique to manage interference while satisfying the requirements of both femto- and macrocell users.

Despite the momentum of femtocells in recent years, modeling and development platforms are still needed in order to test implementation-specific characteristics of femtocells, such as interference mitigation techniques and self-organizing algorithms. Rather than proposing new algorithms to deal with the well-studied problem of interference in regular femtocell networks, in the second section of this chapter we present our developed high-fidelity platform that integrates femtocells into fully standardized networks. Using

OPNET, a high fidelity simulation environment for wireless networks, a femtocell modeling and development platform is created, closely following the specifications dictated by 3GPP regarding the entities, functionalities, procedures, and message formats for femtocell networks. This platform should address not only the link-level characteristics but also the system level behavior associated with Universal Mobile Telecommunications System (UMTS) or HSPA networks. The platform consists of the main elements of a femtocell enhanced UMTS network: the Home Node-B (HNB) and Home Node-B Gateway (HNB-GW), as well as their related procedures and standard messages according to 3GPP's ASN.1 definitions. OPNET provides a platform for high fidelity modeling, simulation and analysis of a broad range of wireless networks, allowing the design and optimization of proprietary wireless protocols [115]. It is shown how the platform reflects the effect of both interference and backhaul degradation on the overall performance of the network, which represent the key concerns for operators nowadays regarding femtocell deployments.

The femtocell interference problem can be classified as cross-tier if it occurs among macrocell and femtocell elements (FAPs or users) or co-tier if the interference happens among different femtocell elements. Numerous approaches have been proposed in the literature to cope with cross-tier interference, usually related to power control [116], [117], spectrum management techniques [118], [119], and open/closed/hybrid access modes of operation [120], [121]. An additional critical issue in all of them is the interference estimation, which triggers all the above procedures but may undermine performance if not correctly tackled. There is not much research done especifically addressing this problem, although most of the works assume that interference can be simply calculated based on distance estimations on the uplink or downlink signal measurements at the FAPs. In this work, we make use of the framework presented in Chapter 3 that allows the creation of interference maps using the reports of the femtocell users. As we will see, this allows the formulation of a resource allocation problem with constraints also on interfered users, instead of only served users. In addition, the estimation of signal at locations without users

is new feature of this technique that can be useful for a variety of network management, diagnostics, and planning problems.

Finally, we will explore the hybrid mode of operation of femtocells to manage interference in the network. The radio interference can be also managed by allowing strong macrocell interferers to connect and acquire some level of service in femtocells [122]. A key mechanism for operators to provide different levels of priority to FUs and MUs is the access control (AC) policy, which is the protocol that regulates the access of the users to a femtocell. For this, three access control modes exist [123]: i) a *closed* access mode where the femtocell resources can be used only for FUs; ii) an *open* access mode where all the femtocell resources are available for MUs; and iii) a *hybrid* access mode where MUs can only access a limited number of femtocell resources. Several studies can be found in the literature which compare open and closed access modes for femtocell networks [124], [125]. On the one hand, in the open access mode, the number of dropped sessions due to cross-tier interference between macrocells and femtocells can be reduced by allowing the most harmful interfering MUs to connect to the femtocell. On the other hand, the closed access mode does not entail security and sharing concerns, and it is more preferred by femtocell customers because they own and install the FAPs in their private environments. The hybrid access mode is proposed as a trade-off between open and closed access modes where the access control has to be carefully chosen depending on the scenario under study and the customer profile [126], [127].

This chapter is organized as follows. In Section 6.2, the assessment of the interference degradation in a femtocell network via a high-fidelity OPNET platform is presented. Then, Section 6.3 introduces the spatio-temporal estimation framework for interference management, and Section 6.4 presents the study on hybrid access femtocells. Finally, conclusions are drawn in Section 6.5.

6.2 Interference Degradation Assessment via High-fidelity Platform

The development of this platform was a joint effort with another BWN lab member. The complete description of our model can be found in [128]. Using the existing reference design of UMTS in OPNET, we developed two new software models to enable the operation of femtocells in the network: The HNB and the HNB-GW. These are the 3GPP names for femtocell and femtocell gateway, respectively. Figure 33(a) depicts a simplified architecture of the network, where the interfaces are also shown. A major part of the development work was focused on the implementation of the Iuh interface between HNB and HNB-GW, consisting of the protocols shown in Figure 33(b) and their corresponding new packet types [129]. The reader is encouraged to go to the published paper to read the implementation details of each of the protocols and packet formats.

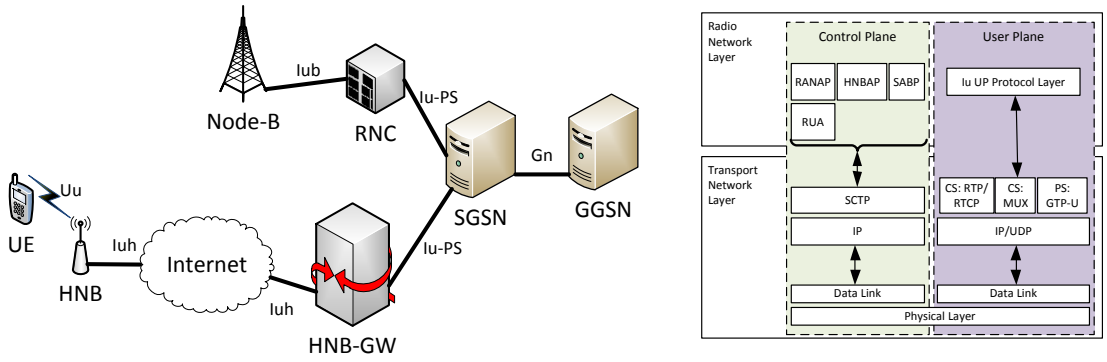

(a) Packet switched section (b) Iuh interface

Figure 33. Femtocell integration within a UMTS network.

Using the above described accurate modeling, we perform simulations on a simple network to validate the interference concerns introduced by femtocells. The femtocell operates in closed-subscriber mode, i.e., it only accepts subscribers. A femtocell is deployed within the coverage region of a macrocell network, both operating in the same frequency. Only one MU and one FU are considered in the system. Here, we show in Fig. 51 a limited set of results that show the impact of interference at the FU and MU's throughput. Figure 51(a) shows the degradation caused in the uplink while Fig. 51(b) does the same with

the downlink. Because the MU is usually far away from the MBS, its transmission power is high and causes a large uplink degradation in the FU. However, the degradation in the downlink is shared between the two users since the received interference power is similar in both users. Finally, Fig. 51(c) shows the dependence of the interference impact with the distance. It can be clearly seen in the graph how the throughput is greatly affected by the distance with the MU: Practically no change in throughput exists when the MU is distant, whereas for the scenario with a close MU, the highest achievable throughput for the FU is only obtained when the MU stops transmitting.

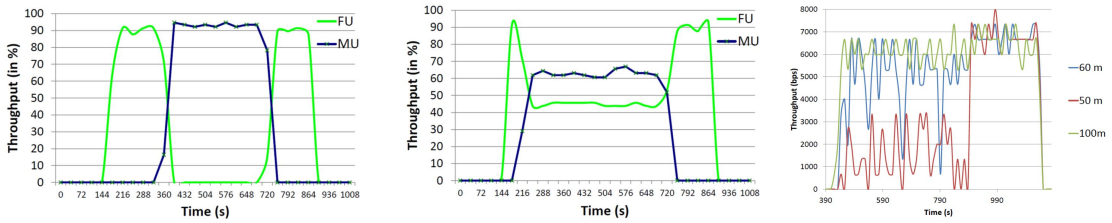

(a) Uplink throughput degradation (b) Downlink throughput degradation (c) Downlink throughput with MU distance to the femtocell

Figure 34. Throughput performance in a femtocell network.

This platform will be used as a reference to compare the performance of femtocells with that of femtorelays. A femtorelay is a novel technology that will be introduced in Chapter 7.

6.3 Spatio-temporal Estimation for Interference Management in Femtocell Networks

In this section, we propose a novel downlink cross-tier interference estimation approach for femtocell networks based on spatio-temporal correlation techniques. The scheme can be applied both at the femtocell and macrocell networks depending on the specific scenario needs for downlink interference management. For instance, downlink interference at the femtocell can be severe if the femtocell is located close to the MBS. Similarly, downlink interference at the macrocell is a serious issue for cell-edge MUs near a femtocell. Without loss of generality, we focus on the former scenario. Therefore, we perform an estimation

of the macrocell interference at the FUs' location.

The estimation consists of spatial and temporal parts. For the spatial estimation portion, we will use the framework presented in Chapter 3: We make use of the Kriging interpolator using semivariogram analysis. At the MBS, MUs' locations and signal attributes are utilized as inputs to the estimation algorithm. The temporal estimation of the signal is subsequently performed using autorregressive models of different orders. With this estimation, the FAP can perform accurate resource allocation functionalities by utilizing the right amount of power so that FUs satisfy their service requirements while the caused cross-tier interference is minimized. We also present an analytical formulation of the resource allocation problem and a suboptimal heuristic algorithm. Finally, we propose a practical network procedure enabling this scheme in the cellular network.

The remainder of this section is organized as follows. Section 6.3.1 describes the topology as well as the system model where the problem is framed. The proposed scheme consisting of the spatio-temporal estimation, the resource allocation step and the overall network procedure, is presented in section 6.3.2. Section 6.3.3 shows performance evaluation results and conclusions are drawn in section 6.5.

6.3.1 System Architecture and Model

The considered topology shown in Fig. 35 consists of an MBS with several MUs in the sourroundings of the femtocell. The femtocell network is located within the coverage region of the macrocell and the FAP serves its FUs by using a closed subscriber group approach. The analyzed interference scenario is cross-tier, i.e. the interference between femtocell and MUs.

In order to maintain the generality of different types of systems, we consider resources as generic channels that are allocated by both macrocell and femtocell base stations to its users. The SINR per channel is obtained by utilizing the following expression:

$$SINR_n = \frac{P_n}{L(I_n + P_N)} \tag{50}$$

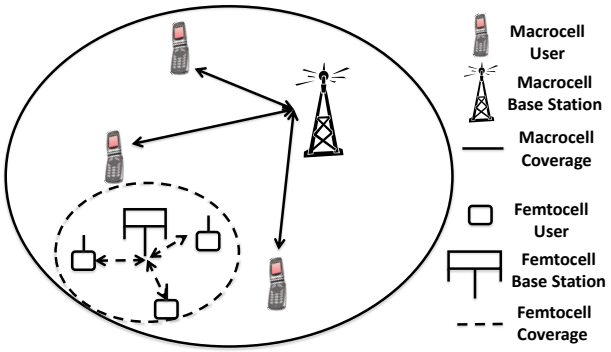

Figure 35. The Considered Topology

where P_n and I_n are the transmitted power and the received interference power on channel n, respectively, and P_N is the noise power. L is the propagation pathloss between transmitter and receiver. The propagation pathloss both for indoor, outdoor and indoor to outdoor environments follow the channel models suggested by 3GPP [130], as shown by Eqs. (51), (52) and (53).

- Indoors

$$L = 38.46 + 20 \log_{10} d_i + 0.7 d_i \quad (dB) \tag{51}$$

- Outdoors

$$L = 15.3 + 37.6 \log_{10} d_o \quad (dB) \tag{52}$$

- Indoors-to-outdoors

$$L = 15.3 + 37.6 \log_{10} d_i + F \quad (dB) \tag{53}$$

Here, f is the frequency in MHz, d_i is transmitter-receiver distance measured in meters and d_o distance measured in kilometers. F is the log-normal shadow fading random variable with a standard deviation of 8.9 dB.

Finally, the signal power can be obtained from the temporal signal $s(k)$, where K is the number of samples:

$$P_s = \frac{1}{K} \sum_{k=1}^{K} s(k)^2 \tag{54}$$

6.3.2 Proposed Interference Management Scheme

In this section, we present our proposed interference management scheme.

6.3.2.1 Spatio-temporal Estimation

In order to estimate the received signal of the MBS at a new unknown location, we propose a spatio-temporal estimation module as shown in Fig. 36 with four basic operations.

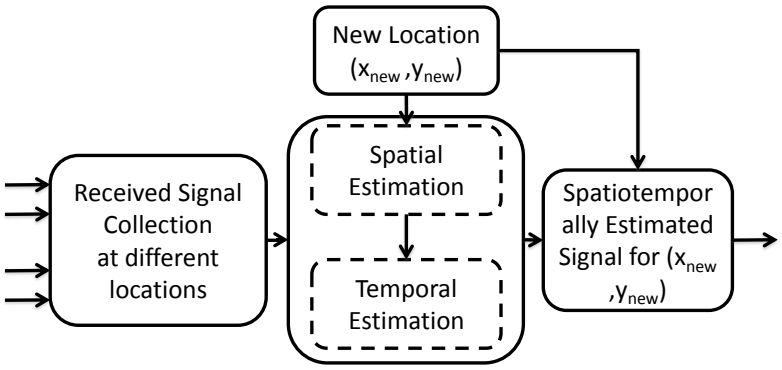

Figure 36. The proposed spatio-temporal estimation module

The module has four basic operations as it can be seen in Fig. 36, which are explained as follows:

- The users located at n different positions estimate their received SINR values $S(t, x_i, y_i)$ (usually via pilot estimation followed by interpolation) for a given time t. These values are sent to the MBS.

- The collected SINR $S(t, x_i, y_i)$ are given as inputs to the spatial estimator as shown in Fig. 36. The spatial estimator uses an ordinary Kriging estimation to predict received signal of the MBS $S(t, x_{new}, y_{new})$ for a new location with coordinates (x_{new}, y_{new}).

- The spatially estimated SINR $S(t, x_{new}, y_{new})$ is then temporally predicted using autoregressive models with orders 1 and 2, AR(1) and AR(2), for a monitoring period $T = 1, 2, .., t$.

- The module outputs $\hat{S}(t, x_{new}, y_{new})$, which is the spatio-temporally estimated received signal of the MBS, for a new location with coordinates (x_{new}, y_{new}).

In the following, the spatial and temporal estimations are analytically described.

The *spatial estimation* is performed by applying the ordinary Kriging interpolation method. This method collects $S(t, x_i, y_i)$, the received signal samples from the MBS at different locations with coordinates (x_i, y_i) at a given time t. It then estimates new SINR value for a new location with coordinates (x_{new}, y_{new}), by using the spatial correlation among the collected values. In order to achieve a spatial correlation based estimation, the Kriging interpolator uses the semivariogram analysis which is the characterization of the spatial correlation of the collected signals in a given random field. The semivariogram $\gamma_{(i,j)}$ of two signals $S(x_i, y_i)$ and $S(x_j, y_j)$ is calculated as:

$$\gamma_{(i,j)} = 0.5 \times E[((S(x_i, y_i) - S(x_j, y_j))^2]. \tag{55}$$

The steps of the Kriging based spatial estimation method are reviewed in the following. The spatially estimated SINR $S(t, x_{new}, y_{new})$ for a new location with coordinates (x_{new}, y_{new}) is given by:

$$S(t, x_{new}, y_{new}) = \sum_{i=1}^{n} [\lambda_i \times S(t, x_i, y_i)] \tag{56}$$

where $S(t, x_i, y_i)$ in Eq. 56 is the received signals from the MBS at different locations with coordinates (x_i, y_i) at a given time t and λ_i is the Kriging coefficient for the i^{th} location with coordinates (x_i, y_i). The λ_i in Eq. 56 is expressed as:

$$\lambda_i = \frac{\gamma_{(new,j)}}{\gamma_{(i,j)}} \; \forall \; i, j \tag{57}$$

where $\gamma_{(new,j)}$ is the semivariogram value of the the signal at position (x_{new}, y_{new}) and the signal with position (x_j, y_j). Note that the signal at (x_{new}, y_{new}) is the new position which we want to estimate and the signal at (x_i, y_i) is one of the collected signal. Moreover, $\gamma_{(i,j)}$ is the semivariogram value of the the signal at position (x_i, y_i) and the signal at position (x_j, y_j).

We consider again three semivariogram models in this work: The exponential semivariogram $\lambda_i^{(exp)}$, the gaussian semivariogram $\lambda_i^{(gauss)}$ and the linear semivariogram $\lambda_i^{(lin)}$. These are expressed respectively by the Eqs. (58), (59) and (60) as follows.

$$\lambda_i^{(exp)} = \frac{\gamma_{(new,j)}}{\gamma_{(i,j)}} = \frac{c(1 - e^{[-3\times\frac{\sqrt{(x_{new}-x_j)^2+(y_{new}-y_j)^2}}{a}]})}{c(1 - e^{[-3\times\frac{\sqrt{(x_i-x_j)^2+(y_i-y_j)^2}}{a}]})} \tag{58}$$

$$\lambda_i^{(gauss)} = \frac{\gamma_{(new,j)}}{\gamma_{(i,j)}} = \frac{c(1 - e^{[-3\times\frac{(x_{new}-x_j)^2+(y_{new}-y_j)^2}{a}]})}{c(1 - e^{[-3\times\frac{(x_i-x_j)^2+(y_i-y_j)^2}{a}]})} \tag{59}$$

$$\lambda_i^{(lin)} = \frac{\gamma_{(new,j)}}{\gamma_{(i,j)}} = \frac{c + a \times \sqrt{(x_{new} - x_j)^2 + (y_{new} - y_j)^2}}{c + a \times \sqrt{(x_i - x_j)^2 + (y_i - y_j)^2}}. \tag{60}$$

In Eqs. (58) ,(59) and (60), the parameter c is the *sill* value which represents the maximum spatial correlation level for any two points and a is the *range* value which represents the longest Euclidian distance between two points at which these two points have reached the sill value. In other words, a is the lag distance for the two points having the highest spatial correlation value.

The spatially estimated SINR, if the received signals in the random field are exponentially distributed, can be expressed by inserting Eq. (58) into Eq. (56) as follows:

$$S^{(exp)}(t, x_{new}, y_{new}) = \sum_{i=1}^{n}[\frac{c(1 - e^{[-3\times\frac{\sqrt{(x_{new}-x_j)^2+(y_{new}-y_j)^2}}{a}]})}{c(1 - e^{[-3\times\frac{\sqrt{(x_i-x_j)^2+(y_i-y_j)^2}}{a}]})} \times S(t, x_i, y_i)] \; \forall \; j. \tag{61}$$

The spatially estimated SINR, if the received signals in the random field are gaussian distributed, can be expressed by inserting Eq. (59) into Eq. (56) as follows:

$$S^{(gauss)}(t, x_{new}, y_{new}) = \sum_{i=1}^{n}[\frac{c(1 - e^{[-3\times\frac{(x_{new}-x_j)^2+(y_{new}-y_j)^2}{a}]})}{c(1 - e^{[-3\times\frac{(x_i-x_j)^2+(y_i-y_j)^2}{a}]})} \times S(t, x_i, y_i)] \; \forall \; j. \tag{62}$$

The spatially estimated SINR of the received signal from the MBS at a new location (x_{new}, y_{new}), if the received signals in the random field are linearly distributed, can be expressed by inserting Eq. (60) into Eq. (56) as:

$$S^{(linear)}(t, x_{new}, y_{new}) = \sum_{i=1}^{n}[\frac{c + a \times \sqrt{(x_{new} - x_j)^2 + (y_{new} - y_j)^2}}{c + a \times \sqrt{(x_i - x_j)^2 + (y_i - y_j)^2}} \times S(t, x_i, y_i)] \; \forall \; j. \tag{63}$$

The *temporal estimation* of the spatially estimated signals which are expressed by Eqs. (58), (59) and (60) can be found by using *AutoRegressive Model* with order p ($AR(p)$). Thus, the spatio-temporal estimation of the received signal from the MBS at a new location with coordinates (x_{new}, y_{new}) is given by $\hat{S}(t, x_{new}, y_{new})$ and expressed as:

$$\hat{S}(t, x_{new}, y_{new}) = \beta_0 + [\sum_{n=1}^{p} \beta_n \times S(t-n, x_{new}, y_{new})] \tag{64}$$

where β_0 and β_n are the coefficients of the autoregressive model which are calculated using ordinary least squares (OLS) method as:

$$\beta_n = \frac{\sum_{i=1}^{n}(S(t-i)S(t) - nE[S(t-i)S(t)])}{\sum_{i=1} n(S^2(t-i) - nE[S_2(t-i)])} \tag{65}$$

and

$$\beta_0 = E[S(t)] - \sum_{i=1}^{n} \beta_i \times E[S(t-i)] \tag{66}$$

6.3.2.2 Resource Allocation

In this section, we formulate the problem of allocating resources at the FAP as an optimization problem exploiting the previously estimated interference at the FUs. Let $\mathcal{F}$ and $\mathcal{M}$ be the number of FUs and MUs, respectively, and N the total number of channels available at the femtocell. Let $\alpha(u, n)$ be a binary indicator that contains 1 if channel n is assigned to user u or 0 otherwise. We define a matrix P^F of $\mathcal{F}$ rows and N columns that contains the femtocell power allocation. If the user i is assigned the channel j with transmission power p, then the ij^{th} element of P^F will contain the value p. Let I_{un} be the interference power estimated at FU u on channel n. Given that we want to minimize the cross-tier interference, the objective function to be minimized is the total employed power, i.e. the sum of all the elements of P^F, as shown by Eq. (67).

The optimization problem can be formulated as follows:

$$\min_{P,\alpha} \sum_{u=1}^{\mathcal{F}} \sum_{n=1}^{N} P^F_{un} \cdot \alpha(u, n), \tag{67}$$

subject to:

$$C1: \frac{P^F_{un}}{L^F_u(I_{un} + \sigma^2)} \geq \beta^F \alpha(u, n) \quad \forall n, \forall u = 1, ..., \mathcal{F}$$

$$C2: \frac{(\sum_{u=1}^{\mathcal{F}}\sum_{n=1}^{N} P_{un}^{F})^2}{M(\sum_{n=1}^{N} P_{un})^2} = 1$$

$$C3: \sum_{u=1}^{\mathcal{F}} \alpha(u,n) = 1 \quad \forall n$$

$$C4: \frac{S_{un}^{M}}{\frac{1}{L_u^M}\sum_{u=1}^{M} P_{un}^{F} + \sigma^2} \geq \beta^M \gamma(u,n) \quad \forall n, \forall u = 1, ..., \mathcal{M}$$

$$P_{un}^{F} \geq 0, \quad \alpha(u,n), \gamma(u,n) \in \{0,1\} \quad \forall n, \forall u = 1, ..., \mathcal{F},$$

where C1 sets the SINR constraint to β^F on every channel n allocated to FU u; C2 is the fairness constraint among FUs implemented by a Jain's fairness index of 1 guaranteeing that all users will receive same power [131]; C3 ensures that no interference will appear among FUs in any channel; and C4 sets the SINR constraint for the MUs, where $\gamma(u,n)$ is a known function containing the macrocell channel allocation.

The problem specified by Eq. (67) and constraints C1 to C4 is not a convex optimization problem and cannot be solved by standard methods in optimization theory. Therefore, we propose an alternative simple heuristic algorithm as shown in Algorithm 1. This algorithm assumes interference minimization is effectively achieved by minimizing femtocell transmit power. The idea is summarized as follows: Channels are assigned to users based on their requested power to achieve the target SINR. Users with channels requesting a lesser amount of power are served first and fairness is guaranteed by trying to assign the same number of channels to each user.

6.3.2.3 Network Implementation Procedure

The above resource allocation procedure must be performed at the FAP. For this, we need a network procedure that allows the exchange of signalling information between the macrocell and the femtocell taking place over the air or via the backhaul network. It is not realistic to assume known at the MBS the position of the MUs; however, the FAP can perform estimations on the location of both the femtocell and close-by MUs since the femtocell itself

Algorithm 1

Maximum number of channels per user
$max\_channels \leftarrow \lceil \frac{N}{M} \rceil$
Power requested for each user in each channel
for $u \leftarrow 1, M$ **do**
    for $n \leftarrow 1, N$ **do**
        $P_{un}^{req} = \beta^F \left(I_{un} + \sigma^2 \right) L_u^F$
    end for
end for
Channel and power allocation
while $P^{req} \neq \emptyset$ **do**
    $[p^*, u^*, n^*] \leftarrow minP^{req}$
    if *Channels assigned to* $u^* < max\_channels$ **then**
        Remove column n^* *from* P^{req}
        $P(u^*) \leftarrow P(u^*) + p^*$
    else
        Remove row u^* *from* P^{req}
    end if
end while

will be aware of its location via e.g., a GPS receiver. Techniques based on signal strength or more sophisticated MIMO approaches based on direction-of-arrival estimation could be employed. The procedure enabling this exchange of information is described as follows:

1. The FAP estimates the users' locations and sends them to the MBS along with their identification. This information is available at the FAP since both femtocell subscribers and non-subscribers can attempt to camp on the femtocell.

2. MUs provide SINR feedback to the MBS, and users interfering with the femtocell will be identified.

3. The MBS, using its own users' location information and their received signal attributes, runs the spatio-temporal framework to estimate the interference at the FUs' location for a certain period of time.

4. Interference power values are sent back from the MBS to the femtocell.

5. The FAP runs a resource allocation algorithm exploiting the estimated interference values.

6. The procedure is repeated once the estimation period expires or the FUs substantially change locations.

Overall, only some signaling information need to be exchanged between macrocell and femtocell. The necessary amount of such information is another interesting research question, since spatial correlation properties of both the femtocell and MUs could be exploited to reduce the amount of exchanged data.

In order to guarantee certain QoS at the MUs, this scheme could be reciprocally triggered at the macrocell to estimate and optimize the amount of interference that FUs are causing to MUs. In addition, this interference estimation approach can be utilized to improve other power control based interference management schemes (such as the one in [117]) whose performance may be undermined by inaccurate interference estimation.

6.3.3 Performance Evaluation

We perform several experiments with the objective of evaluating the performance of the different proposed spatio-temporal estimators. The scenario is similar to the one depicted in Fig. 35, with five MUs radomly deployed in the surroundings of the femtocell (up to 40 meters). We perform simulations for one single femtocell with a varying number of users suffering from cross-tier interference and randomly deployed in a coverage radius of 20 meters. The relevant simulation parameters common to all the experiments are shown in Table 7.

The first experiment investigates how the different estimation approaches affect the total transmit power of the femtocell, i.e., the interference caused to the macrocell. A total number of six spatio-temporal techniques are to be simulated, combining the three spatial schemes (linear, exponential and Gaussian) and two temporal autorregresive models of order one and two, as shown in Fig. 37. The number of FUs is fixed to four and the

Table 7. Simulation parameters

Carrier frequency (f_c)	$2\ GHz$
Simulation time	$500\ ms$
Noise power (σ^2)	$-115\ dBm/channel$
MBS coverage distance	$1km$
MBS transmission power	$42dBm$
Number of MUs	5
Femtocell range	$20m$
FAP maximum transmission power	$0.375mW/channel$
Femto user SINR requirements	$15\ dB$

Y-axis represents the number of available channels at the femtocell. The results show significant differences among the spatial approaches, being the linear estimator the lowest-energy interference estimator and therefore allowing the FAP to satisfy users' requirements causing the lowest cross-tier interference.

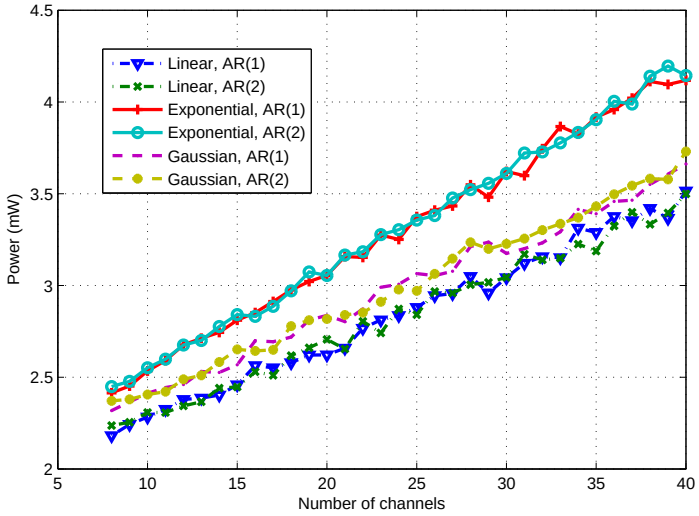

Figure 37. Femtocell transmit power with number of available channels.

Figure 38 shows the results of the next experiment, where we compare the quality of the spatio-temporal linear estimator (of AR order 1) with other interference estimation approaches. The interference signal is generated at the MBS, delivered to the MUs and measured at the FUs. The optimal femtocell power corresponds to the minimum value that is needed to meet SINR constraints at the FUs. We seek the closest scheme to this curve, knowing that excessive power will cause more interference and not enough power will not

allow FUs achieve their requirements. We compare linear estimation with several schemes: An estimation-free approach where power is allocated based on distance and interference is neglected, a maximum power approach delivering the maximum allowable power in each channel, and a conventional FAP interference estimation scheme where macrocell signal is estimated directly at the FAP from the received signal strength and the pathloss formula. The spatio-temporal estimation is the closest curve to the optimal one, and the conventional FAP approach happens to deliver a much larger power value than the spatio-temporal one.

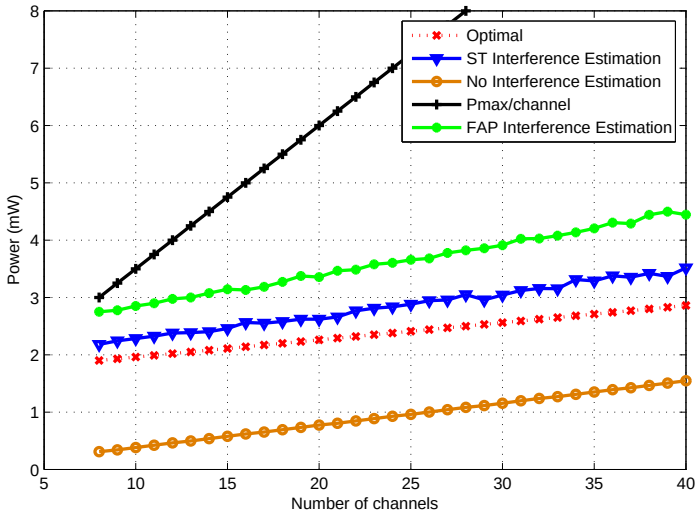

Figure 38. Femtocell transmit power for different interference estimation methods.

The last two experiments are depicted in Fig. 39 and Fig. 40, respectively. The first one shows the total femtocell power allocation for an increasing number of FUs in the three spatial estimation cases. Since requirements are set in terms of SINR per assigned channel and fairness must be satisfied, the larger the number of users the larger the flexibility to minimize total power. Figure 40 explores the inaccuracy of the power assignment when the FUs move away from the locations utilized for the spatial estimation. The X-axis shows the magnitude of the displacement although the distance to the FAP is kept constant. The Y-axis shows the difference of the *old-coordinates* and the *new-coordinates* power allocations. Clearly, the Gaussian estimator is the most sensitive one to the changes in the users' location, an interesting result since the location information exchange is a signalling

overhead that should be kept as low as possible.

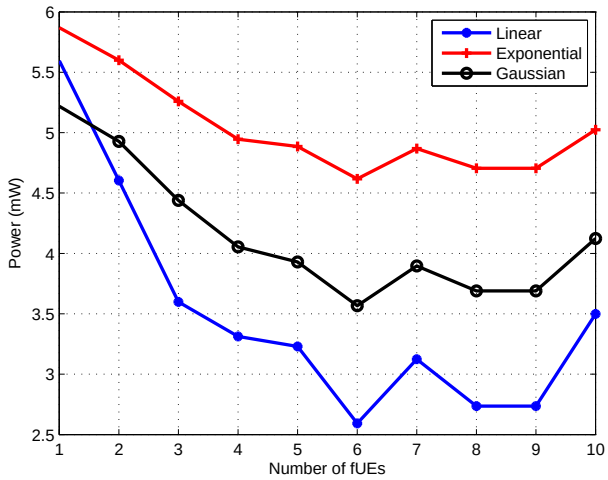

Figure 39. Femtocell transmit power with number of FUs.

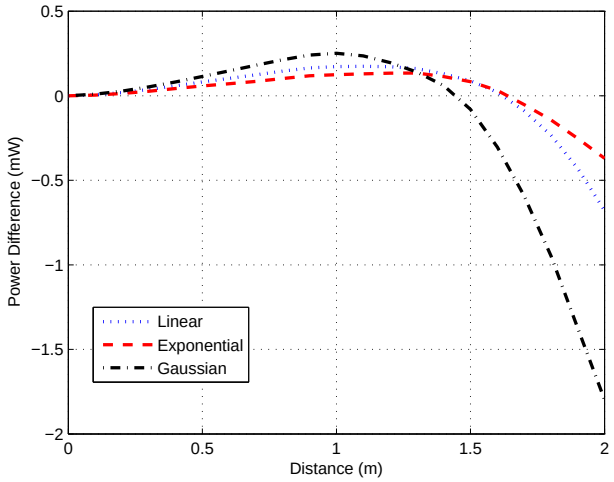

Figure 40. Power mismatch with fUEs movement.

6.4 Resource Management in Hybrid Femtocells

In this section, we explore the hybrid access mode of femtocells to mitigate interference while satisfying users' requirements. Fort this, we develop an analytical model of the FU activity profile to study which channels are the best to be operated in open access mode. Our model assumes that the FUs have priority over the MUs since the femtocell customers

are the owners of the FAPs. In our study, if an MU is connected to the femtocell while an FU is in need of the resources used by the MU, the MU will vacate the channel. To the best of our knowledge, this priority of FUs is not considered in existing works. The study of the hybrid access mode proposed in this paper allows to identify which channels are the best option for MUs depending on the SINR experienced by the users on each channel and the amount of time an FU is using these channels. The results motivate the need for novel resource management schemes which dynamically adapt the set of channels operating open access mode depending on the network conditions.

This section is organized as follows. In Section 6.4.1, we describe the system model to study the activity profile of FUs. In Section 6.4.2, we derive expressions for several performance parameters for MUs from the model in Section 6.4.1. In Section 6.4.3, we discuss and compare the numerical results.

6.4.1 Femtocell User Activity Profile Model

In this section, we present a model of the FU activity profile. We consider a single femtocell with C available channels, from which $C_m \leq C$ are operating open access mode. Each channel experiences different signal and interference levels and therefore the data rate achieved in each channel is different. The data rate on channel i is R_i bit/second. We consider that one specific channel has the same average radio characteristics, e.g., SINR, for all users (FUs and MUs) and which are static during the period of time under consideration.

The traffic can be mainly classified in two different types, namely, elastic traffic and streaming traffic [132]. *Elastic traffic* corresponds to the transfer of digital documents. *Streaming traffic* corresponds to real-time services. In case of elastic traffic, the session duration depends on the data rate received. High data rates entail shorter session durations. In case of streaming traffic, the session duration only depends on the user behavior. We consider that FUs generate streaming traffic, but the model could be extended to the case of elastic traffic.

6.4.1.1 System Model

We model the activity profile of FUs using a multidimensional Continuous-Time Markov Chain (CTMC), which is shown in Fig. 41. The system state vector $\boldsymbol{x}$ is described by the C-tuple $\boldsymbol{x} = (x_1, \ldots, x_C)$, where x_i takes value 0 when the channel i is idle and 1 when it is used by an FU (busy). We consider that one FU session uses one channel, therefore the number of FUs connected to the femtocell at state $\boldsymbol{x}$ is represented by $N(\boldsymbol{x}) = \sum_{i=1}^{i=C} x_i$.

We consider a finite user population with M FUs. The arrival rate λ at state $\boldsymbol{x}$ is given by

$$\lambda(\boldsymbol{x}) = (M - N(\boldsymbol{x}))\lambda_f, \tag{68}$$

where λ_f refers to the arrival rate for one iddle FU.

Incoming FUs access the channels by following an order, namely, the FUs access the channels by choosing the most preferred channel among all the available idle channels. The most preferred channel ($i = 1$) is the channel having the highest data rate, while the least preferred channel ($i = C$) is the channel having the lowest data rate. If there are no idle channels, i.e., all of them are occupied by FUs, an incoming FU is blocked out of the femtocell. For the sake of mathematical tractability, we consider exponentially distributed session durations for FUs, and $1/\mu$ is the average session duration.

We consider that MUs generate packets with a fixed size $L = L_H + L_D$ bits, where L_H and L_D are, respectively, the header and payload lengths. The MUs use the channels operated in open access mode not used by FU traffic. We consider that the MUs are in saturation, i.e., there are always MUs waiting for free channels. Therefore, for this study, it is not relevant which channels the MUs choose first when they access the femtocell. Upon an FU arrival, MUs vacate the channel chosen by the FU and the MU packet that is being transmitted is lost, i.e., we consider a preemptive and non-resume access control policy. Thus, when the MUs access a higher number of preferred channels, MU transmissions are more likely to be interrupted. It is under study in this work, how many channels and which channels are assigned as open access mode to MUs.

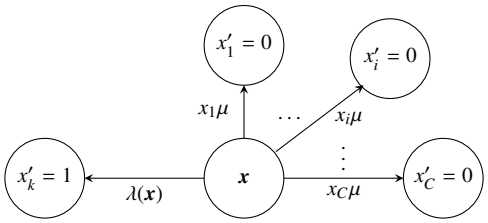

Figure 41. State transitions of the CTMC which model the FU activity profile.

The state transitions of the CTMC under study occur when a new FU session connects to the femtocell or when any FU session is finished. The state $\boldsymbol{x}'$ represents the state achieved by the femtocell after a state transition and $q_{xx'}$ is the transition rate from $\boldsymbol{x}$ to $\boldsymbol{x}'$. The transition matrix $\boldsymbol{Q}$ when the states are lexicographically sorted can be easily obtained by using the $q_{xx'}$. This is shown in Fig. 41. The channel states from $\boldsymbol{x}'$ that are not represented in Fig. 41 keep the same status as in $\boldsymbol{x}$ and the kth channel is the channel with $k = \min\{(i) \mid x_i = 0\}$. Note that in state $\boldsymbol{x}$ only one transition can occur due to an arrival of an FU, while up to $N(\boldsymbol{x})$ different transitions can occur when an FU finishes its service. Let $\boldsymbol{\pi}$ denote the vector of stationary probabilities obtained by using the global balance equations and the normalization equation given by

$$\pi(\boldsymbol{x}) \sum_{\forall \boldsymbol{x} \neq \boldsymbol{x}'} q_{xx'} = \sum_{\forall \boldsymbol{x}' \neq \boldsymbol{x}} q_{x'x}\pi(\boldsymbol{x}'); \quad \sum_{\forall \boldsymbol{x}} \pi(\boldsymbol{x}) = 1. \tag{69}$$

6.4.1.2 Characterization of Idle and Busy Periods

Our goal is to characterize the time intervals when an arbitrary channel is used by an FU (busy period, B_i) and the time intervals when an arbitrary channel is not used by any FU (idle period, I_i). Therefore, the busy period B_i corresponds to the channel holding time of FUs in channel i, which is exponentially distributed with rate μ $\forall i$. The idle period I_i corresponds to the period of time spent in the set of states with $x_i = 0$. Hence, the idle period follows a phase type distribution, which defines the time until absorption ($x_i \rightarrow 1$) in an Absorbing Markov Process (AMP) [133] and it is represented by $PH(\boldsymbol{\alpha}, \boldsymbol{S})$, where $\boldsymbol{S}$ is the transition matrix which conteins the transition rates between the states and $\boldsymbol{\alpha}$ is the initial state probability vector.

For each channel i, a different AMP is defined $PH(\boldsymbol{\alpha}_i, \boldsymbol{S}_i)$. The AMP is initiated when channel i becomes idle and the absorption occurs when it becomes busy. Therefore, the matrix $\boldsymbol{S}_i$ is obtained from $\boldsymbol{Q}$ by removing the rows and the columns corresponding to the states where channel i is busy. The probabilities $\boldsymbol{\alpha}_i$ are the normalized probabilities of initiating the process at each of the states where $x_i = 0$, given by:

$$\boldsymbol{\alpha_i} = \frac{1}{\sum_{\forall \boldsymbol{\pi}_{x_i=1}} \boldsymbol{\pi}_{x_i=1} \boldsymbol{Q}_{x_i=1, x_i'=0}} \boldsymbol{\pi}_{x_i=1} \boldsymbol{Q}_{x_i=1, x_i'=0}, \tag{70}$$

where $\boldsymbol{\pi}_{x_i=1}$ is a row vector with the probabilities for the busy states and $\boldsymbol{Q}_{x_i=1, x_i'=0}$ is a matrix with transition rates from busy states to idle states.

The cumulative distribution function corresponding to the idle period of channel i is $F_{I_i}(t) = 1 - \boldsymbol{\alpha}_i e^{t\boldsymbol{S}_i} \mathbf{1}$, where $\mathbf{1}$ is the unity vector. The average time in which the channel i is idle corresponds to the mean time until absorption in the $PH(\boldsymbol{\alpha_i}, \boldsymbol{S}_i)$ AMP distribution and it is given by

$$E[I_i] = -\boldsymbol{\alpha}_i \boldsymbol{S}_i^{-1} \mathbf{1}. \tag{71}$$

6.4.2 Performance Metrics for Macrocell Users

In this section, we derive the analytical expressions for several performance parameters for MUs, by starting from the model defined in Section 6.4.1.

The probability that at least n packets of length L, corresponding to nL bits, are transmitted during the idle period I_i of the channel i is

$$p_i(n) = P\left(I_i \geq \frac{nL}{R_i}\right) = 1 - F_{I_i}\left(\frac{nL}{R_i}\right) = \boldsymbol{\alpha}_i e^{\frac{nL}{R_i}\boldsymbol{S}_i} \mathbf{1}, \tag{72}$$

where R_i is the data rate on channel i.

The maximum achievable throughput for MUs in the channel i, γ_i, is defined as the average successfully transmitted data bits during an idle period divided by the total average time of idle plus busy periods. The average number of successfully transmitted data bit in

channel i, $\overline{D}_i$, is

$$\begin{aligned}\overline{D}_i &= L_D \sum_{n=1}^{\infty} p_i(n) = L_D \alpha_i \left(\sum_{n=0}^{\infty} \left(e^{\frac{L}{R_i} \boldsymbol{S}_i} \right)^n - 1 \right) \mathbf{1} \\ &= L_D \alpha_i e^{\frac{L}{R_i} \boldsymbol{S}_i} \left(\boldsymbol{I} - e^{\frac{L}{R_i} \boldsymbol{S}_i} \right)^{-1} \mathbf{1},\end{aligned} \tag{73}$$

where $\boldsymbol{I}$ is the identity matrix and L_D refers to the payload length. From (71), (73) and knowing that the busy period B_i is exponentially distributed with mean $1/\mu$, the throughput γ_i for the channel i is given by

$$\gamma_i = \frac{\overline{D}_i}{\overline{I}_i + \overline{B}_i} = \frac{L_D \alpha_i e^{\frac{L}{R_i} \boldsymbol{S}_i} \left(\boldsymbol{I} - e^{\frac{L}{R_i} \boldsymbol{S}_i} \right)^{-1} \mathbf{1}}{-\boldsymbol{\alpha}_i \boldsymbol{S}_i^{-1} \mathbf{1} + 1/\mu}. \tag{74}$$

The total achievable throughput is the sum of the achievable throughputs in the C_m channels operated in open access mode,

$$\gamma_T = \sum_{\forall i \in OA} \gamma_i. \tag{75}$$

During an idle period of time there are $\Phi_i = D_i/L_D$ successfully transmitted packets on the channel i and one packet interrupted by an FU arrival. The probability that an MU packet is interrupted on the channel i is $\xi_i = 1/(\overline{\Phi}_i + 1)$ and the number of transmitted packets per time unit on the channel i is $(\overline{\Phi}_i + 1)/(\overline{I}_i + \overline{B}_i)$. Therefore, the global MU interruption probability ξ_G is obtained by dividing the sum of interrupted transmissions per time unit of each channel operated in open access mode by the total transmissions per time unit in the same channels. This is given by

$$\begin{aligned}\xi_G &= \frac{1}{\sum_{\forall j \in OA} \frac{\overline{\Phi}_j + 1}{\overline{I}_j + \overline{B}_j}} \sum_{\forall k \in OA} \frac{\overline{\Phi}_k + 1}{\overline{I}_k + \overline{B}_k} \xi_k \\ &= \frac{\sum_{\forall k \in OA} \frac{1}{-\boldsymbol{\alpha}_k \boldsymbol{S}_k^{-1} \mathbf{1} + 1/\mu}}{\frac{\gamma_T}{L_D} + \sum_{\forall j \in OA} \frac{1}{-\boldsymbol{\alpha}_j \boldsymbol{S}_j^{-1} \mathbf{1} + 1/\mu}}.\end{aligned} \tag{76}$$

Finally, the consumed energy per successfully transmitted data bit on the channel i for MUs, Eb_i, is computed as the energy consumed by the MUs when they are transmitting

plus the energy consumed due to the channel monitoring when channel i is occupied by an FU. The average consumed energy per successfully transmitted data bit, $\overline{Eb}$, results from weighting the average energy consumed $\overline{Eb_i}$ per successfully transmitted data bit on each channel i operated in open access mode by the corresponding fractions of throughput in each channel i. This leads to

$$\overline{Eb_i} = \frac{P_{TX}\overline{I}_i + P_s\overline{B}_i}{L_D\overline{\Phi}_i}, \quad ; \qquad \overline{Eb} = \sum_{\forall i \in OA} \frac{\gamma_i}{\gamma_T}\overline{Eb_i} \tag{77}$$

where P_{TX} is the FAP average transmission power, P_s is the average power consumed to monitor which channels are occupied by FUs, L_D stands for the payload length and Φ_i refers to the successfully transmitted packets in channel i.

6.4.3 Performance Evaluation

6.4.3.1 Parameter Setting

In this section, we define the values of the parameters considered in the model. In commercial systems such as LTE, OFDMA is used. The frequency domain is divided into non-overlapping subchannels which occupy a bandwidth of 180kHz. The time domain is divided into slots of 1ms. These subdivisions in time and frequency referred to as resource blocks (RBs), are the smallest time-frequency units that can be assigned to an user and correspond to a set of twelve adjacent subcarriers and seven OFDM symbols [134].

As previously pointed out, each channel experiences different SINR levels and therefore the data rate achieved for the MUs in each channel is considered to be different for each channel. In Table 8, the different data rates per RB are detailed depending on the experienced SINR levels [135]. Each RB corresponds here to one channel. We consider a femtocell with $C = 8$ channels. Unless otherwise stated, the data rates achieved by each of the 8 channels are chosen from table 8 by considering the channels with the best data rate, i.e. $R_1 = 792$ kbit/s, $R_2 = 715.96$ kbit/s ... $R_8 = 282.26$ kbit/s.

Since we consider a system with finite population, the offered FU traffic (in Erlangs) to

Table 8. Bitrates achieved per RB as function of the SINR [135]

#	SINR (dB)	R_i (in kbit/s/RB)
1	SINR $\geq$ 22.05	792.00
2	19.91 $\leq$ SINR $<$ 22.05	715.96
3	17.78 $\leq$ SINR $<$ 19.91	640.30
4	15.64 $\leq$ SINR $<$ 17.78	565.27
5	13.50 $\leq$ SINR $<$ 15.64	491.22
6	11.37 $\leq$ SINR $<$ 13.50	418.75
7	9.23 $\leq$ SINR $<$ 11.37	348.69
8	7.09 $\leq$ SINR $<$ 9.23	282.26
9	4.96 $\leq$ SINR $<$ 7.09	221.00
10	2.82 $\leq$ SINR $<$ 4.96	166.64
11	0.68 $\leq$ SINR $<$ 2.82	120.73
12	$-1.45 \leq$ SINR $<$ 0.68	84.09
13	$-3.59 \leq$ SINR <-1.45	56.54
14	$-5.73 \leq$ SINR <-3.59	36.93
15	$-7.86 \leq$ SINR <-5.73	23.60
16	$-10 \leq$ SINR <-7.86	14.85
17	$SINR < -10$	0.00

the system is given by

$$\rho_f = \frac{M}{C}\frac{1/\mu}{1/\lambda_f + 1/\mu} = \frac{M}{C}\frac{\lambda_f}{\lambda_f + \mu}. \tag{78}$$

Unless otherwise stated, the arrival rate per idle FU is chosen to be $\lambda_f = 100\ s^{-1}$, the average channel holding time is $1/\mu = 10$ ms, the packet header length is $L_H = 500$ bits and the total packet size is $L = 4$ kbits. The FU population is $M = 8$. The offered FU traffic as function of these values is $\rho_f = 0.5$. The FAP average transmission power is $P_{TX} = 10$ dBm and the average transmission power consumed to monitor which channels are occupied by FUs is $P_s = 0$ dBm.

6.4.3.2 Numerical Results

In this section, we compare the MU maximum achievable throughput and the interruption probability obtained when the channels operated in open accessmode have the highest data rate, i.e. $i = 1, \ldots, C_m$ and when they have the lowest data rate, i.e. $i = C + 1 - C_m, \ldots, C$.

In Fig. 42, the MU maximum achievable throughput γ_T in (75) is shown as a function of

the packet size L. We can see that for the same value of channels operated in open access-mode C_m, higher throughputs are achieved when the open access channels have the lowest data rate (Fig. 42(a)) than when they have the highest data rate (Fig. 42(b)). This can be explained as follows. The FUs use first the channels with the highest data rate and therefore there are more interruptions which reduce the contribution of these channels to the total throughput, despite having higher data rates. When C_m is small and the open access channels are the channels with the lowest data rates (Fig. 42(a)), having one more open access channel leads to higher gains. When C_m is high, the gain of having one more open access channel is smaller because this channel is used by an FU with a higher probability. This effect is more significant for high L as longer MU packets experience more interruptions. The opposite occurs when the open access channels have the highest data rate (Fig. 42(b)). Regarding the influence of the packet size, the achievable throughput has a maximum for a given L. This is due to the fact that for a smaller packet size L, more header information is transmitted, and for longer packet size L, there are more interruptions.

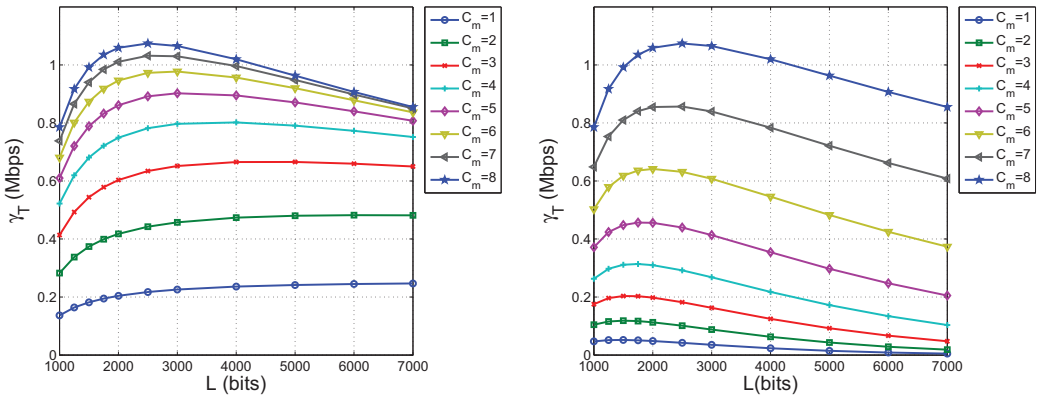

(a) Open access channels with the lowest data rates

(b) Open access channels with the highest data rates

Figure 42. Maximum achievable throughput γ_T in Mbps for MU vs. L for different sets of open channels operated in open access mode.

The interruption probability ϵ_G in (76) is shown in Fig. 43. It can be clearly seen that when the open access channels are the channels with the highest data rate (Fig 43(b)) the interruption probability ϵ_G is higher than when the channels with the lowest data rate are

chosen (Fig. 43(a)). This happens because the FUs use first the channels with the highest data rate.

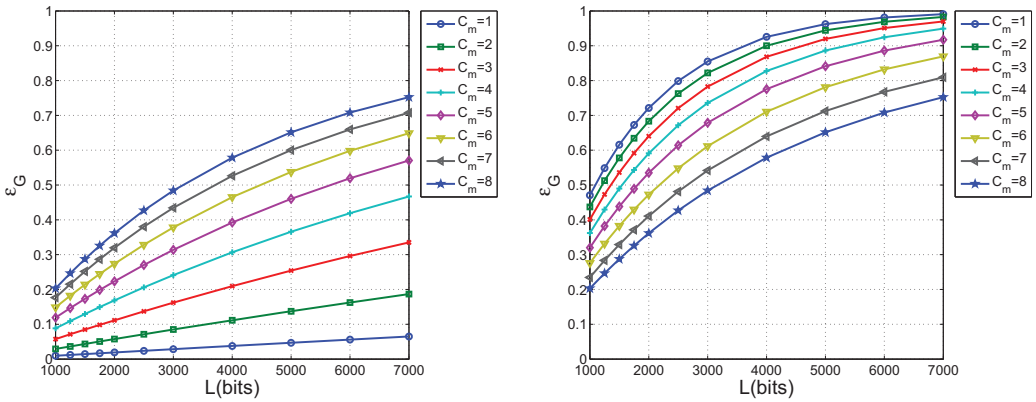

(a) Open access channels with the lowest data rates

(b) Open access channels with the highest data rates

Figure 43. Interruption probability ϵ_G vs. L for different sets of open channels operated in open access mode.

In Fig. 44, results considering different sets of data rates for each channel are shown. We consider $R^{(1)}$ as the set of data rates defined in Section 6.4.3.1 and $R^{(2)}$ are the set of data rates with values from Table 8 corresponding to rows #1, 3, 5, 7, 10, 12, 14 and 16 . We have $R_8^{(1)} = 0.356R_1^{(1)}$ and $R_8^{(2)} = 0.019R_1^{(2)}$. For $R^{(1)}$, it is better to operate in open access mode the channels with the lowest data rate. However, for $R^{(2)}$, the channels with the highest data rate yield better performance. This can be explained as follows. When the difference of data rates among channels is significant, the data rate achieved in the worst channels is too small, and it is better to access the best channels with higher data rates, despite having more interruptions.

When the set of channels operated in open access mode have the highest data rate, the performance only has better results when the difference of data rates among channels is very significant ($R^{(2)}$). Since common scenarios does not present these asymmetrical data rates, from now on $R^{(1)}$ is considered, and the set of channels operated in open access mode are considered to be the channels with the lowest data rate.

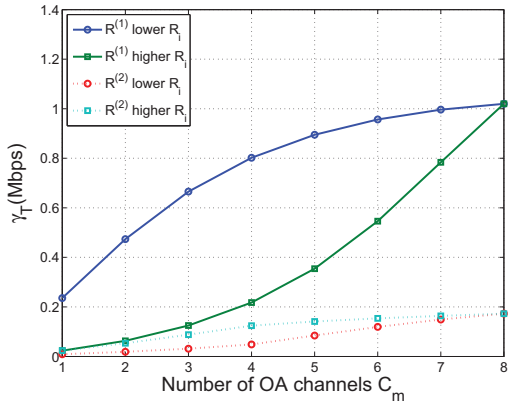

Figure 44. Maximum achievable throughput γ_T in Mbps for MU vs. C_m for different sets of data rates $R^{(1)}$ and $R^{(2)}$.

In Fig. 45, we show the maximum achievable throughput γ_T for MUs in (75) for different session durations while the offered traffic to the system ρ_f in (78) is kept constant. For small μ the FUs are using the same channel for longer time. This happens because the system varies more slowly, there are less interruptions and therefore, the γ_T is higher. The opposite effect can be seen for high μ. This is because the FUs are using and releasing channels faster, the MUs experience more interruptions and therefore γ_T is lower. It can be seen that the number of C_m channels reaches a point at which considering one more channel operated in open access mode does not contribute to increase in the throughput γ_T. This happens because the best channels are occupied and released continuously by the FUs, thus making these channels useless for MUs.

In Fig. 46, the average consumed energy $\overline{Eb}$ per successfully transmitted data bit for MUs in (77) is shown. We can see that given a number of channels operated in open access mode C_m, there is a value of L which makes the $\overline{Eb}$ minimum. This happens because when small packet sizes L are considered, more energy is consumed by the header bits. On the other hand, when long L is considered, more interruptions and more energy is consumed by bits of packets that are not successfully transmitted. Note that the values of L which make the $\overline{Eb}$ minimum are close to the values of L for which the γ_T is maximum, as shown in Fig. 42(a). Regarding the influence of the number of channels operated in open access

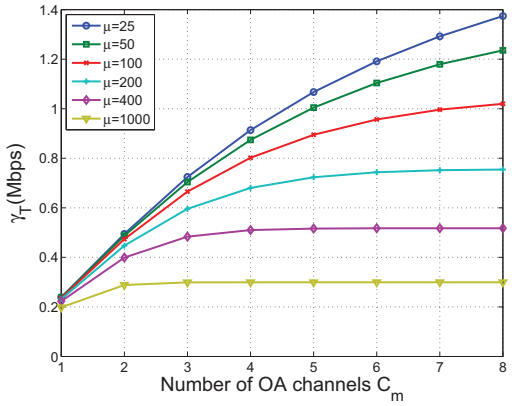

Figure 45. Maximum achievable throughput γ_T in Mbps for MU vs. C_m for different μ.

mode C_m, given a value of L, the value of $\overline{Eb}$ first decreases with C_m, reaches a minimum and then increases again. This happens because for small C_m, the transmission of a bit takes longer since the open access channels have low data rates. For high C_m, more interruptions occur and more power is wasted, despite having high data rates.

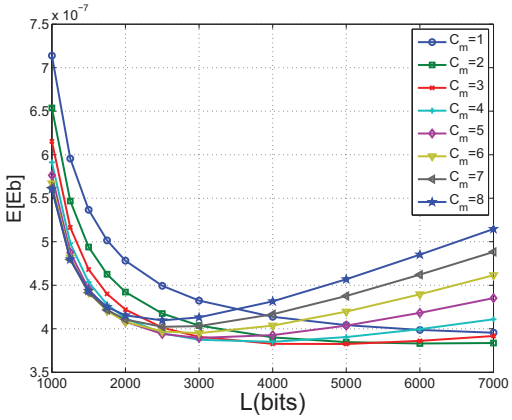

Figure 46. Consumed energy per successfully transmitted data bit $\overline{Eb}$ (J/bit) vs. L for different C_m.

6.5 Conclusions

Femtocells have emerged as an alternative for operators to improve indoor coverage and throughput. In this chapter, we have covered three aspects related to the interference challenge of femtocell networks. They are summarized in the following:

- First, given that several features of femtocells are left as implementation specific by the standard bodies, there exists a need for development and testing tools for femtocells. To fill this need, we created a femtocell modeling and development platform based on OPNET, a high-fidelity simulation environment. This platform closely follows 3GPP specifications regarding femtocells in terms of entities, functionalities, procedures, and message formats. We have shown that the platform effectively reflects the key concern of interference for femtocell networks.

- Second, we presented a spatio-temporal approach to estimate the downlink cross-tier interference in femtocell networks, an important part of the interference management problem that challenges two-tier networks. The scheme is composed of a spatial estimation step that makes use of an ordinary Kriging interpolator using semivariogram analysis followed by a temporal estimation step implemented by an autorregressive model. This estimation is exploited via a resource allocation algorithm, and the whole scheme is enabled through a network procedure. Simulation results show the validity and potential of this approach, establishing the linear estimator followed by an autorregressive model as the most suitable option to solve this problem.

- Third, we studied a hybrid access control mode in femtocell networks. We considered a preemptive and non-resume access control policy for the MUs. Different data rates for each channel were considered depending on the SINR experienced by the users. We assessed several performance parameters for MUs and we computed how many channels and which channels were the best channels to be operated in open access mode. The results show that, if the SINR levels experienced by the users in each channel are comparable, the best channels to be operated in open access are the channels with the lowest data rates. Otherwise, if the SINR achieved by the best channels are significantly higher than for the worst channels, it is better to operate the channels with the highest data rates in open access mode. In addition, we showed that

there is an optimal packet size for MU packets which maximizes the throughput and minimizes the average consumed energy per successfully transmitted data bit. We also demonstrated that for short session durations, the number of channels operated in open access reaches a point at which having more channels operated in open access do not entail any gain to the MU throughput. These results motivate the need for novel resource management schemes which can dynamically adapt the set of open access channels to the channel and network conditions.

CHAPTER 7

FEMTORELAYS

7.1 Introduction

Current deployments of small cell solutions face several major challenges that may inhibit their large-scale adoption: (i) cross-tier interference, (ii) co-tier interference, (iii) backhaul bottleneck, (iv) service degradation due to user mobility, and (v) privacy issues. The first two issues related to interference have been extensively studied in this thesis. The third issue is a generic problem of small cells intensified for the case of femtocells, since the internet-based backhaul may suffer congestion resulting in a backhaul bottleneck [136] that fails to provide consistent and required quality of service (QoS) to satisfy user expectations. In addition, service may be degraded or even interrupted when the mobile users hand over from small cells to macrocells, from macrocells to small cells, or among different small cells. Finally, the privacy issue becomes a major concern when privately-owned small cells such as femtocells are open to MUs and their traffic is routed through the femtocell owner's private backhaul [137].

To address the aforementioned small cell challenges, we introduce the femtorelay technology, a novel, cost-effective small cell solution offering better performance than existing solutions. It aims to offer improved cellular coverage, enhanced system capacity, and guaranteed QoS, and affords their mobile users a seamless wireless broadband experience. At the heart of our idea is the patented femtorelay system architecture [138], [139]. This novel architecture lays the foundations of our innovations in relaying technology, cross-tier and self-interference cancellation, dynamic backhaul switching, co-tier coexistance optimization through our multi-femtorelay centralized coordination technique, and enhanced user mobility. Moreover, a femtorelay does not require careful radio frequency planning or dedicated backhaul to the operator's core network, hence reducing capital expenditure

(CAPEX) and operating expense (OPEX) not only when compared to the expensive deployment of traditional base stations, but also to other small cell solutions. The overall capacity of the system will be enhanced, allowing the accommodation of more data-demanding customers in the network.

Specifically, the femtorelay small cell technology provides the following benefits:

- *Improvement of Cell Coverage:* An architecture capable of relaying the macrocell traffic between MBSs and MUs at the cell edge in order to increase the coverage of macrocells. Moreover, the indoor coverage is simultaneously improved by the deployment of femtorelay for SCUs.

- *Enhancement of System Capacity:* The system capacity is mainly enhanced by minimization and cancellation of cross-tier, co-tier, and self-interference. First, the relaying technology effectively minimizes cross-tier interference between MUs and SCUs. Second, coordination through a centralized management entity in the multi-femtorelay minimizes co-tier interference in large indoor environments. Third, a new self-interference cancellation technique based on both active and passive approaches is developed to cancel the interference from the transmitted signal in the receiving path to enable full-duplex transmission on the same frequency bands, which further enhances system capacity.

- *Guarantee of QoS:* The QoS is guaranteed by two innovations: (i) dynamic backhaul switching and (ii) seamless mobility. First, since industry trials have shown difficulties for femtocell data transfer over a single IP backhaul, a key innovation of this technology is the enabling of a dual backhaul via relaying for QoS enhancement at a single small cell access point. Second, seamless handling of users moving in and out of the small cell coverage area is achieved through novel mobility management procedures. Also supported is the feature of backhaul switching, which performs load balancing to guarantee users' QoS.

- *Transparent Support and Scalability:* A gateway component for the core network to facilitate rapid large-scale adoption is introduced. This gateway, providing standard interfaces to the network elements, helps to significantly minimize the impact of our technology on the network. The gateway also acts as an aggregator of traffic from several of our small cell access points towards the network.

Although our femtorelay patented technology [139] described in this chapter proposes a novel approach to exploit femtocells and relays synergic advantages, there are several other works in the literature that aim to obtain some gain out of the combination of femtocells and relays in cellular networks. In [140], [141], and [142], FUs act as relays for MUs by relaying their data to the serving femtocell. The authors of [143] proposed a concept where signal decoding is not performed at the femtocell but at the MBS, and both FUs and MUs can access the open-access single-backhaul femtocell. Works targeted to improve backhaul performance by using both relay and femtocell internet-based backhauls have also been proposed: In [144] the femtocell backhaul is used to aid the macrocell backhaul when the latter is congested, and [145] proposes a rate-splitting approach where MUs can share their load between the direct macrocell link and an open access femtocell using internet-based backhaul. Femtocells and relays can also coordinate to improve mobility or resource allocation performance as shown in [146] and [147], respectively. All these concepts are very different from ours since no new small cell technology is proposed in any of them. Furthermore, they suffer from the need of re-architecting the network. Only the authors of [148] use a similar concept to ours for a femtocell and relay cooperation framework, but they assume LTE relay-enabled networks and hence their concept is not applicable to 3G networks. Further, femtocells need to be underutilized to be useful for MUs since no additional mechanism for optimizing femtocell resources is applied. Moreover, no self-interference mechanism is applied for an optimal usage of the available resources.

The remainder of this chapter is organized as follows. In Section 7.2 the femtorelay

concept is described along with its main features. Section 7.3 describes the network architecture, i.e. how this technology is compliant with the existing network infrastructure. Performance evaluation results are shown in Section 7.4, and Section 7.5 presents the evolution of this technology for larger coverage scenarios. Finally, conclusions are drawn in Section 7.6.

7.2 Femtorelay Concept Description

A femtorelay is a small cell technology aimed at improving cellular coverage within indoor environments such as dwellings or enterprises while also increasing the overall system capacity through spatial frequency reuse. On the access network, a femtorelay access point (FrAP) serves as the access point providing cellular connectivity for the users within its coverage area. Fig. 47 depicts a FrAP operating in a home environment, which includes a wireless small cell access point with a dual backhaul, one internet-based and another one relay-based, the latter one operating on carrier's licensed spectrum. As shown in Fig. 48, the internet-based backhaul connects to a femtocell gateway acting as an aggregator of several FrAPs traffic towards the CN [149], [150]. The relay-based backhaul is enabled by a relay link between the FrAP and the MBS [151], [152], [153] that is supported from the core network side by means of a femtorelay gateway (FrGW). The FrGW, as part of the core network, enables transparent integration of FrAP into the network. Furthermore, an open access approach is employed for servicing users, which means that the femtorelay users could be pre-registered with the FrAP as in the case of regular FUs or just regular subscribers to the network operator, also referred to MUs [137], [154], [155].

Fig. 49 shows a simplified block diagram of the internal architecture of a FrAP. At a high level, it consists of: (i) a femto processing module that is responsible for providing radio link to both FUs and MUs, (ii) a relaying module that provides a relay-based backhaul with the MBS used primarily for serving MU traffic, (iii) a smart open access resource

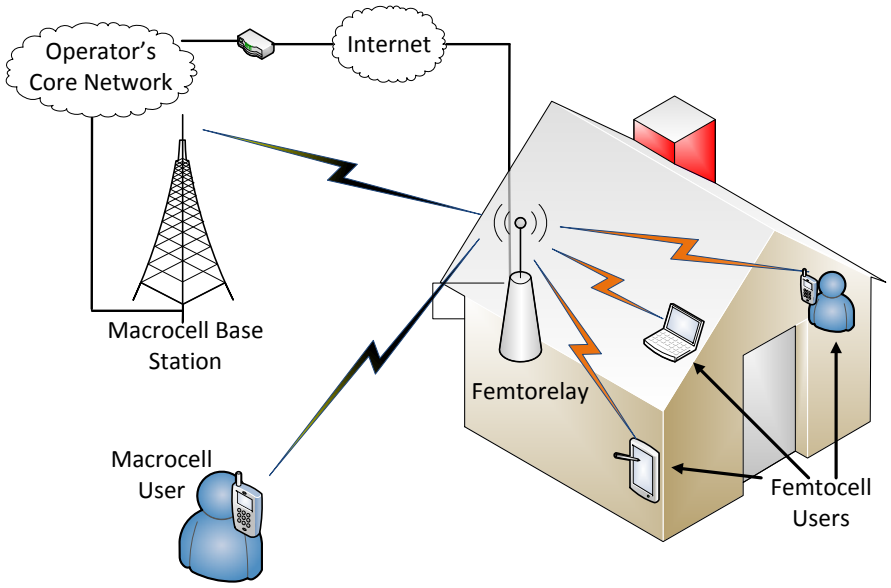

Figure 47. Femtorelay

manager that is able to intelligently allocate resources to both FUs and MUs, (iv) a performance monitor that is able to monitor the backhaul performance of users, (v) a mobility management module that enables handover and backhaul switching procedures for users, and (vi) a self-interference cancellation unit providing full-duplexing capabilities.

There are significant advantages of deploying femtorelays, as it will be further elaborated in the rest of this section. The crucial problem of the radio interference between macrocell and small cells is overcome by serving the interfering MUs residing within the small cell coverage area directly from the small cell through the relay-based backhaul. The dual backhaul feature also promises improved QoS for users and supports novel functions including backhaul switching to enhance user experience. The flexible femtorelay approach of utilizing multiple backhauls to access the core network and minimize the interference improves users QoS and is a unique feature of this technology.

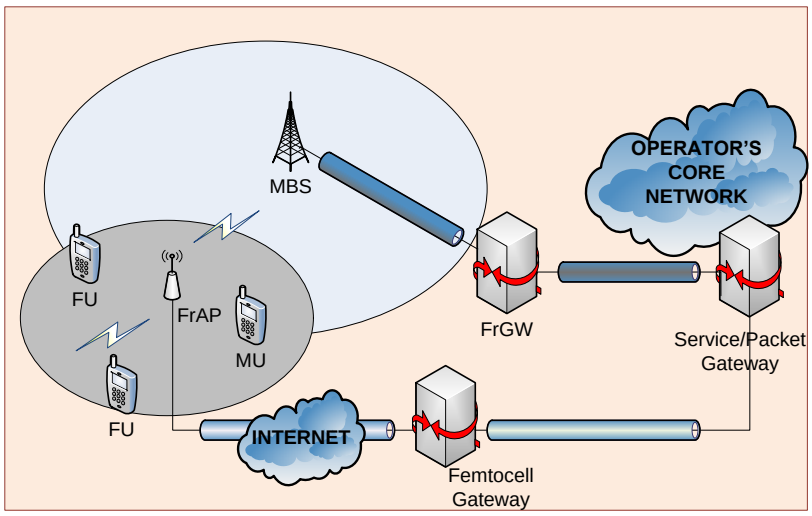

Figure 48. Cellular Network Architecture with FrAP and FrGW

7.2.1 Cross-tier Interference Management

The FrAP provides the radio link for the users under its coverage area. With current technologies, the presence of MUs in the small cell coverage area causes performance degradation to the users of both the macrocell and the small cell [156], [157], [158], [89], [116], [159]. With our technology, the strongly interfering MUs in the coverage area are served by the FrAP. The traffic of these users is forwarded through the relay-based backhaul with the help of the relaying unit. By doing so, the cross-tier interference can be largely mitigated. Since FrAP serves both MU and FU traffic, a smart resource manager allocates resources intelligently between these users.

7.2.2 QoS Guarantee

The relaying module of the FrAP is responsible for establishing a relay link with a nearby macrocell. The relay link acts as a secondary backhaul for the FrAP in addition to the internet-based backhaul and it is mainly used for serving the MUs that are attached to the FrAP. The performance monitor unit tracks the backhaul performance of all the users. The QoS is guaranteed for the users with the help of dynamic backhaul switching and seamless mobility handling. The mobility management module is responsible for performing the above tasks. Dynamic backhaul switching is concerned with switching the backhaul for a

user that experiences service degradation due to congestion in one of the backhauls. Backhaul switching primarily applies to FUs since they are registered users with potentially strict QoS requirements and the Internet-based backhaul is highly prone to performance degradation. However, the switching mechanism is applicable for MUs as well. Seamless mobility handling concerns with hand-in and hand-out of users between FrAP and nearby cells. Whenever a user experiences service degradation, an indication is sent to the mobility management module. It evaluates the service requirement and if possible, performs backhaul switching for the user. If backhaul switching cannot satisfy the service requirement, a novel handover procedure initiates a handover request to a nearby cell [160], [161], [162]. To summarize, our femtorelay tackles the key problems of backhaul limitations and user mobility and ultimately provides superior QoS performance to users.

7.2.3 Self-interference Cancellation

The relaying operation of the FrAP requires radio resources to be used for communication with the macrocell. Typically, the macrocell allocates resources to the relaying unit for the wireless backhaul link. The smart resource manager takes into account this information to assign radio resources for the users it serves. In addition, to achieve better spectral efficiency, each FrAP transmitter may operate in the same frequency band as its receiver and perform simultaneous transmission and reception for the access and relay links [162], [163], [164], [165], [166], [167], [168], resulting in full-duplex operation. It has been shown that full-duplex communication can add capacity to wireless networks [169]. However, the full-duplex operation of the FrAP results in the phenomenon of self-interference, where a signal from the transmitter causes a strong interference at the receiver and makes signal extraction infeasible [170], [171], [172]. The FrAP includes a robust self-interference cancellation scheme to mitigate the undesired feedback signal and operate in full-duplex mode.

The self-interference feedback channel, as shown in Fig. 50, exists between the femtorelay transmitter and receiver. For example, the base station will send downlink traffic

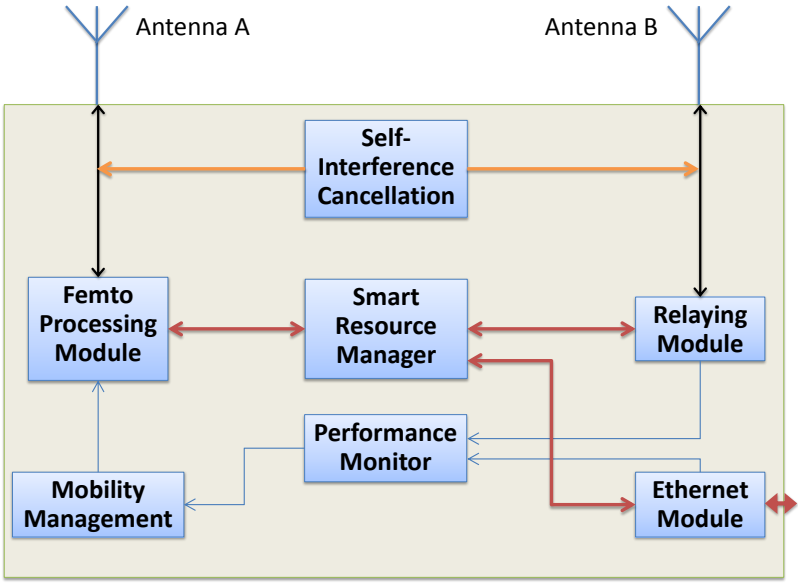

Figure 49. Functional Block Diagram of FrAP

to the FrAP on f_1 while the traffic is then relayed to a user on f_1. Similarly, the user will send uplink traffic to the FrAP on f_2, which will then be relayed to the base station on f_2. The FrAP receivers operating on f_1 and f_2 will suffer from self-interference from their respective transmitters. A similar problem occurs when the FrAP backhaul channel is the same as its access channel. The feedback channel can most often be modeled as an indoor line-of-sight (LOS) channel with AWGN. It has been shown that this channel is slowly time-varying [173].

To achieve full-duplex capability, FrAP includes a self-interference cancellation mechanism. There are several methods that attempt to address the self-interference problem; these include: Physical isolation, active, and passive cancellation schemes.

- Physical isolation includes antenna placement that reduces the interference power by orthogonal arrangement or by increasing the path loss between antennas through physical separation, RF circulators, etc. Physical size constraints from the FrAP hardware design limit the extent to which this method can provide self-interference cancellation. In [174], up to 57 dB self-interference attenuation is achieved within a 13”x9” package with omni-directional antennas. Since path loss is roughly based on

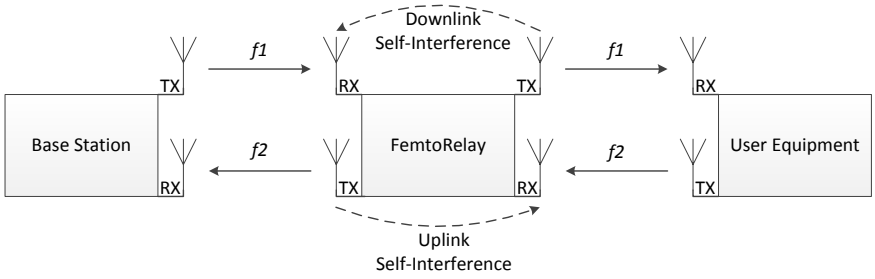

Figure 50. Self-Interference Channel

a carrier frequency, physical isolation provides wide-band self-interference cancellation.

- Active self-interference cancellation involves injecting an auxiliary signal into the receiver channel prior to digitization [175] that, ideally, is an inverted version of the interfering signal. The combined signals destructively interfere and result in reduced self-interference. This operation can be done with such devices as the Qhx module by Intersil [176], which achieves up to 20 dB isolation as an integrated chip. The chip is advertised as good for canceling spurs and phase noise. Similar designs are studied in [177], where 72 dB cancellation is achieved across a 625 kHz bandwidth. Another approach is to place an auxiliary transmit antenna a distance from the receive antenna such that the auxiliary signal arrives π radians of the carrier phase different than the offending signal [178]. One issue with this approach is that the phase difference cannot be uniform across the entire bandwidth of a wide-band signal, making it unsuitable for cellular systems that operate in wide frequency bands or multiple frequency bands. Another issue is far-field nulls in the received signal power of remote nodes resulting from the destructive interference of replica signals from the use of multiple transmission antennas.

- Passive self-interference cancellation involves removing the feedback signal without an auxiliary transmitter, usually with a digital adaptive filter after digitization.

In [179], Independent Component Analysis is used to mitigate an unwanted feedback while leaving desired received signals from remote users unaffected. Numerous passive techniques such as the least mean square (LMS) filter [180] that remove unwanted noise based on a known reference signal are reviewed in the literature. Passive schemes alone are unable to remove powerful self-interference signals when the signal is strong enough to saturate the receiver amplifier, rendering the sampled output bits useless.

Regardless of application, the successful self-interference cancellation scheme will ideally suppress the feedback signal to the noise floor. As described further in section 7.4, FrAP includes a unique combination of active, passive, and physical self-interference cancellation techniques, which blends the features of each method while mitigating their drawbacks, to enable full-duplex operation across a wide bandwidth.

7.2.4 Transparent Support and Scalability

In order to facilitate rapid large-scale adoption of our technology, we introduce the FrGW, as shown in Fig. 48. Its primary purpose is to significantly minimize the impact at the user equipment, base stations, and core network's gateways due to having the relaying module as part of the FrAP. The FrGW is a part of the operator's core network and supports standard interfaces with other network elements. It is able to efficiently decode and forward user data relayed by the FrAP towards the core network gateway. Similarly, it is also responsible for encapsulating data arriving from the core network for the users and route the data to the corresponding FrAP. Thus, it also acts as an aggregator of traffic from several FrAPs towards the network. In addition, the FrGW enables not only the deployment of femtorelays in a cellular network, but also regular relays that otherwise would need to be supported by the standard. This means that by using the FrGW, 3G and 4G relays could be deployed in a standards-compliant way without the need to upgrade the operators network infrastructure.

7.3 Femtorelay-enabled Network Architecture

In this section, we define the functional description of the femtorelay in a typical cellular network. We envision seamless integration of femtorelays into the cellular access and core network. It is, therefore, necessary to provide a generic network architecture to highlight this smooth integration. We explain the interaction between different network elements with the FrAP and the FrGW, also providing the user plane and control plane behavior of femtorelay serving different user categories in the network.

7.3.1 Network Architecture and Connectivity

Femtorelay in a typical cellular network is presented in Fig. 48. The femtorelay provide dual backhaul connectivity to the core network leveraging the relaying capability of the device in addition to the internet-based backhaul that femtocells support. Femtorelays, due to their open access feature, can allow both the FUs and MUs to connect to its access link. The real difference is observed at the backhaul through which the users are served. The FUs who typically own the internet connection from their ISPs are served over the internet-based backhaul to connect to the core network. The MUs, who are typically visitors into the femtorelay network are served on the relay-based backhaul. The internet-based backhaul is analogous to the one that is observed with femtocells. Due to their large scale deployment, traffic from several femtocells are aggregated over the internet and then routed through a femtocell gateway to the cellular operator's network. For the case of the relay-based backhaul, the Layer 3 user packets are forwarded through the relay backhaul in two-hops to the MBS. Our proposed FrGW, which acts as an accumulator for the relayed traffic in the network can intelligently capture the packets sent by the femtorelay and forwards the user packets to the core network. Based on this proposed architecture, network-wide functions carried out by the femtorelay are described in the following.

- *Backhaul Link Establishment*: Using our novel backhaul establishment procedure

and the FrGW, the relay backhaul from the FrAP to the neighboring MBS is established. To establish the backhaul link, the relay module of the FrAP acts as a mobile user and establishes a default session with the network through the FrGW. The FrAP can utilize this default session to exchange the backhaul signaling messages for user attachment.

- *Session Establishment Procedure*: The session establishment procedure can be explained as follows. The FrAP transmits downlink synchronization signals which are received by users and the users can perform initial cell attachment to establish the radio access link. With the help of user classification and the novel resource manager, a decision can be made regarding whether the users are served through the internet-based backhaul or the relay backhaul. If the internet-based backhaul is selected, the session is established in the same way as would be done in a femtocell. In case the users are served by the relay backhaul, the default session setup from the relaying module with the network is utilized to negotiate the session with the core network for the user. The session establishment procedure is completed when the end-to-end connectivity is achieved for the mobile users with the core network.

- *Mobility Procedure*: Femtorelays support both the classical hand-in and hand-out of mobile users. In addition, femtorelays can also perform backhaul switching for the mobile users when one of the backhauls experiences link failure or service degradation. The backhaul switching is achieved with the help of our novel performance monitor unit within the femtorelay.

- *Performance Monitoring*: Femtorelays are enabled with performance monitoring unit which is a software that can intelligently track the performance achieved for the users at the backhaul links. Whenever one of the links experience congestion or failure (due to internet congestion, radio link failure), the performance monitor sends an indication to the mobility management module. The mobility management

module can either trigger a handover or a backhaul switching procedure through the femto processing module to overcome the backhaul link failures. The major advantage of the backhaul switching is that the mobile user can still be connected to the femtorelay network while overcoming backhaul failure issues.

7.3.2 Protocols and network integration

The FrAP, similar to other radio access network (RAN) elements in the service provider network, requires a backhaul connection in order to communicate with the CN. Indeed, the femtorelay has two backhaul connections as mentioned in Section 7.2 . The internet-based backhaul is exactly the same as the one utilized by a typical FAP for backhauling. As such, it utilizes the same procedures, interfaces, and protocol stacks for the user and control plane as the ones used by a femtocell [181], [182], [183], [184], [185]. On the other hand, the protocols, procedures, and interfaces differ for the wireless backhaul link.

From the wireless backhaul link point of view, the FrAP and FrGW jointly provide an extra layer of tunneling that enables a transparent exchange of data and control messages between the mobile user and the CN. The FrAP and FrGW contain the necessary functionality to extract and insert any message into this tunnel without loss of information. This is analogous to how virtual private networks (VPNs) are established between two VPN endpoints. Over this tunnel, any protocol, procedure, and interface can be executed. For example, in the LTE version of the FrAP, this tunnel would support the X2 [184] and S1 [185] interfaces that are already used by eNodeBs and Home eNodeBs. In the UMTS/HSPA version, the tunnel would support the Iu [186] or Iuh [181], [182] interface already used by radio network controllers (RNCs) and Home NodeBs, respectively. From this description, it is clear that adding the FrGW in the CN plays a key role to support the femtorelay concept.

In general, adding a new element to the CN requires either to have this element standardized or to modify the CN in order to be compatible with the new element. Both options have their own advantages and drawbacks. Without standardization of the new element,

modifying the CN to be compatible with the new element represents a very high risk for an operator since there is no guarantee that the modifications will achieve the desired results without causing disruptions to their service. On the other hand, the standardization path takes a long time to achieve, but guarantees that all future networks will support the new element. Nevertheless, even if the standardization path took less time, operators are very cautious regarding upgrading their equipment to newer versions of a standard due to the high impact of any system disruption. Therefore, the time taken for an operator to upgrade their equipments (after standardization is completed) would significantly delay the introduction of the new element. With this in mind, we chose an option that lies between the previous two: Be compliant with existing standards by providing standard interfaces to the new elements we are introducing.

In order to avoid any modifications to the CN, the FrGW presents itself to the rest of CN elements as the RAN element that is serving the end user. In UMTS this corresponds to the RNC, while in LTE this corresponds to the eNodeB. In this way, the rest of the CN elements can talk with the FrGW using the interfaces and protocols they already use to communicate with RNCs and eNodeBs. Similarly, the FrGW presents itself to the RAN as the CN element that is serving the user. In UMTS, this corresponds to the serving GPRS support node (SGSN), while in LTE this corresponds to the service gateway (S-GW) and mobility management entity (MME). In this way, the RAN can communicate with the FrGW using the interfaces and protocols it already uses to communicate with SGSNs, S-GW, and MME.

Even though we have described the femtorelay architecture using 3GPP's terminology for UMTS and LTE, the femtorelay is in no way constrained to be implemented just in these two radio access technologies (RATs). The previous descriptions can be mapped to other networks, such as WiMAX. It is because of this, that we have not gone in more detail regarding the specific protocols that will be used by the femtorelay, since they would depend on the RAT in which it is introduced.

7.4 Performance Evaluation

To evaluate the performance, extensive simulations were conducted for femtorelay to determine the throughput compared with closed access femtocells. Simulations were performed using different configurations by varying the transmit power of the access points, user distances, traffic types and results were obtained. In this paper, we present our initial results where the throughput of MUs and FUs data transmission have been measured to see how they are affected when both users are in close proximity and transmit simultaneously under - 1) closed access femtocells, 2) Femtorelay. The users locations are assumed to be randomly distributed within the coverage area of the access points. The simulation parameters are listed in Table 9.

Table 9. Simulation Parameters

User Traffic Type	CBR
User start times	$[100, 200]s$
User finish times	$[700, 1000]s$
BER Required	10^{-3}
User Traffic Rate	$100kbps$
Mean User Distance	$5m$

7.4.1 Femtorelays vs. Femtocells

The throughput performance of femtocells is computed as a percentage of the data transmission rate and is illustrated in Fig. 51. In Fig. 51(a), the FUs start their transmission ahead of the MUs. As soon as the MUs start their transmission, the throughput for the FUs drop to zero while the throughput of the MUs remain as high as 90 percent. Once the MUs traffic flow comes to an end, the FUs are able to achieve about 90 percent throughput. In the case of Fig. 51(b), the FUs start the transmission first and are able to achieve 90 percent throughput only as long as the MUs haven't started transmitting their data. When both MUs and FUs are transmitting simultaneously, the throughput for both the MUs and FUs drop significantly. A different throughput performance is observed in Fig. 51(c) where the throughput of MUs drop to 30 percent while the FUs' throughput remain close to 90

percent. As seen from these results, the cross-tier interference has a significant role in the achievable performance in the network where closed access femtocells are present.

In Fig. 52, two scenarios where FR distance from the MUs and FUs vary are shown to highlight the throughput performance. It can be observed that in both the scenarios corresponding to Fig. 52(a) and 52(b), both the MUs and FUs achieve more than 90 percent throughput during the entire simulation time. In addition to the throughput vs time computation, the mean total throughput for both femtocells and femtorelay are computed and illustrated in Fig. 52(c). When the cross-tier interference is high for the case of femtocells, the mean total throughput is only about 30 percent as observed for femtorelay. When the interference in the case of femtocells is low due to the user distances, the femtorelay still achieves 1.5x higher mean total throughput than closed access femtocells. These results indicate clearly that femtorelays are a strong candidate to overcome the cross-tier interference that inhibits the throughput performance in small cells, and particularly in femtocells.

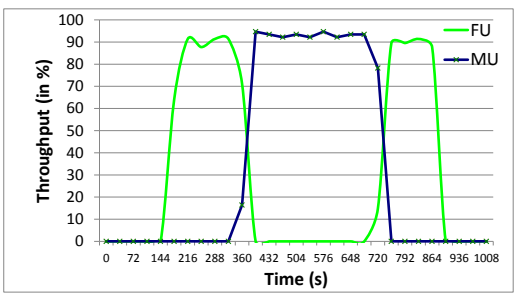

(a) FU throughput degradation

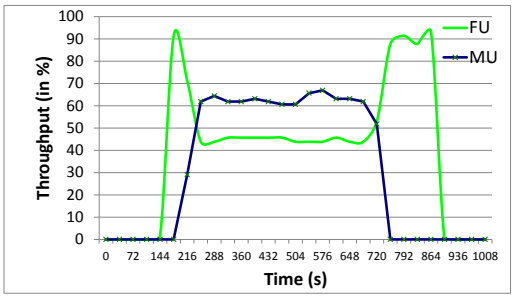

(b) FU and MU throughput degradation

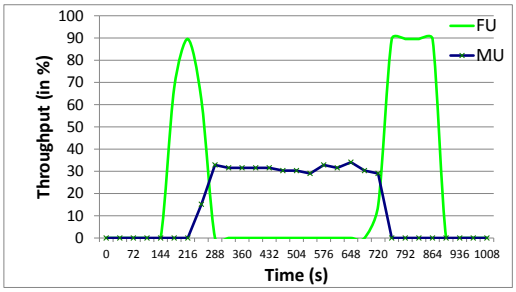

(c) Partial FU throughput degradation

Figure 51. Throughput performance under femtocell

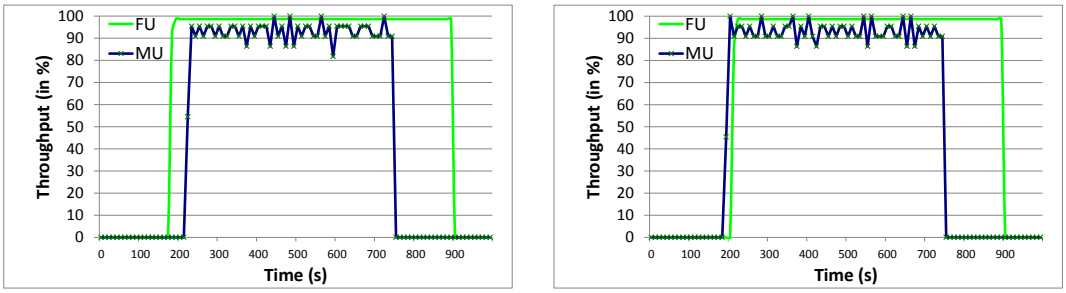

(a) Scenario 1

(b) Scenario 2

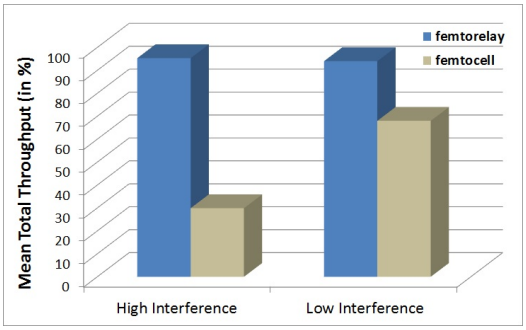

(c) Mean Total Throughput for Femtorelay vs Femtocell

Figure 52. Throughput performance under femtorelay

7.4.2 Self-Interference Cancellation Performance

To evaluate the performance of the femtorelays self-interference cancellation, we used MATLAB to simulate a feedback channel and an adaptive active cancellation mechanism. The performance of any self-interference cancellation scheme can be measured by attenuation power across a certain bandwidth. Adjacent channel power (ACP) and intermodulation intercept points (IIP) are also factors in measuring a receivers performance, which remain part of future work on this concept. The required performance differs by application. In the case of the FrAP, 3G and 4G cellular networks are of interest. For example, for WCDMA, the minimum $\frac{E_b}{N_i}$, where N_i denotes interference plus noise, required for a receiver to handle voice calls is approximately 7 dB. With a processing gain of 25 dB and received signal power, $P_{R,DPCH}$, of -117 dBm, the combined power from self-interference, receiver noise, and nearby transmitters must be less than approximately -99 dBm in order to satisfy this requirement [187]. Fig. 53 shows the simulated performance of the femtorelays novel active self-interference cancellation scheme when transmitting a WCDMA

signal and the self-interference signal is drastically reduced across 5 MHz. Together with path loss and passive interference power reduction, the femtorelay can act as a full-duplex node. In the time domain, the adaptive nature of the cancellation is apparent. Future work includes increasing the convergence rate and over interference attenuation power, as well as implementation on software defined radios for hardware validation.

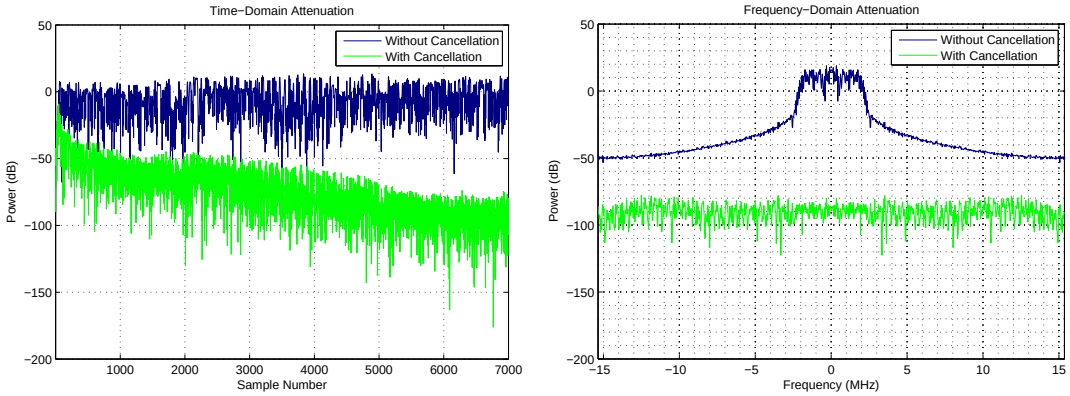

Figure 53. Active self interference cancellation performance

7.5 Technology Evolution for Large Scale Indoor Environments

Femtocells were initially envisioned as devices installed by home users in their dwellings. As femtocells evolved, they were introduced in larger indoor environments such as airports, office buildings, shopping malls, and stadiums in order to improve both capacity and coverage. Nevertheless, the fact that the femtocells are now confined in a larger indoor environments does not eliminate the interference and congestion problems associated with them. With this in mind, we further expanded the femtorelay concept to attack these two problems in larger indoor environments (enterprise environments from now on).

The multi-femtorelay (MFR) is the femtorelay version for enterprise environments [139]. The idea behind it is to have a central entity in charge of managing and coordinating the femtocells belonging to the enterprise environment; therefore, being closely located. Through this, it is able to provide better resource management across the femtocells compared to uncoordinated and distributed management approaches.

While the concept of having a central entity managing multiple femtocells can be mapped to the femtocell gateway (HNB-GW or HeNB-GW in 3GPP terms), the MFR differs in three things. First, the femtocell gateway is meant to be part of the CN of the service provider, while the central entity in the MFR is meant to be located within the local premises of the enterprise environment. This leads to the second difference: in the MFR, the central entity is in charge of managing a small set of femtocells (i.e. just the ones of the enterprise environment), compared to the number of femtocells that are managed by femtocell gateway. This allows the MFR to optimize the performance of the enterprise femtocell networks in ways that are computationally prohibitive for the HNB-GW to apply to all the femtocells in the network. Third, and what makes it unique, is that the central entity in the MFR has the same type of wired and wireless backhaul as the femtorelay, and brings all the benefits of the femtorelay to enterprise environments.

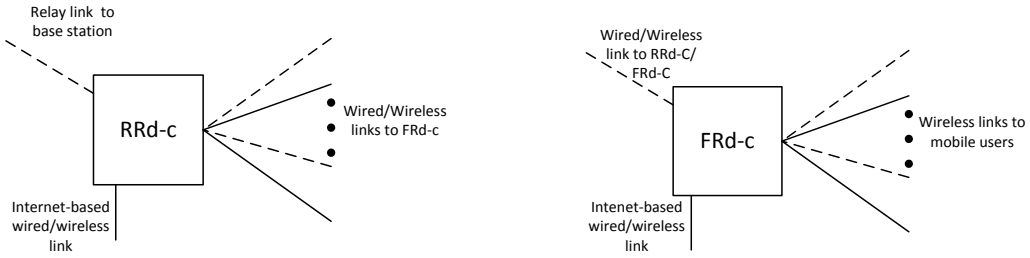

(a) RRd-C (b) FRd-C

Figure 54. MFR components

Fig. 54 illustrates the main components of a MFR. First, there is the Relay Radio Component (RRd-C). The main tasks associated with the RRd-C are to coordinate the usage of resources among the FRd-C and to provide both wireless and wired backhaul to the CN using similar methods as the femtorelay. The second element is the Femto Radio Component (FRd-C). The main role of the FRd-C is to provide radio access to the MUs and FUs within the enterprise environment. The link between the RRd-C and the FRd-C can be done through a wired connection or through wireless connection, depending on the scenario. For

example, in an office building the existing LAN can be used to connect the FRd-C to the RRd-C, as shown in Fig. 55. In tunnels and stadiums, wireless links may be more appropriate if there is no pre-existing wired networks. Regarding the internet-based backhaul, the RRd-C, the FRd-C or both may have it. For example, if all the FRd-C belong to the same owner, having the internet-based backhaul in the RRd-C is sufficient. However, if each FRd-C belongs to a different owner, then each FRd-C may have its own internet-based backhaul.

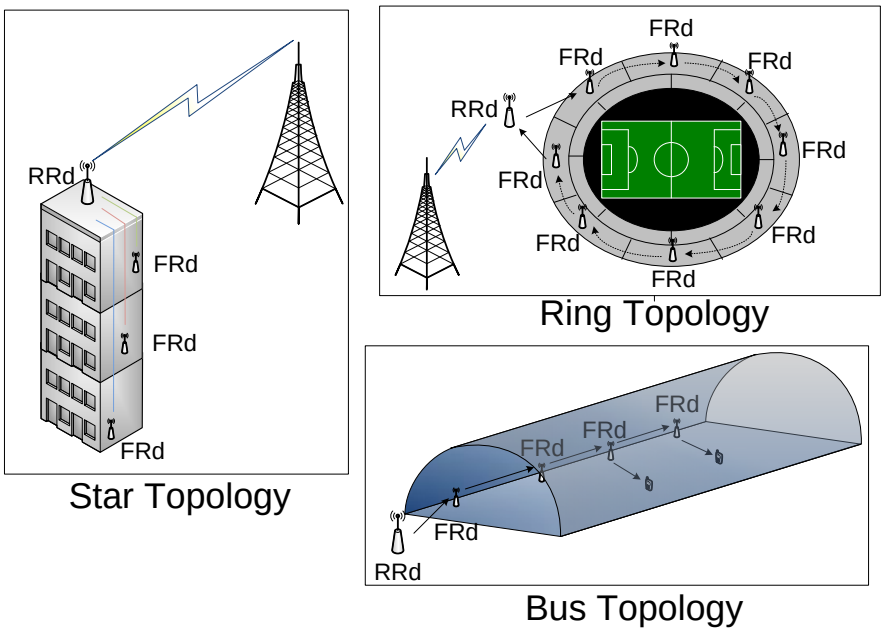

Figure 55. MFR: Scenarios

From the point of view of procedures, interfaces, and protocols, the MFR borrows these directly from the femtorelay. Therefore, it is able to integrate seamlessly into the network. In terms of managing the radio and backhaul resources, both the RRd-C and FRd-C have resource managers that closely interact and coordinate the resources that should be used by each element of the MFR. This coordination allows the MFR to achieve efficient configurations within the enterprise environment to achieve multiple objectives, such as capacity optimization, mobility robustness, load balancing, and energy savings. Currently, we are exploring the methods to perform the coordination functionality of the MFR, while

avoiding unnecessary overhead in the backhaul between the RRd-C and FRd-C. We are also exploring how the capacity of the relay backhaul of the RRd-C may affect the performance within the MFR, and methods to tackle it.

7.6 Conclusions

The demand for ubiquitous and very high speed wireless communications have shifted the paradigm of cellular networks to an architecture of heterogeneous networks composed of a combination of small cells and macrocells. Nevertheless, interference and backhaul issues still hinder the gains achievable through existing small cell technologies. To tackle these issues, a novel solution for next generation small cells, the femtorelay, has been introduced. The internal architecture has been described, as well as how this technology seamlessly integrates into existing 3G and 4G cellular networks. In addition, performance results have been provided, depicting the potential of this technology to outperform existing solutions.

CHAPTER 8

CONCLUSIONS

This thesis has shed new light in the analysis and mitigation aspects of the problem on interference in HetNets. The first overall conclusion of this work is the conviction that interference is a major aspect of HetNets that should guide the design of future network architectures. Its proper handling is an essential tool to efficiently exploit the architecture of a HetNet with the target of boosting the capacity of cellular networks. This observation is, naturally, in line with the rest of research existing in the literature, and to show that is precisely the objective of Chapter 2, where a thorough literature review on the topic is conducted.

We can break down the conclusions of the contributions of this PhD thesis in two large blocks: The first major block, composed of Chapter 3 and Chapter 4, deals with interference aspects of generic HetNets, where the carried out study and proposed solutions are not necessarily attached to a particular type of small cell. The second major block, composed of Chapter 5, Chapter 6, and Chapter 7 deal with interference aspects of specific types of small cells, namely picocells, femtocells, and femtorelays. In the following, we provide a recapitulation of the contributions of each chapter.

In Chapter 3, we address the fundamental issue of the spatial coverage cross-tier correlation between the macrocell and the small cell tiers in the presence of interference by introducing a new mathematical framework. First, we derive analytical expressions for the estimated two-tier coverage fields using techniques from the random field theory. We utilize different estimation models and cross-validate them for an assessment of their suitability for the task at hand. Stemming from these expressions, we derive a novel closed-form expression for the cross-tier correlation function exclusively dependent on the estimator's parameters. Moreover, the framework is applied to the problem of cell association in HetNets, where the coverage correlation level is utilized as a metric to determine a cell-specific

bias for each small cell.

In Chapter 4, we present a novel method to mitigate the strong interference caused by the pilot contamination effect present in a HetNet where the MBS is equipped with a very large number of antennas. The main idea in our proposed design is to prevent the reception of signal at time slots where certain network elements are receiving strong interference from a transmitter that uses a contaminated channel estimate. Besides the main architectural features, we conduct an interference analysis of our design and distinguish different fundamental interference regimes under which the network can operate. We then formalize the problem of a TDD HetNet grid and present two strategies to fill it out. Results show the potential of increasing the user rates via massive MIMO if the pilot contamination effect is properly managed with an appropiate TDD design.

In Chapter 5, we introduce codeword-level interference cancellation and almost blank subrames as interference suppression techniques for clustered picocell deployments. We also present a subframe-level coordination scheme for each picocell cluster so that the gains of these techniques can be maximized. We show that moderate gains can be obtained by applying either of these techniques but special care should be put on the system fairness. These results could be further improved by applying a biased cell association policy or a combination of interference suppression with other key LTE-Advanced technologies.

In Chapter 6, several interference-related aspects of femtocell deployments are tackled. First, we create a femtocell modeling and development platform based on OPNET, a high-fidelity simulation environment, to realistically assess the degrading effects of femtocells in the network without propoer interference management. Then, we present a spatio-temporal estimation approach based on the framework of Chapter 3 to estimate the downlink cross-tier interference in femtocell networks and enhance the performance of the resource allocation step at the FAP. Finally, we investigate the hybrid access control mode in femtocell networks as a means to control interference. A thorough investigation on the amount of resources that should dedicated to each type of user indicates the need for novel resource

management schemes which can dynamically adapt the set of open access channels to the channel and network conditions.

In Chapter 7, we introduce a novel solution for next generation small cells, the femtorelay, that overcomes the interference and backhaul limitations of current femtocells. The internal architecture is described, as well as how this technology seamlessly integrates into existing 3G and 4G cellular networks. In addition, performance results are provided, depicting the potential of this technology to outperform classical femtocell deployments.

In the future, we intend to incoporate in our research arguably the most significant feature of next generation cellular systems: The higher frequencies of transmission. The properties of the so-called mm-Wave band need to be incorporated in the design of interference solutions for HetNets. Although it seems intuitive that problems arising from the reuse of the spectrum would have a smaller impact, other aspects of these systems to guarantee the needed performance will have to be investigated. Examples of potential enablers for the systems of the future are massive MIMO and multi-stream carrier aggregation: First, the properties of massive MIMO can be used to counteract the high propagation loss of higher frequencies; second, multi-stream carrier aggregation in small cell networks transmitting in the mm-Wave could be an excellent option to mitigate the high rate of connectivity loss inherent to those high frequencies.

PUBLICATIONS

Journal Papers

1. Gutierrez-Estevez, D. M. and Akyildiz, I. F., "Architecture Design for Massive MIMO-enabled Time Division Duplex Heterogeneous Networks," submitted for journal publication, 2014.

2. Ameigeiras, P., Gutierrez-Estevez, D. M., and Navarro-Ortiz, J., "Dynamic Deployment of Small Cells in TV White Spaces," submitted for journal publication, 2014.

3. Akyildiz, I. F., Gutierrez-Estevez, D. M., Balakrishnan, R., and Chavarria Reyes, E., "LTE-Advanced and the Evolution to Beyond 4G (B4G) Systems," in Physical Communications (Elsevier) Journal, Vol. 10, pp. 31-60, March 2014.

4. Gutierrez-Estevez, D. M. and Akyildiz, I. F., "Spatial Coverage Cross-Tier Correlation Analysis for Heterogeneous Cellular Networks," in IEEE Transactions on Vehicular Technology, *in press*, 2014.

5. Akyildiz, I. F., Chavarria Reyes, E., Gutierrez-Estevez, D. M., Balakrishnan, R., and Krier, J. R., "Enabling Next Generation Small Cells through Femtorelays," in Physical Communications (Elsevier) Journal, Vol. 9, pp. 1-15, Dec. 2013.

6. Akyildiz, I. F., Gutierrez-Estevez, D. M., and Chavarria Reyes, E. "The Evolution to 4G Cellular Systems: LTE-Advanced," in Physical Communications (Elsevier) Journal, Vol. 3, No. 4, Dec. 2010.

Conference Papers

1. Al-Khansa, R., Artail, H. A., and Gutierrez-Estevez, D. M., "A Study of LTE-WiFi Carrier Aggregation for Future Multi-RAT Systems in Small Cells Environments," submitted for conference publication, 2014.

2. Doumiati, S., Artail, H. A., and Gutierrez-Estevez, D. M., "A System Design of LTE-A D2D-based Service Discovery and Communications," submitted for conference publication, 2014.

3. Gutierrez-Estevez, D. M., Somasundararam, K., and Damnjanovic, A., "Interference Suppression Techniques for Clustered Small Cell Deployments", in QTech, Qualcomm Internal Conference, San Diego, CA, June 2014.

4. Bernal-Mor, E., Pla, V., Gutierrez-Estevez, D. M., and Martinez-Bauset, J., "Resource Management for Macrocell Users in Hybrid Access Femtocells," in Proc. of IEEE Global Communications Conference (GLOBECOM), Anaheim, CA, December 2012.

5. Chavarria Reyes, E., Gutierrez-Estevez, D. M., and Akyildiz, I. F., "A Complete Femtocell Network Modeling and Development Platform," in Proc. of IEEE Global Communications Conference (GLOBECOM), Anaheim, CA, December 2012.

6. Gutierrez-Estevez, D. M., Canberk, B., and Akyildiz, I. F., "Spatio-Temporal Estimation for Interference Management in Femtocell Networks," in Proc. of IEEE Personal, Indoor & Mobile Radio Communications (PIMRC), Sydney, Australia, September 2012.

Patents

1. Somasundaram, K., Gutierrez-Estevez, D. M., Damnjanovic, A., Luo, T., Mallik, S., Xu, H. "Measurement and Signaling for Network Assistance to Enable Data-IC in Small Cell Clusters", Provisional Patent Application, Sept. 2013.

2. Akyildiz, I. F., Gutierrez-Estevez, D. M., and Chavarria Reyes, E. ”Femto-Relay Systems And Methods of Managing Same,” US Patent Application No. 20120076027, Pub. March 29, 2012.

REFERENCES

[1] I. F. Akyildiz, D. M. Gutierrez-Estevez, R. Balakrishnan, and E. Chavarria-Reyes, "LTE-Advanced and the Evolution to Beyond 4G (B4G) Systems," *Physical Communication (Elsevier) Journal*, vol. 10, pp. 31–60, Mar. 2014.

[2] 3GPP, "TR 36.912 Feasibility study for Further Advancements for E-UTRA (LTE-Advanced)," tech. rep., Jun. 2010.

[3] S. Parkvall and D. Astely, "The Evolution of LTE towards IMT-Advanced," *Journal of Communications*, vol. 4, no. 3, 2009.

[4] A. Ghosh, R. Ratasuk, B. Mondal, N. Mangalvedhe, and T. Thomas, "LTE-Advanced: Next-Generation Wireless Broadband Technology," *IEEE Wireless Communications*, vol. 17, no. 3, pp. 10–22, 2010.

[5] P. Mogensen, T. Koivisto, K. Pedersen, I. Kovacs, B. Raaf, K. Pajukoski, and M. Rinne, "LTE-Advanced: The Path Towards Gigabit/s in Wireless Mobile Communications," in *International Conference on Wireless Communication, Vehicular Technology, Information Theory and Aerospace Electronic Systems Technology (Wireless VITAE)*, pp. 147–151, 2009.

[6] 4G Americas, "4G Mobile Broadband Evolution: Release 11 & Release 12 and Beyond," tech. rep., Feb. 2014.

[7] ITU-R, "Assessment of the global mobile bradband deployments and forecasts for International Mobile Telecommunications," Report M.2134, 2011.

[8] 3GPP, "RP-13xxxx, Draft Report of 3GPP TSG RAN meeting #58," tech. rep., Dec. 2012.

[9] 3GPP, "RWS-120052, Report of 3GPP TSG RAN Workshop on Release 12 and onwards," tech. rep., Jun. 2012.

[10] Huawei, "On the Advanced 5G Network Infrastructure for the Future Internet," tech. rep., Apr. 2014.

[11] Qualcomm, "The 1000x Data Challenge," tech. rep.

[12] F. Boccardi, R. W. Heath, A. Lozano, T. L. Marzetta, and P. Popovski, "Five disruptive technology directions for 5G," *IEEE Communications Magazine*, vol. 52, pp. 74–80, Feb. 2014.

[13] J. G. Andrews, S. Buzzi, W. Choi, S. Hanly, A. Lozano, A. C. Soong, and J. C. Zhang, "What Will 5G Be?," *IEEE Journal on Selected Areas in Communications*, Sept. to appear, 2014.

[14] A. Osseiran, F. Boccardi, V. Braun, K. Kusume, P. Marsch, M. Maternia, O. Queseth, M. Schellmann, H. Schotten, H. Taoka, *et al.*, "Scenarios for 5G Mobile and Wireless Communications: The Vision of the METIS Project," *IEEE Communications Magazine*, vol. 52, no. 5, pp. 26–35, 2014.

[15] G. Wunder, P. Jung, M. Kasparick, T. Wild, F. Schaich, Y. Chen, S. ten Brink, I. Gaspar, N. Michailow, A. Festag, *et al.*, "5GNOW: Non-orthogonal, Asynchronous Waveforms for Future Mobile Applications," *IEEE Communications Magazine*, vol. 52, no. 2, pp. 97–105, 2014.

[16] 3GPP, "TS 22.011 Service accessibility," tech. rep., Dec. 2011.

[17] Y. Li, Q. Mu, L. Liu, L. Chen, M. Peng, and W. Wang, "Control Channel Design for Carrier Aggregation between LTE FDD and LTE TDD Systems," in *Proc. IEEE Vehicular Technology Conference (VTC)*, pp. 1–5, May 2012.

[18] L. Juho, H. Jin-Kyu, and J. Zhang, "MIMO technologies in 3GPP LTE and LTE-Advanced," *EURASIP Journal on Wireless Communications and Networking*, Jul. 2009.

[19] L. Liu, R. Chen, S. Geirhofer, K. Sayana, Z. Shi, and Y. Zhou, "Downlink MIMO in LTE-advanced: SU-MIMO vs. MU-MIMO," *IEEE Communications Magazine*, vol. 50, no. 2, pp. 140–147, 2012.

[20] F. Boccardi, B. Clerckx, A. Ghosh, E. Hardouin, G. Jogren, K. Kusume, E. Onggosanusi, and Y. Tang, "Multiple-Antenna Techniques in LTE-Advanced," *IEEE Communications Magazine*, vol. 50, no. 3, pp. 114–121, 2012.

[21] C. Park, Y.-P. Wang, G. Jogren, and D. Hammarwall, "Evolution of Uplink MIMO for LTE-Advanced," vol. 49, pp. 112–121, Feb. 2011.

[22] F. Rusek, D. Persson, B. K. Lau, E. Larsson, T. Marzetta, O. Edfors, and F. Tufvesson, "Scaling Up MIMO: Opportunities and Challenges with Very Large Arrays," *IEEE Signal Processing Magazine*, vol. 30, pp. 40–60, Jan. 2013.

[23] L. Lu, G. Li, A. Swindlehurst, A. Ashikhmin, and R. Zhang, "An Overview of Massive MIMO: Benefits and Challenges," *IEEE Journal of Selected Topics in Signal Processing*, vol. PP, no. 99, pp. 1–1, to appear, 2014.

[24] E. Larsson, O. Edfors, F. Tufvesson, and T. Marzetta, "Massive MIMO for Next Generation Wireless Systems," *IEEE Communications Magazine*, vol. 52, pp. 186–195, Feb. 2014.

[25] T. L. Marzetta, "Noncooperative Cellular Wireless with Unlimited Numbers of Base Station Antennas," *IEEE Transactions on Wireless Communications*, vol. 9, pp. 3590–3600, Nov. 2010.

[26] H. Q. Ngo, E. G. Larsson, and T. L. Marzetta, "Energy and spectral efficiency of very large multiuser MIMO systems," *IEEE Transactions on Communications*, vol. 61, p. 14361449, Apr. 2013.

[27] "RP-121805 Work plan for MIMO-related topics in Rel-12," TSG RAN WG1 Meeting #58, Samsung, AT&T, CMCC, Nokia, Nokia Siemens Networks, NTT DOCOMO, Dec. 2012.

[28] "RP-122015 Study on Full Dimension MIMO for LTE," TSG RAN WG1 Meeting #58, Samsung, Dec. 2012.

[29] Huawei, "Active Antenna System: Utilizing the Full Potential of Radio Sources in the Spatial Domain," *White paper*, Nov. 2012.

[30] J. Lee, Y. Kim, H. Lee, B. L. Ng, D. Mazzarese, J. Liu, W. Xiao, and Y. Zhou, "Coordinated Multipoint Transmission and Reception in LTE-Advanced Systems," *IEEE Communications Magazine*, vol. 50, no. 11, pp. 44–50, 2012.

[31] Q. Li, R. Hu, Y. Qian, and G. Wu, "Cooperative Communications for Wireless Networks: Techniques and Applications in LTE-Advanced Systems," *IEEE Wireless Communications*, vol. 19, no. 2, pp. 22–29, 2012.

[32] ArrayComm, "Coopers Law.," tech. rep.

[33] A. Ghosh, N. Mangalvedhe, R. Ratasuk, B. Mondal, M. Cudak, E. Visotsky, T. A. Thomas, J. G.Andrews, P. Xia, H. Jo, H. S. Dhillon, and T. D. Novlan, "Heterogeneous Cellular Networks: From Theory to Practice," *Communications Magazine, IEEE*, vol. 50, pp. 54 –64, June 2012.

[34] S. Hanly, "An Algorithm for Combined Cell-site Selection and Power Control to Maximize Cellular Spread Spectrum Capacity," *IEEE Journal on Selected Areas in Communications*, vol. 13, pp. 1332–1340, Sep. 1995.

[35] A. Sang, X. Wang, M. Madihian, and R. D. Gitlin, "Coordinated Load Balancing, Handoff/Cell-site Selection, and Scheduling in Multi-cell Packet Data Systems," in *Proc.10th annual international conference on Mobile Computing and Networking*, pp. 302–314, 2004.

[36] D. López-Pérez, X. Chu, and I. Guvenc, "On the expanded region of picocells in heterogeneous networks," *IEEE Journal of Selected Topics in Signal Processing (JSTSP)*, vol. 6, pp. 281–294, Jun. 2012.

[37] H.-S. Jo, Y. J. Sang, P. Xia, and J. Andrews, "Heterogeneous Cellular Networks with Flexible Cell Association: A Comprehensive Downlink SINR Analysis," *IEEE Transactions on Wireless Communications*, vol. 11, no. 10, pp. 3484–3495, 2012.

[38] A. Damnjanovic, J. Montojo, Y. Wei, T. Ji, T. Luo, M. Vajapeyam, T. Yoo, O. Song, and D. Malladi, "A survey on 3gpp heterogeneous networks," *IEEE Wireless Communications Magazine*, vol. 18, no. 3, pp. 10–21, 2011.

[39] 3GPP, "TS 36.839 Evolved Universal Terrestrial Radio Access (E-UTRA); Mobility enhancements in heterogeneous networks (Release 11)," tech. rep., Dec. 2012.

[40] E. MCC, "R2-101881: Report of 3GPP TSG RAN WG2 Meeting 68bis," tech. rep., 3GPP TSG RAN WG2 Meeting #68bis, 2010.

[41] "R2-122368: Enhanced MSE based small cell detection," TSG-RAN WG2 meeting #78, Nokia Siemens Networks, Nokia Corporation, 2012.

[42] "R2-121621: Small cell signal based control of inter-frequency measurements," TSG-RAN WG2 meeting #77bis, Nokia Siemens Networks, Nokia Corporation, 2012.

[43] EARTH, "Energy Aware Radio and Network Technologies," tech. rep.

[44] "Cognitive Radio and Cooperative Strategies for POWER saving in multi-standard wireless devices," tech. rep.

[45] Ericsson, "Ericsson Mobility Report," tech. rep., Jun. 2013.

[46] "Worldwide Cellular M2M Modules Forecast Market Brief," tech. rep., Beecham Research, Aug. 2010.

[47] S. Lucero, "Maximizing Mobile Operator Opportunities in M2M: The Benefits of an M2M-Optimized Network," tech. rep., ABI Research, 2010.

[48] 3GPP, "Study on Facilitating Machine to Machine Communication in 3GPP Systems; (Release 8)," tech. rep., TR 22.868, Mar. 2007.

[49] 3GPP, "TS 22.368 Service requirements for Machine-Type Communications (MTC); Stage 1 (Release 10)," tech. rep., Dec. 2010.

[50] K. Doppler, M. Rinne, C. Wijting, C. Ribeiro, and K. Hugl, "Device-to-Device Communication as an underlay to LTE-Advanced Networks," *IEEE Communications Magazine*, vol. 47, no. 12, pp. 42–49, 2009.

[51] L. Lei, Z. Zhong, C. Lin, and X. Shen, "Operator Controlled Device-to-device Communications in LTE-Advanced Networks," *IEEE Wireless Communications*, vol. 19, no. 3, pp. 96–104, 2012.

[52] N. Golrezaei, M. Ji, A. Molisch, A. Dimakis, and G. Caire, "Device-to-device Communications for Wireless Video Delivery," in *Conference Record of the 46th Asilomar Conference on Signals, Systems and Computers (ASILOMAR)*, pp. 930–933, 2012.

[53] P. Phunchongharn, E. Hossain, and D. Kim, "Resource Allocation for Device-to-Device Communications Underlaying LTE-Advanced Networks," *IEEE Wireless Communications*, vol. 20, no. 4, pp. 91–100, 2013.

[54] H. Min, J. Lee, S. Park, and D. Hong, "Capacity Enhancement Using an Interference Limited Area for Device-to-Device Uplink Underlaying Cellular Networks," *IEEE Transactions on Wireless Communications*, vol. 10, no. 12, pp. 3995–4000, 2011.

[55] D. Feng, L. Lu, Y. Yuan-Wu, G. Li, G. Feng, and S. Li, "Device-to-Device Communications Underlaying Cellular Networks," *IEEE Transactions on Communications*, vol. 61, no. 8, pp. 3541–3551, 2013.

[56] B. Zhou, H. Hu, S.-Q. Huang, and H.-H. Chen, "Intracluster Device-to-Device Relay Algorithm With Optimal Resource Utilization," *IEEE Transactions on Vehicular Technology*, vol. 62, no. 5, pp. 2315–2326, 2013.

[57] K. Doppler, C. B. Ribeiro, and J. Kneckt, "Advances in D2D communications: Energy efficient service and device discovery radio," in *Proc. 2nd International Conference on Wireless Communication, Vehicular Technology, Information Theory and Aerospace & Electronic Systems Technology (Wireless VITAE)*, pp. 1–6, IEEE, 2011.

[58] G. Fodor, E. Dahlman, G. Mildh, S. Parkvall, N. Reider, G. Miklos, and Z. Turanyi, "Design Aspects of Network Assisted Device-to-Device Communications," *IEEE Communications Magazine*, vol. 50, no. 3, pp. 170–177, 2012.

[59] S. Rangan, T. Rappaport, and E. Erkip, "Millimeter-Wave Cellular Wireless Networks: Potentials and Challenges," *Proceedings of the IEEE*, vol. 102, pp. 366–385, March 2014.

[60] Z. Pi and F. Khan, "An Introduction to Millimeter-wave Mobile Broadband Systems," *IEEE Communications Magazine*, vol. 49, pp. 101–107, June 2011.

[61] T. Rappaport, S. Sun, R. Mayzus, H. Zhao, Y. Azar, K. Wang, G. Wong, J. Schulz, M. Samimi, and F. Gutierrez, "Millimeter Wave Mobile Communications for 5G Cellular: It Will Work!," *IEEE Access*, vol. 1, pp. 335–349, 2013.

[62] Small Cell Forum, "Small Cells - What's the Big Idea?," Feb. 2012.

[63] A. Bleicher, "A Surge in Small Cell Sites," *IEEE Spectrum*, Dec. 2012.

[64] J. G. Andrews, F. Baccelli, and R. K. Ganti, "A Tractable Approach to Coverage and Rate in Cellular Networks," *IEEE Transactions on Communications*, vol. 59, no. 11, pp. 3122–3134, 2011.

[65] H. S. Dhillon, R. K. Ganti, F. Baccelli, and J. G. Andrews, "Modeling and Analysis of K-Tier Downlink Heterogeneous Cellular Networks," *IEEE Journal on Selected Areas in Communications (JSAC)*, vol. 30, pp. 550 – 560, April 2012.

[66] S. Mukherjee, "Distribution of Downlink SINR in Heterogeneous Cellular Networks," *IEEE Journal on Selected Areas in Communications*, vol. 30, pp. 575–585, April 2012.

[67] T. Novlan, R. Ganti, A. Ghosh, and J. Andrews, "Analytical Evaluation of Fractional Frequency Reuse for Heterogeneous Cellular Networks," *IEEE Transactions on Communications*, vol. 60, pp. 2029–2039, July 2012.

[68] V. Chandrasekhar, M. Kountouris, and J. Andrews, "Coverage in Multi-antenna Two-tier Networks," *IEEE Transactions on Wireless Communications*, vol. 8, pp. 5314–5327, October 2009.

[69] R. Heath, M. Kountouris, and T. Bai, "Modeling Heterogeneous Network Interference Using Poisson Point Processes," *IEEE Transactions on Signal Processing*, vol. 61, pp. 4114–4126, Aug 2013.

[70] R. Madan and et al., "Cell Association and Interference Coordination in Heterogeneous LTE-A Cellular Networks," *IEEE Journal on Selected Areas in Communications*, vol. 28, no. 9, pp. 1479–1489, 2010.

[71] S. Deb, P. Monogioudis, J. Miernik, and J. Seymour, "Algorithms for Enhanced Inter-Cell Interference Coordination (eICIC) in LTE HetNets," *IEEE/ACM Transactions on Networking*, vol. 22, pp. 137–150, Feb 2014.

[72] D. Lopez-Perez, X. Chu, and I. Guvenc, "On the Expanded Region of Picocells in Heterogeneous Networks," *IEEE Journal of Selected Topics in Signal Processing*, vol. 6, no. 3, pp. 281–294, 2012.

[73] S. Corroy and R. Mathar, "Semidefinite Relaxation and Randomization for Dynamic Cell Association in Heterogeneous Networks," in *Global Communications Conference (GLOBECOM), 2012 IEEE*, pp. 2373–2378, 2012.

[74] Q. Ye, B. Rong, Y. Chen, M. Al-Shalash, C. Caramanis, and J. Andrews, "User Association for Load Balancing in Heterogeneous Cellular Networks," *IEEE Transactions on Wireless Communications*, vol. 12, no. 6, pp. 2706–2716, 2013.

[75] J. Jose, A. Ashikhmin, T. Marzetta, and S. Vishwanath, "Pilot Contamination and Precoding in Multi-Cell TDD Systems," *IEEE Transactions on Wireless Communications*, vol. 10, pp. 2640–2651, Aug. 2011.

[76] H. Huh, S.-H. Moon, Y.-T. Kim, I. Lee, and G. Caire, "Multi-Cell MIMO Downlink With Cell Cooperation and Fair Scheduling: A Large-System Limit Analysis," *IEEE Transactions on Information Theory*, vol. 57, pp. 7771–7786, Dec. 2011.

[77] H. Huh, A. Tulino, and G. Caire, "Network MIMO With Linear Zero-Forcing Beamforming: Large System Analysis, Impact of Channel Estimation, and Reduced-Complexity Scheduling," *Information Theory, IEEE Transactions on*, vol. 58, pp. 2911–2934, May 2012.

[78] A. Ashikhmin and T. Marzetta, "Pilot Contamination Precoding in Multi-cell Large Scale Antenna Systems," in *IEEE International Symposium on Information Theory Proceedings (ISIT)*, pp. 1137–1141, Jul. 2012.

[79] R. Mueller, L. Cottatellucci, and M. Vehkapera, "Blind Pilot Decontamination," *IEEE Journal of Selected Topics in Signal Processing*, vol. PP, no. 99, pp. 1–1, to appear, 2014.

[80] H. Q. Ngo and E. Larsson, "EVD-based Channel Estimation in Multicell Multiuser MIMO Systems with Very Large Antenna Arrays," in *IEEE International Conference on Acoustics, Speech and Signal Processing (ICASSP)*, pp. 3249–3252, Mar. 2012.

[81] F. Fernandes, A. Ashikhmin, and T. Marzetta, "Inter-Cell Interference in Noncooperative TDD Large Scale Antenna Systems," *IEEE Journal on Selected Areas in Communications*, vol. 31, pp. 192–201, Feb. 2013.

[82] V. Chandrasekhar, J. Andrews, and A. Gatherer, "Femtocell Networks: A Survey," *IEEE Communications Magazine*, vol. 46, pp. 59 – 67, September 2008.

[83] J. G. Andrews, H. Claussen, M. Dohler, S. Rangan, and M. C. Reed, "Femtocells: Past, Present, and Future," *IEEE Journal on Selected Areas in Communications (JSAC)*, vol. 30, pp. 497–508, Apr. 2012.

[84] M. Yavuz, F. Meshkati, S. Nanda, A. Pokhariyal, N. Johnson, B. Raghothaman, and A. Richardson, "Interference Management and Performance Analysis of UMTS/HSPA+ Femtocells," vol. 47, pp. 102–109, Sep. 2009.

[85] Y. Tokgoz, F. Meshkati, Y. Zhou, M. Yavuz, and S. Nanda, "Uplink Interference Management for HSPA+ and 1xEVDO Femtocells," in *Proc. of IEEE Global Telecommunications Conference (GLOBECOM)*, pp. 1–7, Dec. 2009.

[86] D. Lopez-Perez, A. Valcarce, G. de la Roche, and J. Zhang, "OFDMA Femtocells: A Roadmap on Interference Avoidance," vol. 47, pp. 41–48, Sep. 2009.

[87] H. de Lima Carlos, M. Bennis, K. Ghaboosi, and M. Latva-aho, "On interference analysis of self-organized femtocells in indoor deployment," in *Proc. of IEEE GLOBECOM Workshops (GC Wkshps)*, pp. 659 –663, Dec. 2010.

[88] M. Nazir, M. Bennis, K. Ghaboosi, A. MacKenzie, and M. Latva-aho, "Learning based mechanisms for interference mitigation in self-organized femtocell networks," in *Conference Record of Asilomar Conference on Signals, Systems and Computers (ASILOMAR)*, pp. 1886 –1890, Nov. 2010.

[89] D. Lopez-Perez and et al., "Enhanced Intercell Interference Coordination Challenges in Heterogeneous Networks," *IEEE Wireless Communications*, vol. 18, no. 3, pp. 22–30, 2011.

[90] 3GPP, "TS 36.814 Evolved Universal Terrestrial Radio Access (E-UTRA); Further advancements for E-UTRA physical layer aspects (Release 9);," tech. rep., Mar. 2010.

[91] G. Boudreau, J. Panicker, N. Guo, R. Chang, N. Wang, and S. Vrzic, "Interference Coordination and Cancellation for 4G Networks," *IEEE Communications Magazine*, vol. 47, pp. 74–81, Apr. 2009.

[92] B. Soret, Y. Wang, and K. Pedersen, "CRS Interference Cancellation in Heterogeneous Networks for LTE-Advanced Downlink," in *Proc. IEEE International Conference on Communications (ICC)*, pp. 6797–6801, Jun. 2012.

[93] S. Ye, S. H. Wong, and C. Worrall, "Enhanced physical downlink control channel in lte advanced release 11," vol. 51, pp. 82–89, Feb. 2013.

[94] "R1-125335 PRB Indication for EPDCCH," TSG RAN WG1 Meeting #71, Huawei, Nov. 2012.

[95] M. Haenggi, J. G. Andrews, F. Baccelli, O. Dousse, and M. Franceschetti, "Stochastic geometry and random graphs for the analysis and design of wireless networks," *IEEE Journal on Selected Areas in Communications (JSAC)*, vol. 27, pp. 1029 – 1046, September 2009.

[96] N. Cressie, *Statistics for Spatial Data*. Wiley, 1993.

[97] B. D. Ripley, *Spatial Statistics*. Wiley, 2004.

[98] J. Riihijarvi and P. Mahonen, "Spatial statistics for wireless networks research," *Procedia Environmental Sciences*, vol. 7, no. 0, pp. 86 – 91, 2011.

[99] J. Riihijarvi, P. Mahonen, M. Wellens, and M. Gordziel, "Characterization and modelling of spectrum for dynamic spectrum access with spatial statistics and random fields," in *Proc. of IEEE Personal, Indoor and Mobile Radio Communications*, pp. 1–6, September 2008.

[100] J. Riihijarvi and P. Mahonen, "Estimating wireless network properties with spatial statistics and models," in *International Symposium on Modeling and Optimization in Mobile, Ad Hoc and Wireless Networks (WiOpt)*, pp. 331–336, May 2012.

[101] G. Bohling, "Introduction to geostatistics and variogram analysis," *Available: http://gismyanmar.org/geofocus/wp-content/uploads/2013/01/Variograms.pdf*, 2005.

[102] H.-S. Jo, Y. J. Sang, P. Xia, and J. Andrews, "Heterogeneous cellular networks with flexible cell association: A comprehensive downlink sinr analysis," *IEEE Transactions on Wireless Communications*, vol. 11, pp. 3484–3495, Oct. 2012.

[103] A. Goldsmith, *Wireless Communications*. Cambridge University Press, 2005.

[104] J. Nam, A. Adhikary, J.-Y. Ahn, and G. Caire, "Joint Spatial Division and Multiplexing: Opportunistic Beamforming, User Grouping and Simplified Downlink Scheduling," *IEEE Journal of Selected Topics in Signal Processing*, vol. PP, no. 99, pp. 1–1, to appear, 2014.

[105] Y. Han, J. Ni, and G. Du, "The Potential Approaches to Achieve Channel Reciprocity in FDD System with Frequency Correction Algorithms," in *International ICST Conference on Communications and Networking in China (CHINACOM)*, pp. 1–5, Aug. 2010.

[106] S. L. H. Nguyen and A. Ghrayeb, "Compressive Sensing-based Channel Estimation for Massive Multiuser MIMO Systems," in *IEEE Wireless Communications and Networking Conference (WCNC)*, pp. 2890–2895, Apr. 2013.

[107] 3GPP, "TS 36.211 Evolved Universal Terrestrial Radio Access (E-UTRA); Physical Channels and Modulation," tech. rep., Mar. 2014.

[108] J. Hoydis, K. Hosseini, S. ten Brink, and M. Debbah, "Making Smart Use of Excess Antennas: Massive MIMO, Small Cells, and TDD," *Bell Labs Technical Journal*, vol. 18, no. 2, pp. 5–21, 2013.

[109] K. Hosseini, J. Hoydis, S. ten Brink, and M. Debbah, "Massive MIMO and Small Cells: How to Densify Heterogeneous Networks," in *IEEE International Conference on Communications (ICC)*, pp. 5442–5447, Jun. 2013.

[110] 3GPP, "TS 36.300 Evolved Universal Terrestrial Radio Access (E-UTRA) and Evolved Universal Terrestrial Radio Access Network (E-UTRAN); Overall description," Dec. 2012.

[111] D. Tse and P. Viswanath, *Fundamentals of Wireless Communication*. Cambridge University Press, 2005.

[112] 3GPP, "TS 36.932 Scenarios and Requirements for Small Cell Enhancements for E-UTRA and E-UTRAN," Dec. 2012.

[113] 3GPP, "TS 36.814 Further Advancements for E-UTRA Physical Layer," Mar. 2009.

[114] A. Weber and O. Stanze, "Scheduling Strategies for HetNets using eICIC," in *IEEE International Conference on Communications (ICC)*, pp. 6787–6791, Jun. 2012.

[115] OPNET, "Wireless Network Simulation: Opnet Modeler Wireless Suite,"

[116] H.-S. Jo, C. Mun, J. Moon, and J.-G. Yook, "Interference mitigation using uplink power control for two-tier femtocell networks," vol. 8, pp. 4906–4910, Oct. 2009.

[117] V. Chandrasekhar, J. Andrews, T. Muharemovic, S. Zukang, and A. Gatherer, "Power Control in Two-tier Femtocell Networks," *IEEE Transactions on Wireless Communications*, vol. 8, pp. 4316–4328, Aug. 2009.

[118] C. Young-June, K. C. Seung, and B. Saewoong, "Flexible design of frequency reuse factor in ofdma cellular networks," in *Proc. of IEEE International Conference on Communications (ICC)*, pp. 1784–1788, June 2006.

[119] I. Guvenc, J. Moo-Ryong, F. Watanabe, and H. Inamura, "A hybrid frequency assignment for femtocells and coverage area analysis for co-channel operation," *IEEE Communications Letters*, vol. 12, pp. 880–882, December 2008.

[120] D. Choi, P. Monajemi, K. Shinjae, and J. Villasenor, "Dealing with load neighbours: the benefits and tradeoffs of adaptive femtocell access," in *Proc. of IEEE Global Telecomm. Conf. (GLOBECOM)*, pp. 1–5, Nov-Dec 2008.

[121] A. Valcarce, D. Lopez-Perez, G. de la Roche, and Z. Jie, "Limited access to ofdma femtocells," in *Proc. of IEEE Int. Sympo. on Personal, Indoor and Mobile Radio Comm. Systems*, pp. 1–5, September 2009.

[122] G. de la Roche, A. Valcarce, D. Lopez-Perez, and J. Zhang, "Access cCntrol Mechanisms for Femtocells," vol. 48, pp. 33–39, Jan. 2010.

[123] A. Golaop, M. Mustapha, and L. B. Patanapongpibul, "Femtocell Access Control Strategy in UMTS and LTE," vol. 47, pp. 117–123, Sept. 2009.

[124] Nortel and Vodafone, "Open and closed access for home NodeBs," tech. rep., 3GPP TSG-RAN WG 4(Radio), Athens, Greece, Aug. 2007.

[125] P. Xia, V. Chandrasekhar, and J. G. Andrews, "Femtocell Access Control in the TDMA/OFDMA Uplink," in *IEEE GLOBECOM 2010*, (Miami, FL), pp. 1–5, Dec. 2010.

[126] D. Das and V. Ramaswamy, "Co-channel Femtocell-Macrocell Deployments - Access Control," in *IEEE 70th Vehicular Technology Conference Fall (VTC 2009-Fall)*, (Anchorage, AK), pp. 1–6, Sept. 2009.

[127] Y.-Y. Li, L. Yen, and E. Sousa, "Hybrid user access control in HSDPA femtocells," in *IEEE GLOBECOM 2010*, (Miami, FL), pp. 679–683, Dec. 2010.

[128] E. Chavarria-Reyes, D. Gutierrez-Estevez, and I. Akyildiz, "A Complete Femtocell Network Modeling and Development Platform," in *IEEE Global Communications Conference (GLOBECOM)*, pp. 5142–5147, 2012.

[129] 3GPP, "TS 25.467 UTRAN architecture for 3G Home Node B (HNB)," Dec. 2012.

[130] 3GPP, "TR 36.814 Evolved Universal Terrestrial Radio Access (E-UTRA); Further Advancements for E-UTRA Physical Layer Aspects v9.0.0.," Mar. 2010.

[131] R. K. Jain, D. Chiu, and W. R. Hawe, "A Quantitative Measure of Fairness and Discrimination for Resource Allocation in Shared Computer Systems," tech. rep., DEC.

[132] T. Bonald and J. Roberts, "Congestion at Flow Level and the Impact of User Behaviour," *Computer Networks*, vol. 42, pp. 521–536, 2003.

[133] M. Neuts, *Matrix-geometric Solutions in Stochastic Models: An Algorithmic Approach*. The Johns Hopkins University Press, 1981.

[134] 3GPP, "TS 36.211: Physical Channels and Modulation (Release 8)," Mar. 2014.

[135] H. van den Berg, I. Fernandez-Diaz, R. Litjens, K. Spaey, and E. U. Warriach, "Self-optimisation Methods for Stand-alone Functionalities in Wireless Access Networks: Packet Scheduling Parameter Optimisation," tech. rep., INFSO-ICT-216284 SOCRATES,D3.1B, 2009.

[136] O. Tipmongkolsilp, S. Zaghloul, and A. Jukan, "The evolution of cellular backhaul technologies: Current Issues and Future Trends," *IEEE Communications Surveys and Tutorials*, vol. 13, pp. 97 – 113, first quarter 2011.

[137] P. Xia, V. Chandrasekhar, and J. Andrews, "Open vs. Closed Access Femtocells in the Uplink," *IEEE Transactions on Wireless Communications*, vol. 9, pp. 3798 –3809, Dec. 2010.

[138] I. F. Akyildiz, E. Chavarria-Reyes, D. M. Gutierrez-Estevez, R. Balakrishnan, and J. R. Krier, "Enabling Next Generation Small Cells through Femtorelays," *Physical Communication (Elsevier) Journal*, 2013.

[139] I. F. Akyildiz, D. M. Gutierrez-Estevez, and E. Chavarria-Reyes, "Femto-Relay Systems And Methods of Managing Same," Pub. Mar. 2012.

[140] D. Zhou and W. Song, "Interference-Controlled Load Sharing with Femtocell Relay for Macrocells in Cellular Networks," in *Proc. of IEEE Global Telecommunications Conference (GLOBECOM)*, pp. 1–5, Dec. 2011.

[141] P. Jacob and A. Madhukumar, "Interference Reduction through Femto-relays," *Communications, IET*, vol. 6, pp. 2208 –2217, Sep. 2012.

[142] P. Jacob and A. S. Madhukumar, "Femto-relays: A power Efficient Coverage Extension Mechanism for Femtocells," in *Proc. of IEEE Int. Symp. on Personal Indoor and Mobile Radio Communications (PIMRC)*, pp. 975–979, Sep. 2011.

[143] T. Elkourdi and O. Simeone, "Femtocell as a Relay: An Outage Analysis," vol. 10, pp. 4204–4213, Dec. 2011.

[144] A. Rath, S. Hua, and S. S. Panwar, "FemtoHaul: Using Femtocells with Relays to Increase Macrocell Backhaul Bandwidth," in *Proc. of IEEE Conference on Computer Communications (INFOCOM) Workshops*, pp. 1–5, Mar. 2010.

[145] S. Samarakoon, M. Bennis, W. Saad, and M. Latva-aho, "Enabling Relaying over Heterogeneous Backhauls in the Uplink of Femtocell Networks," in *Proc. of Int. Symp. on Modeling and Optimization in Mobile, Ad Hoc and Wireless Networks (WiOpt)*, pp. 75–80, May 2012.

[146] Y.-S. Chen, C.-C. Li, and W.-L. Chiang, "A Femtocell-Assisted Data Forwarding Protocol in Relay Enhanced LTE Networks," in *Proc. of Int Parallel Processing Workshops (ICPPW) Conference*, pp. 127–136, Sep. 2011.

[147] A. T. Gamage, N. Rajatheva, and M. Codreanu, "Resource Allocation for OFDMA-based Relay Assisted Two-tier Femtocell Networks," in *Proc. of Int Wireless Communication Systems (ISWCS) Symp*, pp. 834–838, Nov. 2011.

[148] N. Nomikos, P. Makris, D. N. Skoutas, D. Vouyioukas, and C. Skianis, "A Cooperation Framework for LTE Femtocells' Efficient Integration in Cellular Infrastructures based on Femto Relay Concept," in *Proc. of IEEE Int Computer Aided Modeling and Design of Communication Links and Networks (CAMAD) Workshop*, pp. 318–322, Sep. 2012.

[149] D. Knisely, T. Yoshizawa, and F. Favichia, "Standardization of Femtocells in 3GPP," vol. 47, pp. 68–75, Sep. 2009.

[150] D. Knisely and F. Favichia, "Standardization of Femtocells in 3GPP2," vol. 47, pp. 76–82, Sep. 2009.

[151] J. Sydir and R. Taori, "An Evolved Cellular System Architecture Incorporating Relay Stations," vol. 47, pp. 115–121, Jun. 2009.

[152] N. Krishnan, R. D. Yates, N. B. Mandayam, and J. S. Panchal, "Bandwidth Sharing for Relaying in Cellular Systems," vol. 11, pp. 117–129, Jan. 2012.

[153] C. Raman, G. J. Foschini, R. A. Valenzuela, R. D. Yates, and N. B. Mandayam, "Half-Duplex Relaying in Downlink Cellular Systems," vol. 10, pp. 1396–1404, May 2011.

[154] H.-S. Jo, P. Xia, and J. G. Andrews, "Downlink Femtocell Networks: Open or Closed?," in *Proc. IEEE Int. Communications Conference (ICC)*, pp. 1–5, Jun. 2011.

[155] S.-Y. Yun, Y. Yi, D.-H. Cho, and J. Mo, "The Economic Effects of Sharing Femtocells," vol. 30, pp. 595–606, Apr. 2012.

[156] D. M. Gutierrez-Estevez, B. Canberk, and I. F. Akyildiz, "Spatio-temporal estimation for interference management in femtocell networks," in *Proc. of IEEE Int. Sympo. on Personal, Indoor and Mobile Radio Comm. Systems (PIMRC)*, pp. 1137 –1142, September 2012.

[157] E. Chavarria-Reyes, D. Gutierrez-Estevez, and I. Akyildiz, "A Complete Femtocell Network Modeling and Development Platform," in *Proc. of IEEE Global Telecommunications Conference (GLOBECOM)*, Dec. 2012.

[158] E. Bernal-Mor, V. Pla, D. M. Gutierrez-Estevez, and J. Martinez-Bauset, "Resource Management for Macrocell Users in Hybrid Access Femtocells," in *Proc. of IEEE Global Telecommunications Conference (GLOBECOM)*, Dec. 2012.

[159] T. Zahir, K. Arshad, A. Nakata, and K. Moessner, "Interference Management in Femtocells," *IEEE Communications Surveys Tutorials*, vol. 15, pp. 293 –311, First Quarter 2013.

[160] T. Guo, A. ul Quddus, and R. Tafazolli, "Seamless Handover for LTE Macro-Femto Networks Based on Reactive Data Bicasting," vol. 16, pp. 1788–1791, Nov. 2012.

[161] T. Guo, A. ul Quddus, N. Wang, and R. Tafazolli, "Local Mobility Management for Networked Femtocells Based on X2 Traffic Forwarding," vol. 62, pp. 326–340, Jan. 2013.

[162] R. Singoria, T. Oliveira, and D. P. Agrawal, "Reducing Unnecessary Handovers: Call Admission Control Mechanism between WiMAX and Femtocells," in *Proc. of IEEE Global Telecommunications Conference (GLOBECOM)*, pp. 1–5, Dec. 2011.

[163] D. W. K. Ng and R. Schober, "Dynamic Resource Allocation in OFDMA Systems with Full-Duplex and Hybrid Relaying," in *Proc. of IEEE Int. Communications Conference (ICC)*, pp. 1–6, Jun. 2011.

[164] Y. Y. Kang and J. H. Cho, "Capacity of MIMO wireless channel with full-duplex amplify-and-forward relay," in *Proc. of IEEE Int. Symp. on Personal, Indoor and Mobile Radio Communications (PIMRC)*, pp. 117–121, Sep. 2009.

[165] T. Riihonen, S. Werner, and R. Wichman, "Comparison of Full-Duplex and Half-Duplex Modes with a Fixed Amplify-and-Forward Relay," in *Proc. of IEEE Wireless Communications and Networking Conference (WCNC)*, pp. 1–5, Apr. 2009.

[166] T. Riihonen, S. Werner, and R. Wichman, "Hybrid Full-Duplex/Half-Duplex Relaying with Transmit Power Adaptation," vol. 10, pp. 3074–3085, Sep. 2011.

[167] Q. Li, K. H. Li, and K. C. Teh, "Achieving Optimal Diversity-Multiplexing Tradeoff for Full-Duplex MIMO Multihop Relay Networks," vol. 57, pp. 303–316, Jan. 2011.

[168] V. R. Cadambe and S. A. Jafar, "Degrees of Freedom of Wireless Networks With Relays, Feedback, Cooperation, and Full Duplex Operation," vol. 55, pp. 2334–2344, May 2009.

[169] A. Host-Madsen and J. Zhang, "Capacity bounds and power allocation for wireless relay channels," vol. 51, pp. 2020–2040, Jun. 2005.

[170] P. Lioliou, M. Viberg, M. Coldrey, and F. Athley, "Self-interference suppression in full-duplex MIMO relays," in *Conf. Record of Asilomar Conference Signals, Systems and Computers (ASILOMAR)*, pp. 658–662, 2010.

[171] H. Ju, E. Oh, and D. Hong, "Improving efficiency of resource usage in two-hop full duplex relay systems based on resource sharing and interference cancellation," vol. 8, pp. 3933–3938, Aug. 2009.

[172] T. Riihonen, S. Werner, and R. Wichman, "Mitigation of Loopback Self-Interference in Full-Duplex MIMO Relays," vol. 59, pp. 5983–5993, Dec. 2011.

[173] M. Duarte, C. Dick, and A. Sabharwal, "Experiment-Driven Characterization of Full-Duplex Wireless Systems," *IEEE Transactions on Wireless Conmmunications*, vol. 11, pp. 4296 –4307, Dec. 2012.

[174] A. Sahai, G. Patel, and A. Sabharwal, "Pushing the limits of Full-duplex: Design and Real-time Implementation," *Rice University Technical Report TREE1104*, vol. abs/1107.0607, Jun. 2011.

[175] W. Schacherbauer, A. Springer, T. Ostertag, C. C. W. Ruppel, and R. Weigel, "A flexible multiband frontend for software radios using high IF and active interference cancellation," in *Proc. of IEEE MTT-S Int. Microwave Symp. Digest*, vol. 2, pp. 1085–1088, 2001.

[176] "The QHX220 by Intersil," 2013.

[177] M. Duarte and A. Sabharwal, "Full-duplex wireless communications using off-the-shelf radios: Feasibility and first results," in *Conf. Record of Asilomar Conference on Signals, Systems and Computers (ASILOMAR)*, pp. 1558–1562, Nov. 2010.

[178] J. I. Choi, M. Jain, K. Srinivasan, P. Levis, and S. Katti, "Achieving single channel, full duplex wireless communication," in *Proc. of International Conference on Mobile computing and networking (MobiCom)*, pp. 1–12, 2010.

[179] J. Yuan, J. Shi, B. Tang, and H. Chen, "An Adaptive Feedback Interference Cancelling Algorithm Based on Independent Component Analysis for Wireless Repeaters," in *Proc. of Int. Conference on Wireless Communications Networking and Mobile Computing (WiCOM)*, pp. 1–4, Sep. 2010.

[180] B. Widrow, J. R. Glover, Jr., J. M. McCool, J. Kaunitz, C. S. Williams, R. H. Hearn, J. R. Zeidler, J. Eugene Dong, and R. C. Goodlin, "Adaptive noise cancelling: Principles and applications," vol. 63, pp. 1692–1716, Dec. 1975.

[181] 3GPP, "TS 25.444 Iuh Data Transport," Sep. 2012.

[182] 3GPP, "TS 25.468 UTRAN Iuh Interface RANAP User Adaption (RUA) Signalling," Dec. 2012.

[183] 3GPP, "TS 25.469 UTRAN Iuh Interface Home Node B (HNB) Application Part (HNBAP) Signalling," Jun. 2012.

[184] 3GPP, "TS 36.420 Evolved Universal Terrestrial Radio Access Network (E-UTRAN); X2 General Aspects and Principles," Sep. 2012.

[185] 3GPP, "TS 36.410 Evolved Universal Terrestrial Radio Access Network (E-UTRAN); S1 General Aspects and Principles," Sep. 2012.

[186] 3GPP, "TS 25.410 UTRAN Iu Interface: General Aspects and Principles," tech. rep., Sep. 2012.

[187] O. K. Jensen, T. E. Kolding, C. R. Iversen, S. Laursen, R. V. Reynisson, J. H. Mikkelsen, E. Pedersen, M. B. Jenner, and T. Larsen, "RF receiver requirements for 3G W-CDMA mobile equipment," *Microwave Journal*, vol. 43, p. 22, Feb. 2000.

VITA

David M. Gutierrez Estevez was born in Madrid, Spain in 1985. In July 2009 he obtained his Engineering Degree in Telecommunications from the Escuela Tecnica de Ingenierias Informatica y de Telecomunicacion within the Universidad de Granada, Spain. In May 2011 he obtained his MS degree in Electrical and Computer Engineering from the Georgia Institute of Technology with a fellowship of la Caixa. During the summer of 2007 he held a three-month long internship position at the Audio Department of Fraunhofer Institut fuer Integrierte Schaltungen in Erlangen, Germany, where he worked on watermarking techniques for audio signals and delay optimization for advanced audio codecs. From April 2008 to June 2009, he worked as a student research assistant at the Broadband Mobile Communications Networks Department of the Fraunhofer Heinrich Hertz Institute in Berlin, Germany, on projects linked to Long Term Evolution (LTE) cellular systems. Furthermore, during the summer of 2013 he was an intern within the Corporate Research and Development division of Qualcomm, Inc., where he worked on interference cancellation techniques for small cell networks.

Since March 2010, David has been a PhD student with the Broadband Wireless Networking Lab at Georgia Institute of Technology under the supervision of Prof. Ian F. Akyildiz. He received the BWN Lab Researcher of the Year Award for his outstanding research achievements in 2013. Previously, he had also received a full two-year fellowship from Fundacion Caja Madrid for the years 2011-2013. His research interests are focused on enabling technologies for next generation cellular networks with a special emphasis on heterogeneous networks. David is also a member of IEEE.